

AD-A123 783

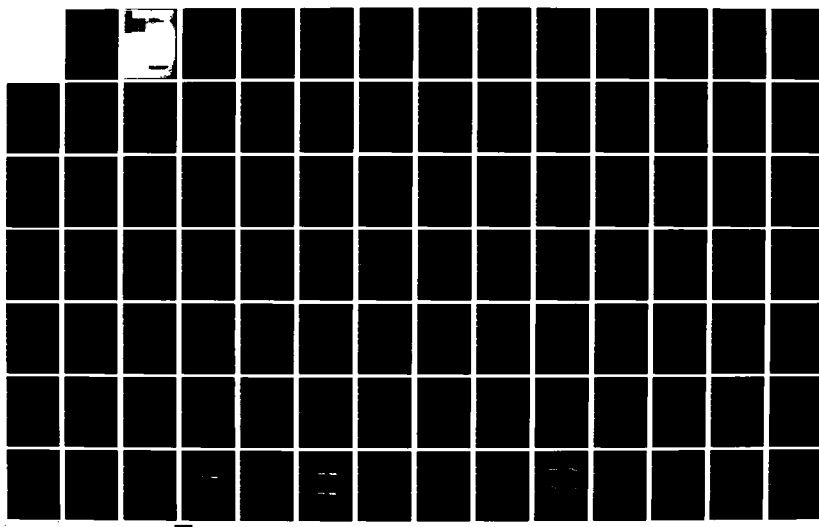
FAILURE DETECTION AND LOCATION METHOD (FDLM) (U)
MASSACHUSETTS INST OF TECH CAMBRIDGE MAN-MACHINE
SYSTEMS LAB U TSACH 30 SEP 82 N00014-77-C-0256

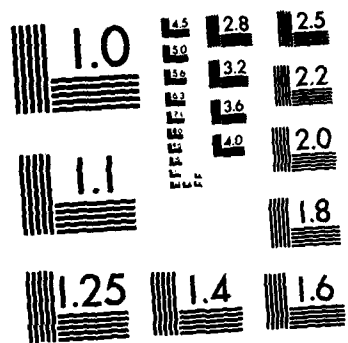
1/2

UNCLASSIFIED

F/G 5/8

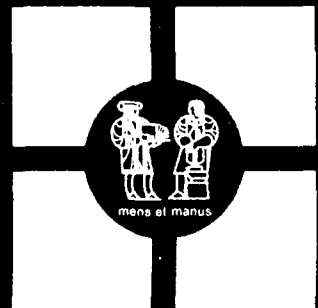
NL





MICROCOPY RESOLUTION TEST CHART
NATIONAL BUREAU OF STANDARDS-1963-A

ADA123783



**Man-Machine
Systems Laboratory**

Department of Mechanical Engineering
Massachusetts Institute of Technology
Cambridge, Massachusetts 02139

SECURITY CLASSIFICATION OF THIS PAGE (When Data Entered)

disaggregating the model and utilizing the causal description of the resultant submodels. This method eliminates the necessity to pre-program the system's possible failure modes, but requires an efficient failure location procedure. System, sensor, and control input failures can be identified by FDLM. The display interfacing FDLM to the human operator was designed to minimize the rate of missings and false alarms as well as the operator's reaction time.

A simulation test of FDLM applied to a part of a ship's engine demonstrates the advantages of the method.

Accession For	
NTIS GRA&I <input checked="" type="checkbox"/>	
DTIC TAB <input type="checkbox"/>	
Unannounced <input type="checkbox"/>	
Justification	
By _____	
Distribution/	
Availability Codes	
Dist	Avail and/or Special
A	



FAILURE DETECTION AND LOCATION METHOD
(FDLM)

by

URI TSACH

B.Sc. Technion, Israel Institute of Technology, Haifa
(1976)

M.Sc. I.I.T., Illinois Institute of Technology, Chicago
(1978)

Submitted in Partial Fulfillment of the
Requirements for the Degree of

DOCTOR OF PHILOSOPHY

at the

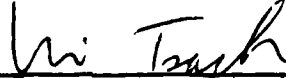
MASSACHUSETTS INSTITUTE OF TECHNOLOGY

September 7, 1982

© Uri Tsach, 1982

The author hereby grants to M.I.T. permission to reproduce and to dis-
tribute copies of this thesis document in whole or in part.

Signature of Author


Department of Mechanical Engineering
September 7, 1982

Certified by



Thomas B. Sheridan
Thesis Supervisor

Accepted by


Warren M. Rohsenow
Chairman, Department Graduate Committee

ACKNOWLEDGEMENTS

The author wishes to thank his thesis committee: Professor Thomas B. Sheridan, Chairman, who suggested the topic and continuously provided direction during the conduct of this research, Professor Elias P. Gyftopoulos, whose critical analysis was a constant source of guidance, and Professor Henry M. Paynter, who developed the theoretical foundations upon which this research is built and was very instrumental in guiding the theoretical aspects of this work. Their help and inspiration are deeply appreciated. I want to express my special appreciation to Professor Thomas B. Sheridan who always has been more than fair with his students.

I wish to thank the Office of Naval Research for supplying financial support under Contract N00014-77-C-0256 and to all my friends in the Man-Machine Systems Laboratory who provided a pleasant working atmosphere.

Special thanks are due to Joseph Tzelgov who helped designing and analyzing the experiments and Ahmet Buharali who prepared the computer graphics.

I want to thank Professor Asher H. Shapiro who provided helpful advice during my stay in M.I.T., and Sandra Tepper who always has the time to listen and to provide very experienced advice.

Special thanks are due to Mark L. Nagurka who helped debugging and rephrasing this work, and to Leslie Regan who typed accurately the final manuscript.

Most of all I would like to thank my wife Dafna and my daughter
Vered whose patience and moral support during the years made the
completion of this thesis possible.

TABLE OF CONTENTS

	<u>Page</u>
TITLE PAGE.....	1
ABSTRACT.....	2
ACKNOWLEDGEMENTS.....	3
TABLE OF CONTENTS.....	5
LIST OF FIGURES.....	8
LIST OF TABLES.....	16
CHAPTER 1 - INTRODUCTION.....	17
CHAPTER 2 - DESCRIPTION OF THE FAILURE DETECTION AND LOCATION METHOD (FDLM).....	21
2.1 Definition of Failure.....	21
2.2 A System's Causal Description.....	21
1. Bilateral energy bonds.....	21
2. Unilateral bonds.....	25
3. Multilateral bonds.....	25
2.3 A Failure Detection Method.....	25
2.4 Failure Detection and Location Method (FDLM).....	29
2.4.1 Bilateral Energy Bonds.....	29
2.4.2 Unilateral Energy Bonds.....	33
2.4.3 Multilateral Energy Bonds.....	33
2.4.4 Refining the Failure-Causes Location.....	36
2.4.5 Updating the Model Using FDLM.....	36
2.5 An Example of FDLM Applied to Bilateral Energy Bonds..	39
CHAPTER 3 - ADVANTAGES AND LIMITATIONS OF FDLM.....	46
3.1 System/Model Comparison.....	46
3.1.1 Early Failure Detection.....	46
3.1.2 Efficient Failure Location Procedure.....	48
3.2 FDLM and the disaggregated Model Technique.....	55
3.3 Sensitivity Analysis.....	58
3.4 Sensor Failures.....	61

	<u>PAGE</u>
CHAPTER 4 - MORE COMPLEX APPLICATIONS OF FDLM.....	62
4.1 Applications of FDLM to Non-Linear Systems.....	62
4.2 Multi-Connected Systems.....	69
4.3 Dependent Energy Storing Components.....	69
4.4 Thermofluidic Systems.....	73
CHAPTER 5 - HUMAN FACTOR CONSIDERATIONS.....	82
5.1 Aiding the Operator Detecting System Failures.....	82
5.1.1 Raw Variables Display.....	83
5.1.2 Averaged Variables Display.....	87
5.1.3 Percentage Error Display (PED).....	89
5.1.4 Standard Score Display (SSD).....	91
5.1.5 Probabilities Display.....	98
5.2 Incorporating a Statistical Model within FDLM.....	100
5.2.1 Classical Hypothesis Testing.....	105
5.2.2 Bayesian Approach.....	106
5.3 Computer/Human Operator Interaction in Applying FDLM.....	111
CHAPTER 6 - EXPERIMENTAL DETERMINATION OF AN OPTIMAL DISPLAY.	114
6.1 Experimental Goals.....	114
6.2 Experimental Design.....	115
6.3 Experimental Method.....	121
6.4 Experimental Results.....	121
6.4.1 Accuracy Analysis.....	122
6.4.2 Analysis of the Subjects' Reaction Times....	122
6.5 Summary and Conclusions.....	128
CHAPTER 7 - SHIP'S ENGINE SIMULATION.....	129
7.1 A Description of the Ship's Engine Simulation.....	129
7.2 Tracing the Non-Linear Ship's Engine Simulation by Solving a Linear Set of Differential Equations..	133
7.3 Elimination Derivative Calculations when Dependent Energy Storing Components are Included in the Model.....	134
7.4 Comparing ac Power Versus Its Corresponding Effort and Flow Variables.....	134
7.5 Different Failure Location Procedures.....	138

	<u>PAGE</u>
CHAPTER 8 - CONCLUSIONS AND FUTURE WORK.....	148
REFERENCES.....	153
APPENDIX A - INSTRUCTIONS TO THE EXPERIMENTAL SUBJECTS.....	156
APPENDIX B - SHIP'S ENGINE SIMULATION.....	160
APPENDIX C - UTILIZING MEASUREMENT POINT 1 IN APPLYING FDLM TO THE SHIP'S ENGINE.....	164
APPENDIX D - UTILIZING MEASUREMENT POINTS 1 AND 2 IN APPLYING FDLM TO THE SHIP'S ENGINE.....	167

LIST OF FIGURES

<u>FIGURE NUMBER</u>	<u>FIGURE TITLE</u>	<u>PAGE</u>
2.1	Causal description of system ($S_1 S_2$) with bilateral energy bonds. from reference 18.....	23
2.2	A two-tank hydraulic system.....	24
2.3	Causal description of the two-tank hydraulic system shown in Figure 2.2.....	24
2.4	Causal description of a system ($S_1 S_2$) with unilateral energy bond. In 2.4a the independent power variable is e and in 2.4b it is f ...	26
2.5	A modified two-tank hydraulic system.....	27
2.6	Causal description of the modified two-tank hydraulic system shown in Figure 2.5.....	27
2.7	Causal description of a system ($S_1 S_2$) with multilateral energy bond.....	28
2.8	Comparing the system transferred power values P_{12} and P_{23} , with their model values, P_{12}^n and P_{23}^n . u is a vector of the system's input variables.....	30
2.9	FDLM system-model setup where the system power, P_{12} , is compared with its model values, $P_{n_1}^n$ and $P_{n_2}^n$	31
2.10	FDLM application to a system with unilateral energy bond. If f_m differs from f_s the failure is in subsystem 1.....	34
2.11	FDLM application to a system with multilateral energy bonds (3 independent power variables). If P_m differs from P_s the failure is in subsystem 1 and if F_m or T_m differs from F_s or T_s , respectively, the failure is in subsystem 2.....	35
2.12	FDLM simultaneous mode. All the available system measured variables are utilized simultaneously and the model is disaggregated into small submodels.....	37

<u>FIGURE NUMBER</u>	<u>FIGURE TITLE</u>	<u>PAGE</u>
2.13	FDLM sequential mode. The system measured outputs of each point are utilized sequentially (test 1, test 2 ...) to pin-point the system failure.....	38
2.14	A description of an hydraulic-mechanical-electrical system. There are 5 measurement points available (Points 1-5).....	40
2.15	Causal description of the hydraulic-mechanical electrical system shown in Figure 2.14.....	41
2.16	A sequence of three FDLM single tests applied to the system shown in Figure 2.14.....	42
2.17a	FDLM test 1. Pressure and flow measured at point 1 in the system compared with the values predicted by the model. Since FS and FM are different the failure is in the right subsystem.....	43
2.17b	FDLM test 2. Pressure and flow measured at point 2 in the system compared with the values predicted by the model. Since FS and FM are different the failure is in the right subsystem.....	44
2.17c	FDLM test 3. Torque and angular velocity measured at point 3 in the system compared with the values predicted by the model. Since TS and TM are different the failure is in the left subsystem.....	45
3.1	The system output x_s crosses its safety limit at time t_2 , whereas the system model deviation ($ x_s - x_m $) exceeds its allowable threshold, δ^n , at time t_1	47
3.2	A sequence of three single FDLM tests applied to a third order model. S_1-S_3 are the state variables, and X is a defective system component.....	50
3.3	A third order electric network utilized to generate the outputs depicted in Figures 3.4-3.6. The three measurement point (points 1-3) correspond to the measurement points shown in Figure 3.2.....	51

<u>FIGURE NUMBER</u>	<u>FIGURE TITLE</u>	<u>PAGE</u>
3.4	The system and model outputs of the left and right submodels. These outputs are obtained by applying the FDLM test 1 and indicate that the failure is in the right subsystem.....	52
3.5	The system and model outputs of the left and right submodels. These outputs are obtained by applying the FDLM test 2 and indicate immediately that the failure is still in the right subsystem.....	53
3.6	The system and model outputs of the left and right submodels. These outputs are obtained by applying the FDLM test 3 and indicate that the failure is in the right subsystem only, after the left system and model outputs coincide.....	54
3.7	The right submodel obtained by applying FDLM to the system shown in Figure 2.12 utilizing measurement point 4. The submodel input is W_{S4} and outputs are $\tau_4, \tau_5, W_5, E_6, I_6$	56
4.1	A non-linear fifth order electric network. The transformer coefficient G is a function of the current I_1	64
4.2	The system and model state variables of the electric network shown in Figure 4.1. The model state variables M_3 and M_4 do not follow their corresponding system state variables S_3 and S_4 . The integration time step is 0.05 seconds.....	66
4.3	The system and model state variables of the electric network shown in Figure 4.1. The model state variables follow their corresponding system state variables. FDLM linear transformation is applied and the integration time step is 0.05 seconds.....	67
4.4	The system and model state variables of the electric network shown in Figure 4.1. The model state variables follow their corresponding system state variables. The integration time step is 0.005 seconds.....	68
4.5	Causal description of the electric network shown in Figure 4.1. This system is multi-connected.....	70

<u>FIGURE NUMBER</u>	<u>FIGURE TITLE</u>	<u>PAGE</u>
4.6	Multiconnected systems cannot be partitioned into two subsystems by applying a single cut..	71
4.7	Multiconnected system is partitioned into two subsystems by cutting multi energy bonds..	72
4.8	The causality of the submodel is such that I_{S1} is the submodel input and E_{M1} is its output.....	74
4.9	The causality of the submodel is such that E_{S1} is the submodel input and I_{M1} is its output.....	74
4.10	A general thermofluidic component. Fluid flows in and out with mass flow F_1 and F_2 . E is the energy and M is the mass of fluid in the component. Q and W are the heat and work rates, respectively.....	75
4.11	The input and output variables of the system shown in Figure 4.10. E and M are the system state variables.....	75
4.12	Choke flow resistor. F is the flow, P_1 and P_2 are the input and output pressure, A is the nozzle area.....	78
4.13	The input and output variables of the choke flow resistor.....	78
4.14	FDLM method applied to a simple thermofluidic system. Deviations of P_S from P_m and T_S from T_m indicate that the tank has failed, and deviations of F_S from F_m indicate that the valve has failed.....	80
5.1	FDLM system and model outputs for a single measurement point. The system output is noisy. The left submodel output is smooth, whereas the right submodel output is noisy....	84
5.2	Raw variables display. The standard deviation of the noise is 0.15 in the output units. In 5.2a the failure located in the right subsystem and in 5.2b in the left subsystem.....	85

<u>FIGURE NUMBER</u>	<u>FIGURE TITLE</u>	<u>PAGE</u>
5.3	Raw variables display. The standard deviation of the noise is 0.55 in the output units. In 5.3a the failure located in the right subsystem and in 5.3b in the left subsystem....	86
5.4	Averaged raw variables display. The standard deviation of the noise is 0.55 in the output units in 5.4a the failure is in the right subsystem and in 5.4b in the left subsystem....	88
5.5	Raw system and averaged model outputs display..	90
5.6	Percentage error and raw variables display. The standard deviation of the noise is 0.15 in the output units. In 5.6a the failure is in the right subsystem and in 5.6b is in the left subsystem.....	92
5.7	Percentage error coupled with the raw variables display. The standard deviation of the noise is 0.55 in the output units. In 5.7a the failure is in the right subsystem and in 5.7b is in the left subsystem.....	93
5.8	Standard score and raw variables display. The standard deviation of the noise is 0.15 in the output units. In 5.8a the failure is in the right subsystem and in 5.8b is in the left subsystem.....	95
5.9	Standard score and raw variables display. The standard deviation of the noise is 0.55 in the output units. In 5.9a the failure is in the right subsystem and 5.9b is in the left subsystem.....	96
5.10	Standard score and raw variables display. The standard deviation of the noise is 1.0 in the output units. In 5.10a the failure is in the right subsystem and in 5.10b is in the left subsystem.....	97
5.11	The odds ratio, Ω versus the probability of a system failure, $p[\text{failure}]$	99
5.12	Raw system averaged model outputs display and the odd calculated by a Bayesian statistical model. The system is under normal conditions...	101

<u>FIGURE NUMBER</u>	<u>FIGURE TITLE</u>	<u>PAGE</u>
5.13	Raw system averaged model outputs display and the odds calculated by a Bayesian statistical model. There is a failure in the right subsystem.....	102
5.14	Raw system averaged model outputs display and the odds calculated by a Bayesian statistical model. There is a failure in the left subsystem:.....	103
5.15	Raw system averaged model outputs display and the odds calculated by a Bayesian statistical mdoel. There is a multiple failure in the left and the right subsystems.....	104
5.16	The classical hypothesis testing centers the probability density function on zero. The crossed area is the probability that \bar{x}_d exceeds the absolute obtained value, $ \bar{x}_d $	107
5.17	The Bayesian model centers the probability density function on x_d . The crossed area is the probability that the system has failed.....	109
5.18	The Bayesian model centers the probability density function on x_d . The crossed area is the probability that the system has failed. $p(\text{failure})$ is increased when \bar{x}_d increases.....	109
5.19	The Bayesian model is able to accumulate information. The probability calculation is changed by accumulating the information of two samples of size n	110
5.20	Proposed FDLM computer/human operator interface. A schematical description as well as the system and model outputs are displayed to the operator.....	113
6.1	Raw system and model outputs in 6.1a, raw system and averaged model outputs in 6.1b, and averaged system and model outputs in 6.1c. The submodels generating these outputs include state variables.....	117
6.2	Raw system and model outputs in 6.2a, raw system and averaged model outputs in 6.2b, and averaged system and model outputs in 6.2c. The submodels generating these outputs do not include state variables.....	118

<u>FIGURE NUMBER</u>	<u>FIGURE TITLE</u>	<u>PAGE</u>
6.3	Digital information display. No digital information in 6.3a the odds ratio, Ω in 6.3b, the time Ω exceeds 1, t_Ω , in the 6.3c, and Ω plus t_Ω in 6.3d.....	119
6.4	The operators' reaction times versus the different digital information displays.....	125
6.5	The operators' reaction times versus the different analog outputs for state and no-state variables cases.....	127
7.1	The ship's engine simulation consists of a turbine, three phase ac generator, switch, motor and propeller.....	130
7.2	Causal description of the ship's engine simulation. There are 4 measurement points (Points 1-4). The pressure and temperature of the gas at the turbine's inlet are input variables.....	131
7.3	Schematical description of the ship's engine. The four measurement points and the calculated probability ratios are displayed. When Ω exceeds 1, the time during which it has happened is displayed as well.....	132
7.4	The system and model outputs of FDLM utilizing measurement point 1. The non-linear system is traced by a linear model.....	135
7.5	FDLM test applied utilizing measurement points 1 plus 2 (in 7.5a) and 1 plus 3(in 7.5b).....	136
7.6	FDLM system and model outputs. The power of measurement point 2 in 7.6b, and the alternating voltage in 7.6c.....	137
7.7a	FDLM sequential test application utilizing measurement point 1. The failure is to the right of point 1.....	139
7.7b	FDLM sequential test application utilizing measurement point 1 plus 2. The failure is to the right of point 2.....	140
7.7c	FDLM sequential test application utilizing measurement points 1 plus 3. The failure is to the left of point 3. Hence, the failure is between point 2 to 3.....	141

<u>FIGURE NUMBER</u>	<u>FIGURE TITLE</u>	<u>PAGE</u>
7.8	FDLM simultaneous test application the failure is between point 2 to 3.....	142
7.9a	FDLM sequential test application utilizing measurement point 1. The failure is to the right of point 1.....	143
7.9b	FDLM sequential test application utilizing measurement points 1 plus 2. There is a multiple failure between points 1 and 2 and to the left of point 2.....	144
7.9c	FDLM sequential test application utilizing measurement points 1 plus 3. There is a multiple failure between points 1 and 3 and on the right of point 3.....	145
7.9d	FDLM sequential test application utilizing measurement points 1 plus 4. The failure is between points 1 and 4.....	146
7.10	FDLM simultaneous test application. There is a multiple failure between points 1 and 2 and points 3 and 4.....	147
B.1	Bond graph description of the ship's engine simulation.....	161
C.1	FDLM test applied utilizing measurement point 1 results in transforming the non-linear model to a linear one.....	165

LIST OF TABLES

<u>TABLE NUMBER</u>	<u>TABLE TITLE</u>	<u>PAGE</u>
2.1	Effort and flow variables of various systems...	22
3.1	The transfer functions of the outputs of the submodel shown in Figure 3.7.....	57
3.2	The results of sensitivity analysis applied to the system shown in Figure 2.12.....	59
5.1	Z values for different noise levels of system measured outputs.....	94
6.1	The combinations of analog and digital displayed information each having 20 experimental trials.....	115
6.2	Percentages of False Alarms (FA) and Misses (MS) for the No-State-Variable Case.....	123
6.3	Percentages of False Alarms (FS) and Misses (MS) for the State-Variable Case.....	123
6.4	Subjects' Average Reaction Times for the State-Variable Case. Time in Seconds.....	124
6.5	Subjects' Average Reaction Time for the No-State Variables Case. Time in Seconds.....	124
6.6	The Interaction Between the Different Analog Outputs and the State Variable/No-State Variable Cases.....	126

CHAPTER 1

INTRODUCTION

The purpose of this thesis is to develop a computerized method which aids the operators of complex dynamic systems to detect failures and to locate the causes in real-time. This method is designed to eliminate the necessity to preprogram the possible system failure-modes. The displays interfacing the method with the human operators include probabilities of system failures calculated by a statistical model.

The increasing complexity and size of systems like chemical plants, power stations (fossil or nuclear), ships, and airplanes impose on the human operators high cognitive work load. This load is increased further when the system malfunctions because then the operators are required to take corrective actions rapidly and promptly. Under such imposed stress the operators' reliability is decreased [1], and as a result severe accidents may occur [2]. This has been recognized by many researchers, who suggested that somehow operators be aided by computers.

Many of the existing failure detection methods rely on preprogramming the possible system failure-modes, all of which cannot practically be considered. Therefore, a method which avoids this requirement is advantageous.

Displaying the probabilities of failures has been found to be very helpful to the operators [3]. Therefore displays which include these updated probabilities are advantageous.

During the last three decades many computerized on-line methods have been developed for failure detection and location. One of these methods is based on a fault/event tree analysis. Here the potential significant failure modes, their logical interrelations and their consequences are preprogrammed and stored in a computer. The computer checks the system status and compares it with the stored failure modes. When one of these modes is activated an alarm is triggered and the operator is informed.

In 1968 Patterson [4] and Welbourne [5] designed a computerized alarm and display system for a nuclear power plant. But this was not used because its cost was prohibitive.

In 1980, with the advent of cheaper computers, Frogner and Meijer [6] and Bastle and Felkel [7] developed a failure detection and location system which they call Disturbance Analysis System (DAS). Recently, it has been recognized that DAS should be designed to allow real-time modification and extension of information, which will enable the operators to test unconsidered failure modes. This concept is currently motivating the development of DAS in a second generation: Disturbance Analysis and Surveillance System (DASS).

Another method which implements the fault/event tree analysis was suggested by Gimmy and Nomme [8]. They constructed the preprogrammed failure modes into special tabulated forms. These tables can easily be modified to include unconsidered failure modes in the fault/event tree.

A system that poses a high degree of redundancy can be diagnosed using Voting Techniques. In the standard voting scheme the outputs of

three or more identical instruments are compared and simple logic is utilized to detect and eliminate faulty instruments. Deckert et al. [9], Gilmore and McKern [10], Pejsa [11], and Broen [12] have developed voting schemes, and Louie [13] discusses the method's different applications. Ray et al. [14] proposed a voting scheme which includes analytic redundancy to test the consistency of the different system outputs.

Nicholson and Lanning [15], and Lind [16] have independently proposed to use the model of the system normal operation mode to diagnose system failures. Here failures are detected when the measured system outputs diverge from their corresponding model values. This method is advantageous because a single model is compared with the physical system. Its disadvantage is that it does not locate the causes of the failures because a system-model disparity does not uniquely locate the causes.

To obtain the location capability, it has been proposed by Sheridan [1] and Hassan [17] to break the aggregated model into submodels, each of which is forced by the appropriate system measured variables. The outputs of these submodels are compared with their corresponding system outputs. A deviation of the outputs of any submodel indicates that its corresponding subsystem has failed. The disadvantage of this method is that it does not specify the compared system-model outputs. In practice, only a partial set of the many system-model outputs is compared. This chosen set of outputs does not necessarily detect all possible system failures.

A method that disaggregates the model of the system's normal operation mode and specifies the compared system and model outputs is

required. This method has to be able (1) to detect system failures by comparing several system and model outputs, and (2) to locate these failures quickly and reliably.

The objective of the Failure Detection and Location Method (FDLM) presented in this thesis is to meet these requirements.

The thesis is organized as follows. Chapter 2 defines a system failure and describes the new Failure Detection and Location Method (FDLM). The advantages and limitations of FDLM are discussed in Chapter 3. Chapter 4 describes more complex applications of the method. Human factors, considerations and experimental determination of human operator/FDLM interface are discussed in Chapters 5 and 6, respectively. An example of the method's application is described in Chapter 7. The conclusions and the proposed future work are summarized in Chapter 8.

CHAPTER 2

DESCRIPTION OF THE FAILURE DETECTION AND LOCATION METHOD (FDLM)

2.1 Definition of System's Failure

The definition of failure applies to systems that operate by transferring power between adjacent subsystems in order to produce a desired rate of work. A fossil power plant is an example in which coal or oil is burnt to generate steam. The steam is expanded through turbine stages which rotate generators to provide the desired electric power. The value of the transferred power between two adjacent subsystems is denoted by P , and its reference value under normal conditions of operation by P^n . The system is said to have failed if the absolute value of the difference between P and P^n lies outside preset limits, δ^n . To locate the failure causes the system's causality should be considered.

2.2 A System's Causal Description

In 1960 Paynter [18] introduced the concept that power in physical systems flows in communication channels named "energy bonds". According to the number of independent variables, which determine the transferred power in these bonds, one can categorize the energy bonds into three classes:

1. Bilateral energy bonds.

These bonds are characterized by two variables: effort, e , and flow, f . The product of these variables is the transferred power, P .

$$P = e \cdot f \quad (2.1)$$

The effort and the flow variables of various systems are summarized in Table 2.1. In electrical systems, for example, voltage and current are the effort and flow variables, respectively.

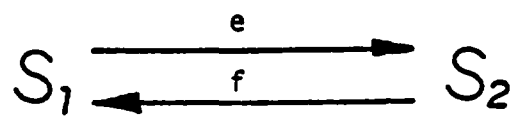
TABLE 2.1: EFFORT AND FLOW VARIABLES OF VARIOUS SYSTEMS

SYSTEM	EFFORT (e)	FLOW(f)
Mechanical	Force	Velocity
	Torque	Angular Velocity
Hydraulic	Pressure	Volumetric Flow
Electrical	Voltage	Current

In thermal systems the effort is the temperature and the flow is the entropy rate which can be evaluated by indirect temperature measurements.

The concept of energy bonds leads to causal descriptions of physical systems. The causal description of a system consisted of bilateral energy bonds is constructed as follows. Consider two interacting subsystems, S_1 and S_2 , shown in Figure 2.1, in which the effort is supplied by subsystem S_1 . This effort causes the flow to achieve a value which depends on the impedance of subsystem S_2 . Hence, a means of communicating the impedance of S_2 back to S_1 must be provided. In this example, the effort is determined by subsystem S_1 and communicated to S_2 , where the flow is determined by subsystem S_2 and communicated to S_1 . This bilateral causal description is shown in Figure 2.1.

An example of an hydraulic system which can be described using the bilateral energy bonds is the two-tank system shown in Figure 2.2. The causal description of this system is shown in Figure 2.3.



equivalent to:



Figure 2.1 Causal description of system $(S_1 S_2)$ with bilateral energy bonds. from reference 18.

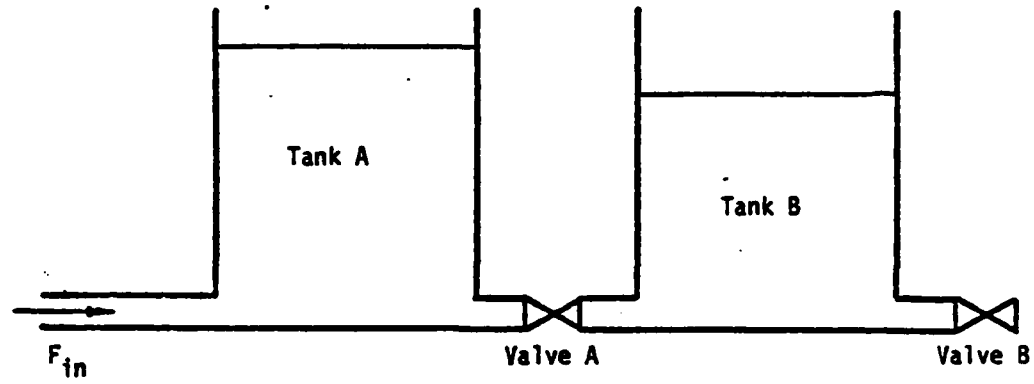


Figure 2.2 A two-tank hydraulic system.

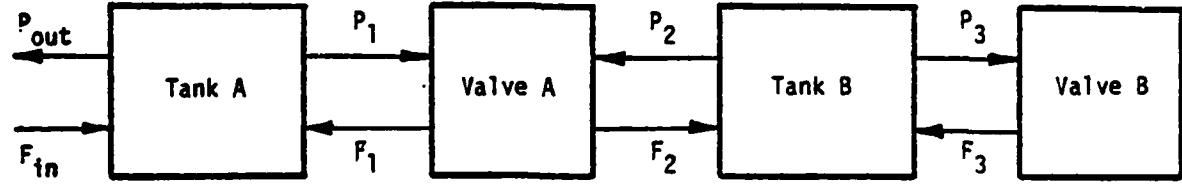


Figure 2.3 Causal description of the two-tank hydraulic system shown in Figure 2.2.

2. Unilateral bonds

These bonds are characterized by a single independent variable, either effort or flow, as shown in Figure 2.4. The covariate of the unilateral bond's independent variable is, in most cases, constant in its value. The modified two-tank hydraulic system shown in Figure 2.5 can be described using bi-lateral and uni-lateral energy bonds. The causal description of this system is shown in Figure 2.6. This description indicates that the energy bond connecting valve A and tank B is uni-lateral. The independent variable of this bond is the flow F_2 , and its covariate is set to be a constant atmospheric pressure.

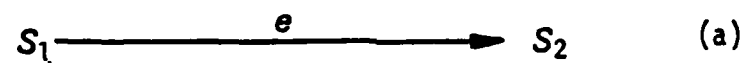
3. Multilateral bonds

When the number of independent power variables exceeds two, the energy bonds are categorized as multilateral bonds. These bonds are used to simulate thermofluid systems in which the power of single phase matter is a function of three variables. Paynter [19] has shown that pressure, flow and temperature form an advantageous set of variables. These power variables are shown in Figure 2.7. Paynter has decomposed the thermofluidic power into two terms: fluidic power, which is dominated by the pressure and the flow variables, and thermal power, dominated by the flow and the temperature.

The causal descriptions of systems with multilateral bonds are discussed in Section 4.4.

2.3 A Failure Detection Method

The detection of a system failure can proceed as follows. A computerized mathematical model of the system is established. The sys-



or:

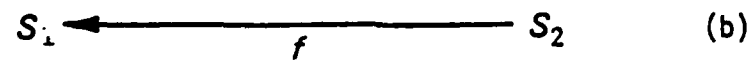


Figure 2.4 Causal description of a system ($S_1 S_2$) with unilateral energy bond. In 2.4a the independent power variable is e and in 2.4b it is f .

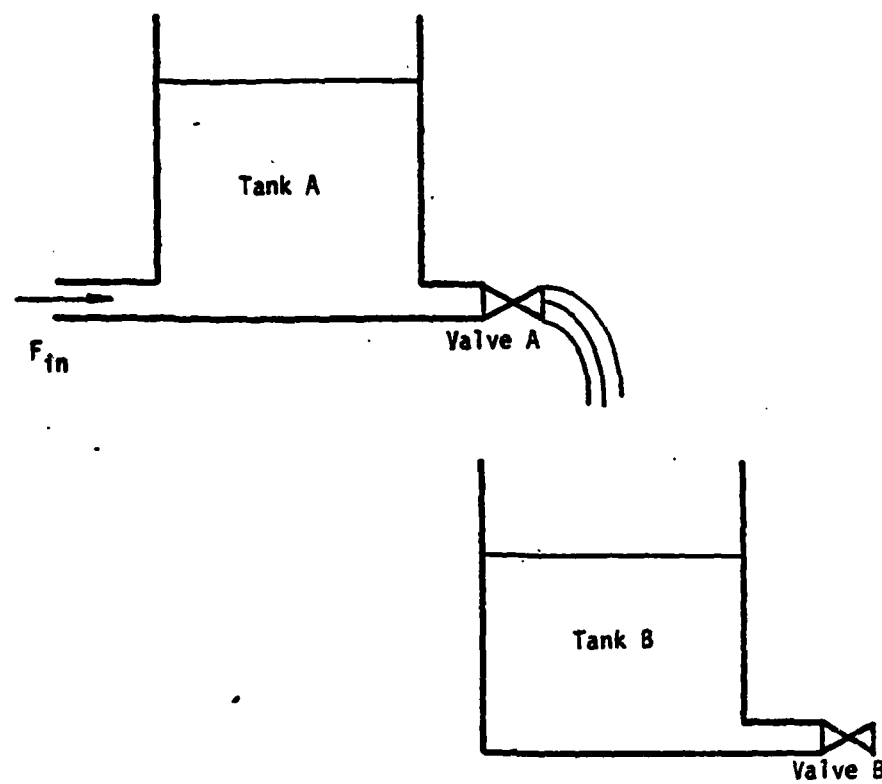


Figure 2.5 A modified two-tank hydraulic system.

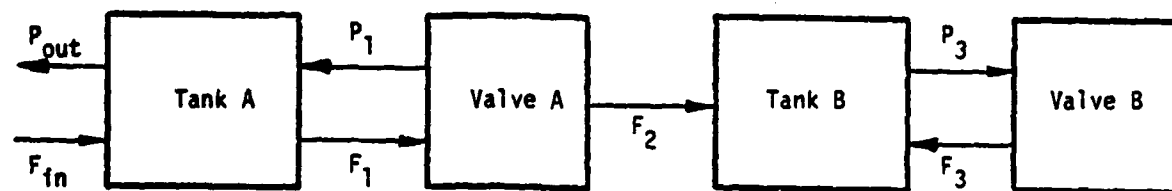


Figure 2.6 Causal description of the modified two-tank hydraulic system shown in Figure 2.5.

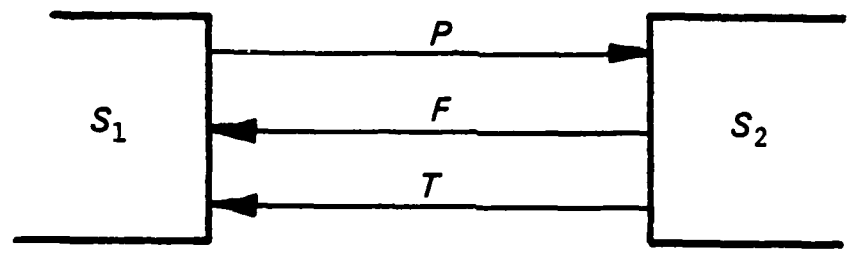


Figure 2.7 Causal description of a system (S_1, S_2) with multilateral energy bond.

tem and the model are excited by the same input. The power transferred between two adjacent subsystems, i , and j P_{ij} is measured and compared with its corresponding model value P_{ij}^n . If the absolute value of the difference between P_{ij} and P_{ij}^n exceeds prespecified limits, δ^n , then a failure is detected. This system-model setup depicted in Figure 2.8, detects failures but does not locate the causes. Clearly, a malfunction in either of the subsystems could result in the observed power deviation. Furthermore, in the case of a multiple system failure, P_{ij} might not deviate from its normal value, P_{ij}^n , although the system has failed.

2.4 Failure Detection and Location Method (FDLM)

The method developed in this thesis is called Failure Detection and Location Method (FDLM). This method is designed to overcome the described difficulties and its applications to bi-, uni-, and multilateral energy bonds are as follows.

2.4.1 Bilateral Energy Bonds

The independent variables, e_s and f_s , of the power transferred from subsystem 1 to subsystem 2, P_{12} , are measured. A model of each of the two subsystems (submodel 1 and submodel 2) is constructed, as shown in Figure 2.9. According to the causalities of these submodels, the measured system effort and flow variables are used as the model inputs.

In Figure 2.9 it is assumed that the causalities of the submodels are such that e_s and f_s are the input variables of submodels 1 and 2, respectively. The complementary variables, f_m and e_m , calculated by the model are the model output variables. Hence, the input to each

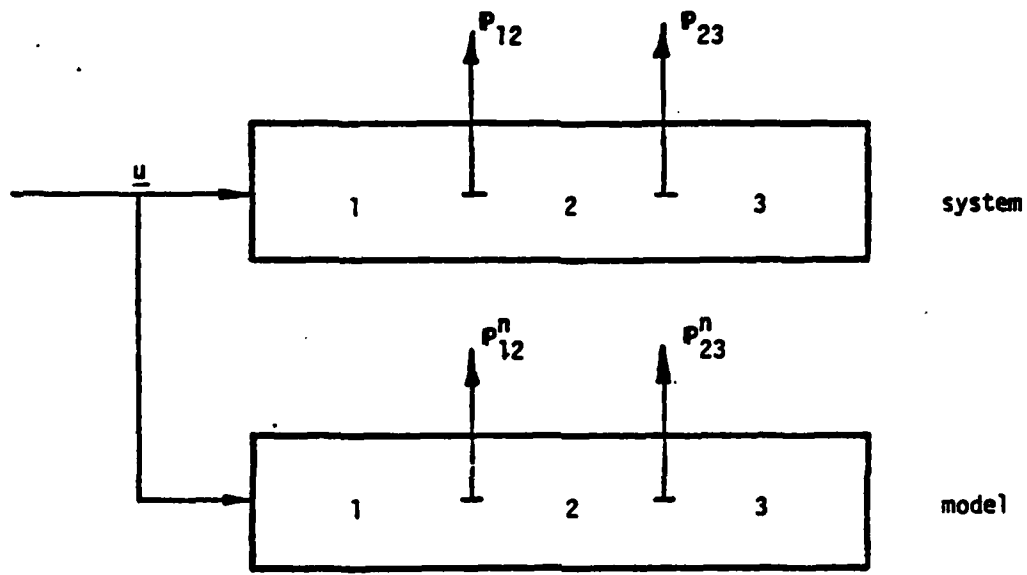


Figure 2.8 Comparing the system transferred power values, P_{12} and P_{23} , with their model values, P_{12}^n and P_{23}^n . \underline{u} is a vector of the system's input variables.

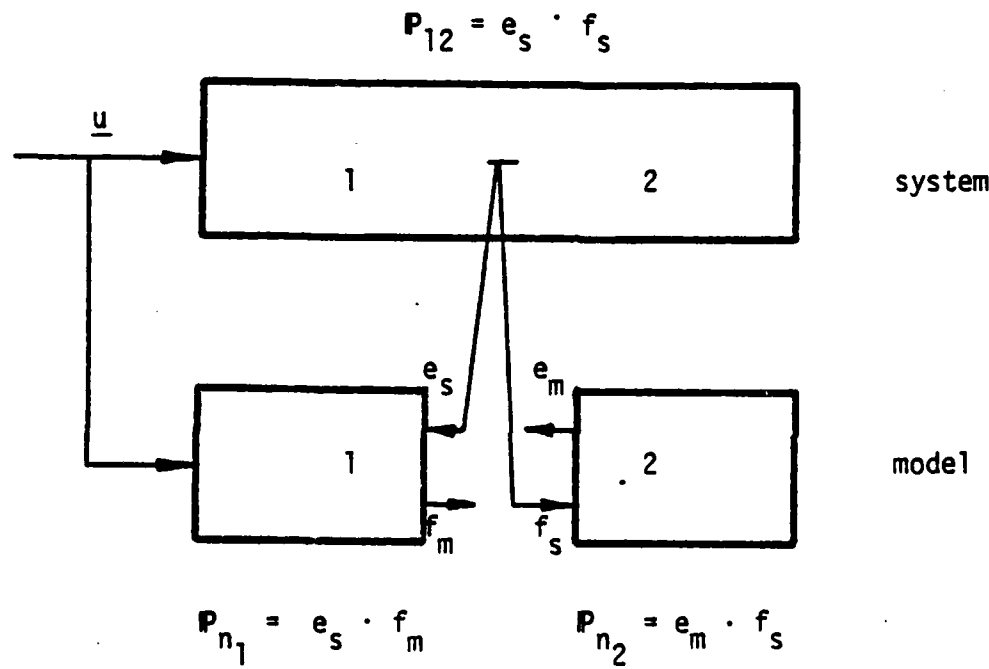


Figure 2.9 FDLM system-model setup where the system power, P_{12} , is compared with its model values, P_{n1} and P_{n2} .

submodel is a measured system variable, the covariable of which is calculated by the submodel. The product of the input and the output of each submodel is the submodel calculated power. In Figure 2.9 the power values of submodel 1 and 2 are

$$P_{n1} = e_s f_m \quad (2.2)$$

$$P_{n2} = e_m f_s \quad (2.3)$$

By comparing these values with the system power P_{12} , system failures can be detected and the location of their causes can be identified. If the model is reliable and P_{n1} differs from P_{12} , the cause of the failure is located in subsystem 1, and if P_{n2} differs from P_{12} the cause is located in subsystem 2. A multiple system failure causes both P_{n1} and P_{n2} to differ from P_{12} . Thus, FDLM is capable of both detecting multiple system failures and locating their causes.

A comparison of the system and model power values is equivalent to the comparison of the corresponding effort or flow variables. The comparison of f_m and f_s (Figure 2.9) is equivalent to the comparison of P_{n1} and P_{12} , and comparison of e_m and e_s is equivalent to comparison of P_{n2} and P_{12} . In most applications the effort and flow comparison is advantageous. However, in applications where the efforts and flows change their values rapidly, the power comparison is advantageous. This is true since the power in these cases is relatively constant. Electrical alternating current (ac) machines belong to this class of systems.

2.4.2 Unilateral Energy Bonds

The system power variable, e_s or f_s , is measured and a model of each of the subsystems (submodel 1 and submodel 2) is constructed, as shown in Figure 2.10. According to the causalities of these submodels, the measured system variable is used as an input to one of the submodels.

In Figure 2.10 it is assumed that the causalities of the submodels are such that f_s is the input of submodel 2. f_m is the model output which is compared with the measured f_s variable. If the model is reliable and f_s differs from f_m the cause of the failure is located in subsystem 1. Thus, in the unilateral energy bond, the failure causes are located in the subsystem which is on the tail side of the causality arrow.

2.4.3 Multilateral Energy Bonds

The scope of this thesis is limited to applications of FDLM to multilateral energy bonds in which there are three independent power variables. Here the three system variables pressure, mass flow, and temperature (P_s , F_s , and T_s , respectively) are measured at a point in the system. A model of each of the two subsystems (Submodel 1 and Submodel 2) is constructed, as shown in Figure 2.11. According to the causalities of the submodels P_s , F_s , and T_s are used as the model inputs.

In Figure 2.11 the causalities are assumed to be such that F_s , and T_s are used as input to submodel 1 and P_s is used as input to submodel 2. The complementary variables P_m , F_m , and T_m are the model output variables. By comparing P_s , F_s , and T_s with the corresponding model

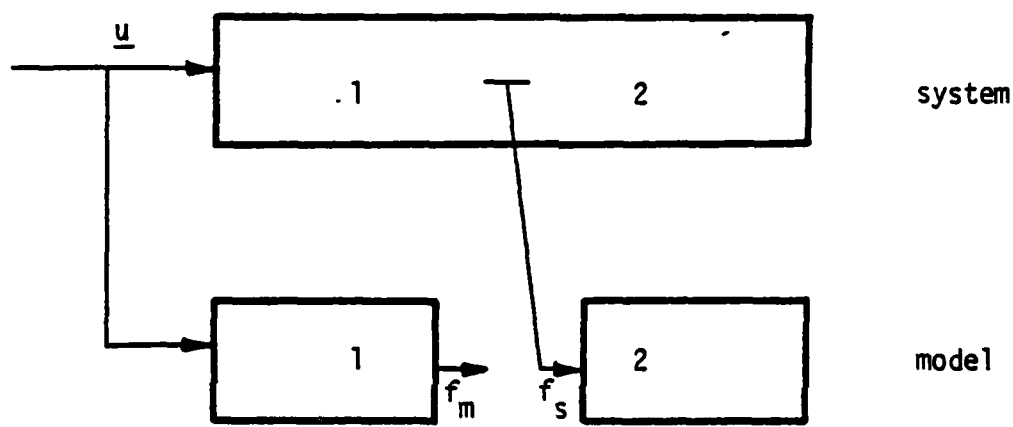


Figure 2.10 FDLM application to a system with unilateral energy bond.
If f_m differs from f_s the failure is in subsystem 1.

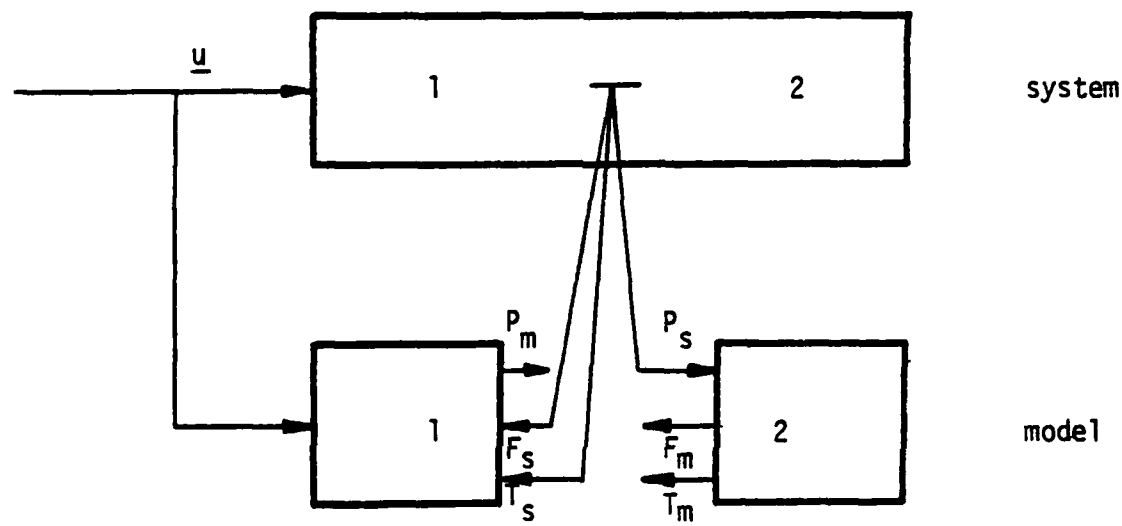


Figure 2.11 FDLM Application to a system with multilateral energy bonds (3 independent power variables). If P_m differs from P_s the failure is in subsystem 1 and if F_m or T_m differs from F_s or T_s , respectively, the failure is in subsystem 2.

variables P_m , F_m , and T_m failures can be detected and the causes can be located. If the model is reliable and P_s differs from P_m the failure is located in subsystem 1, and if F_s differs from F_m and/or T_s differs from T_m it is located in subsystem 2. Similarly to the bilateral energy bonds, a multiple failure may cause all the three variables to differ from their corresponding model values.

2.4.4 Refining the Failure-Causes Location

In order to refine the location of a failure cause, one has to divide the system into smaller subsystems and to perform a number of comparison tests as described in Sections 2.3.1 - 2.3.3. These tests can be performed in simultaneous or sequential FDLM modes. The FDLM simultaneous mode applied to bilateral energy bonds is shown in Figure 2.12. Here, all the available system measured variables are utilized simultaneously. This results in refining the locations of the failure causes at the expense of increasing the simultaneous scanned system and model output variables. The FDLM sequential mode applied to bilateral energy bonds is shown in Figure 2.13. In this mode, the FDLM tests are performed sequentially. In each test the system and model outputs of a single measurement point are utilized. Here, the locations of the failure causes are refined at the expense of a longer search procedure. The trade-off between simultaneous and sequential FDLM modes is discussed further in Chapter 3.

2.4.5 Updating the Model Using FDLM

In the described Failure Detection and Location Method it is assumed that the model is reliable and a discrepancy between the system

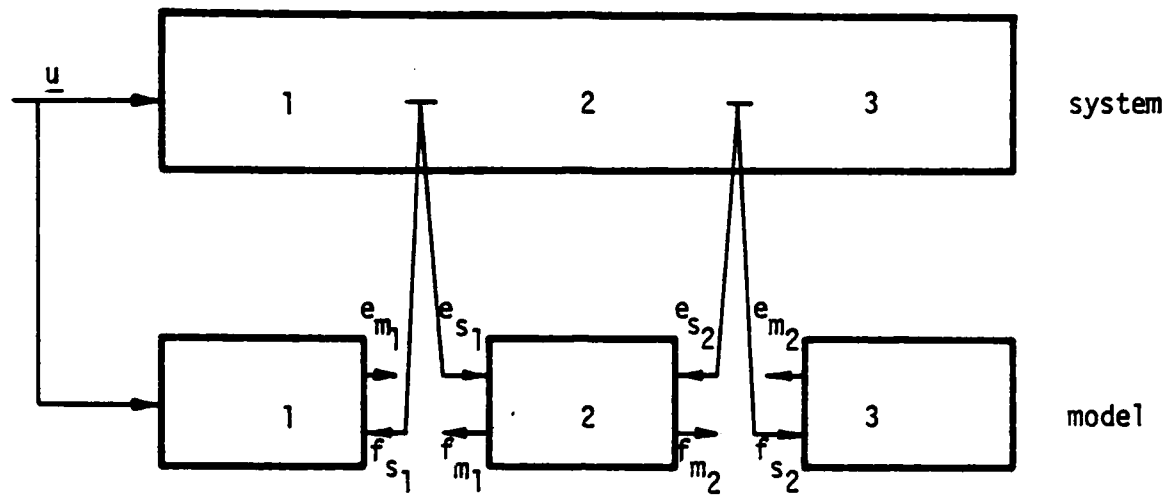


Figure 2.12 FDLM simultaneous mode. All the available system measured variables are utilized simultaneously and the model is disaggregated into small submodels.

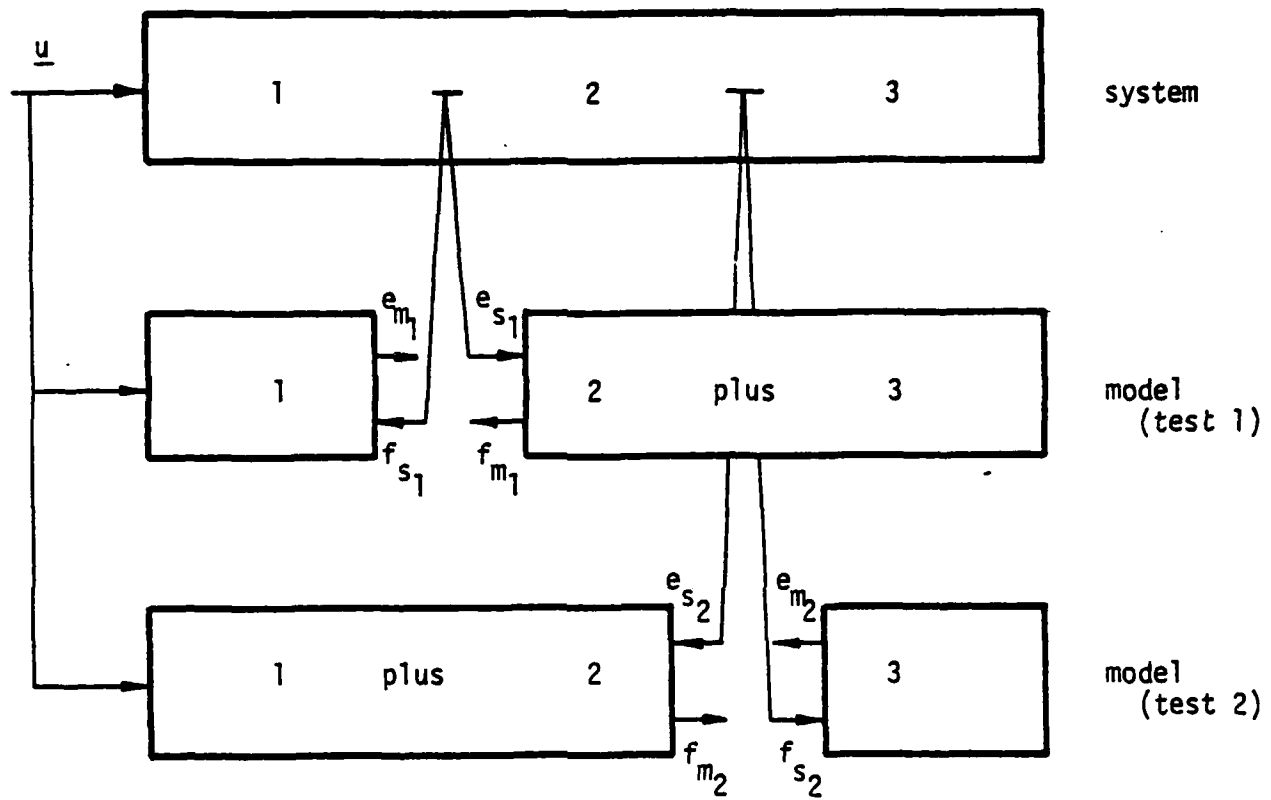


Figure 2.13 FDLM sequential mode. The system measured outputs of each point are utilized sequentially (test 1, test 2 ...) to pinpoint the system failure.

and the model outputs is used to indicate a system failure. However, if the system has been readjusted, or new components have been installed, one can use the FDLM in a reverse way to tune or update the model. This is done by modifying the parameters of the submodels in which the causes of the observed system-model disparity are located. Such modifications should be in a direction to reduce this disparity, and the procedure repeated several times until the disparity is insignificant.

Thus this method can be used either to detect system failures, or to update the model components, depending on the circumstances of its application.

2.5 An Example of FDLM Applied to Bilateral Energy Bonds

Consider a simple hydraulic-mechanical-electrical system, shown in Figure 2.14. This system has been simulated on a computer and its model is depicted in Figure 2.15. A system failure in the hydraulic motor has been simulated by changing its coefficient. We assume that measurements can be taken at five different locations in the system, points 1-5 in Figure 2.14. We apply FDLM using three single tests as shown in Figure 2.16. The outputs of the various submodels and the corresponding measured variables are shown in Figure 2.17. The variables of point 1 (Figure 2.17a) indicate that the failure is in the right subsystem. The variables of point 2 (Figure 2.17b) indicate that the failure is still in the right subsystem. The variables of point 3 (Figure 2.17c) indicate that the failure is in the left subsystem. Thus, the failure is between points 2 and 3, namely it is the hydraulic motor.

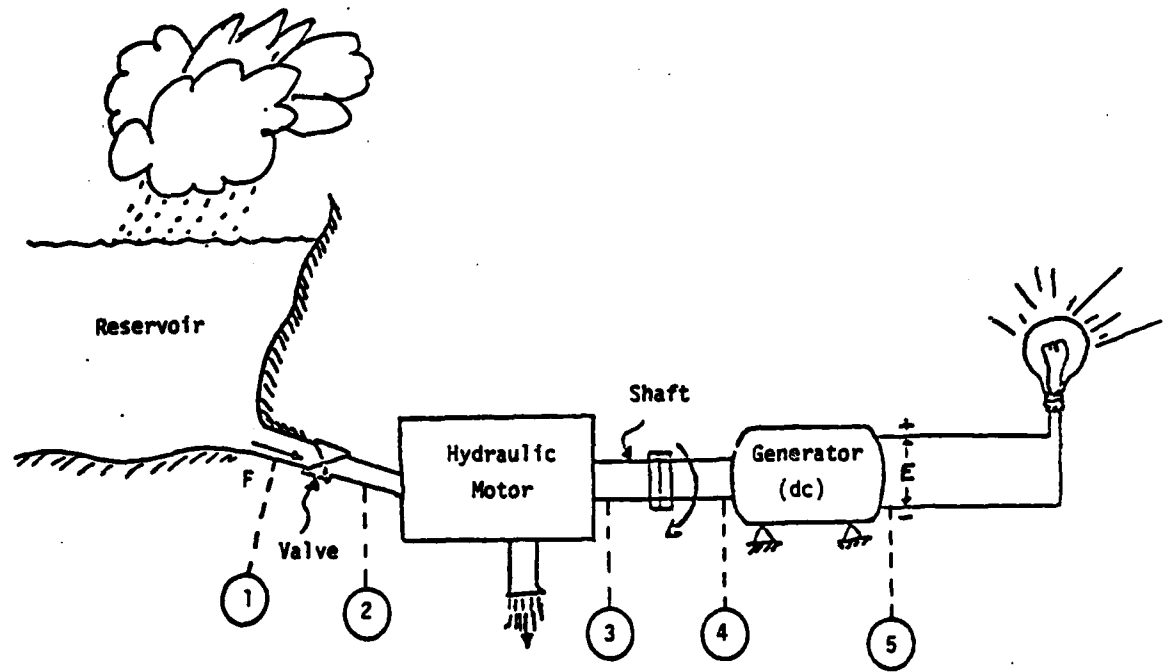


Figure 2.14 A description of an hydraulic-mechanical-electrical system. There are 5 measurement points available (Points 1-5).

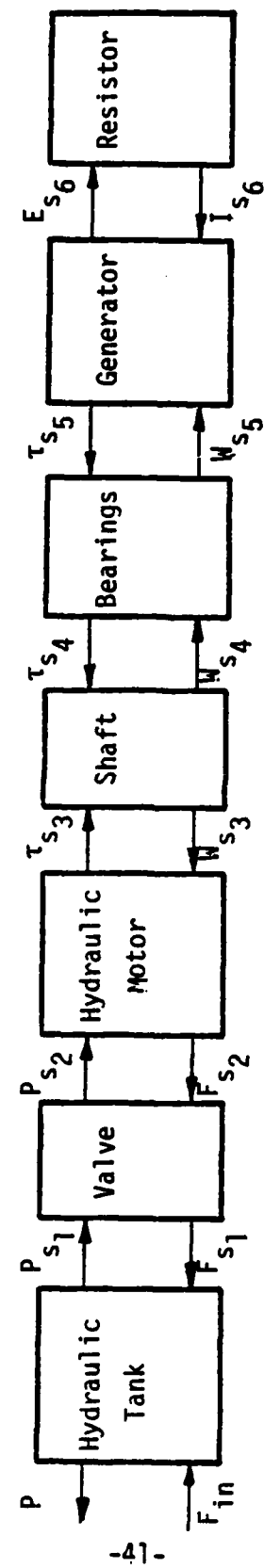


Figure 2.15 Causal description of the hydraulic-mechanical-electrical system shown in Figure 2.14.

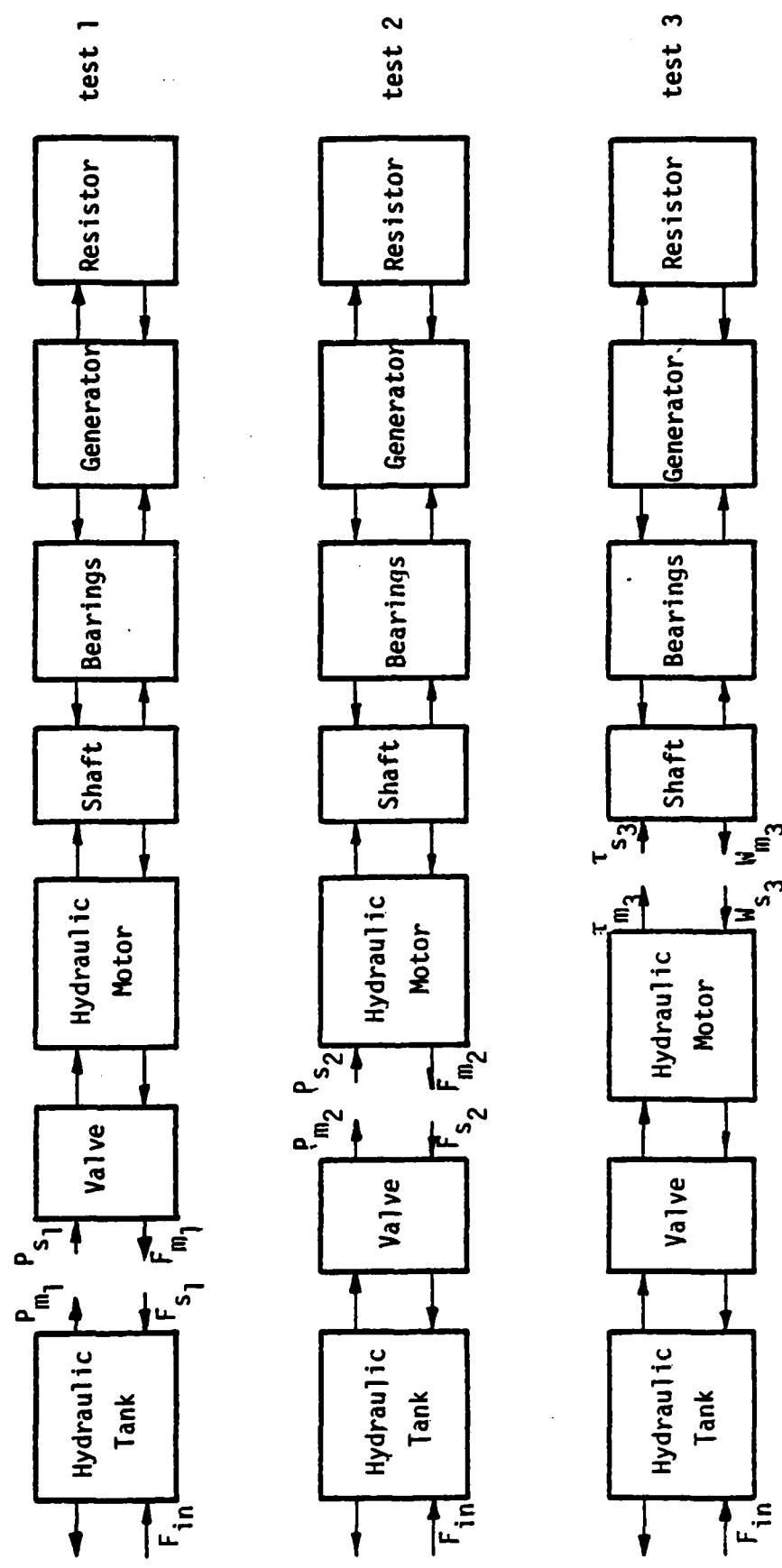


Figure 2.16 A sequence of three FDLM single tests applied to the system shown in Figure 2.14.

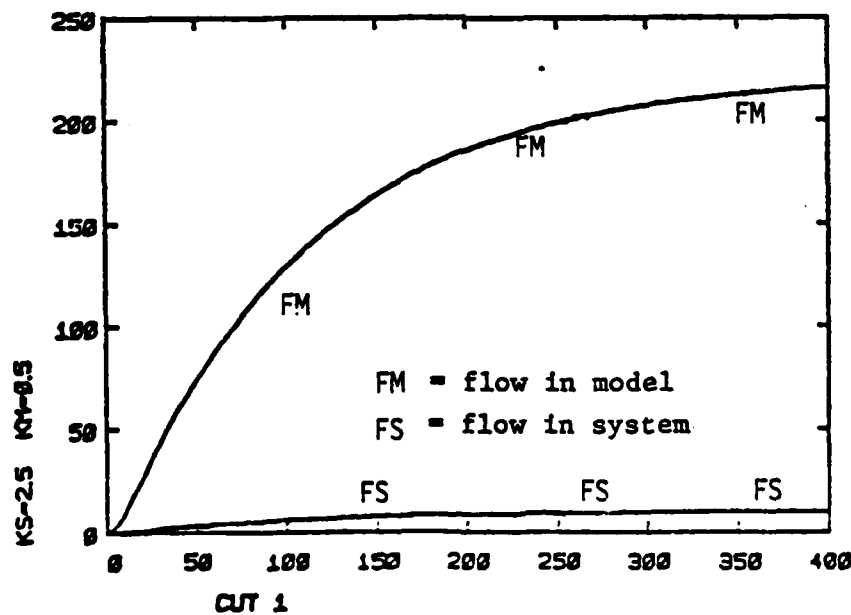
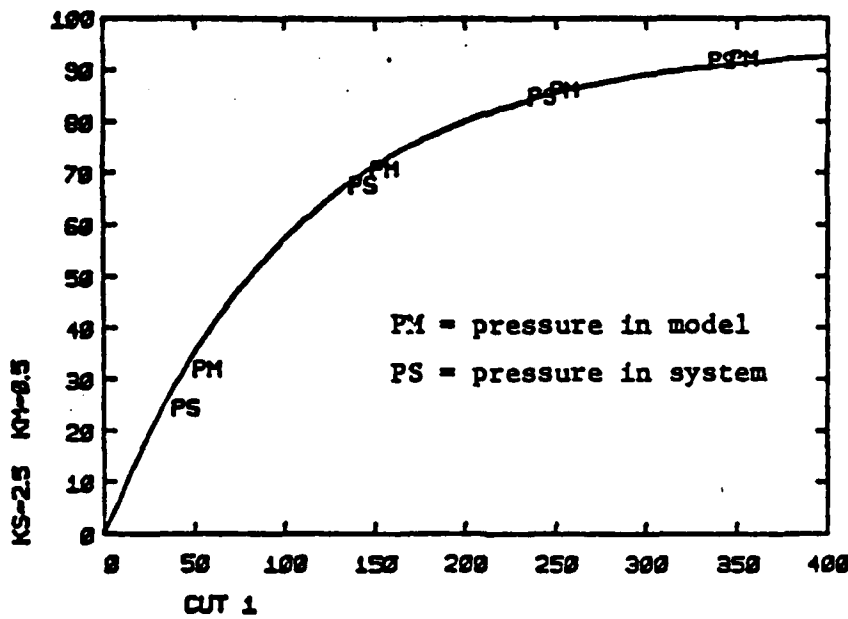


Figure 2.17a FDLM test 1. Pressure and flow measured at point 1 in the system compared with the values predicted by the model. Since FS and FM are different the failure is in the right subsystem.

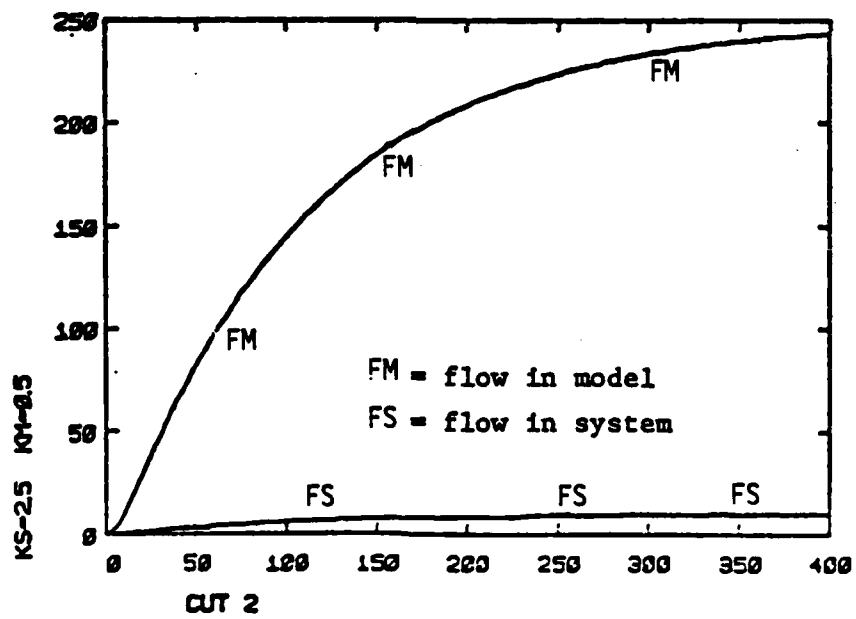
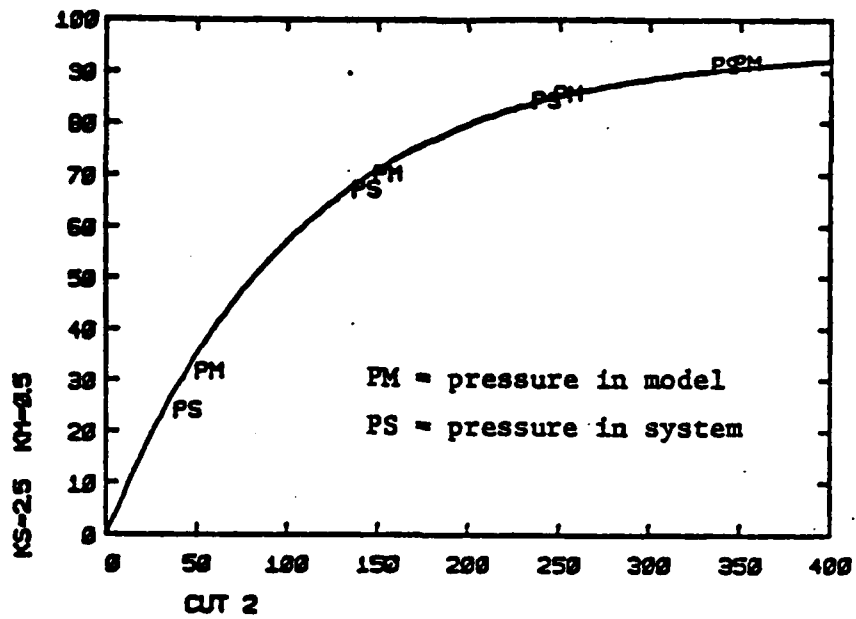


Figure 2.17b FDLM test 2. Pressure and flow measured at point 2 in the system compared with the values predicted by the model. Since FS and FM are different the failure is in the right subsystem.

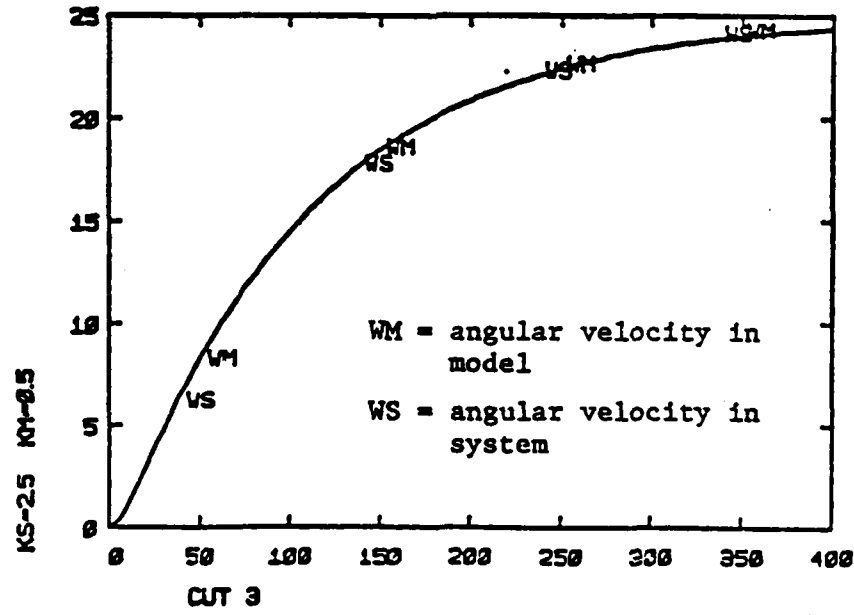
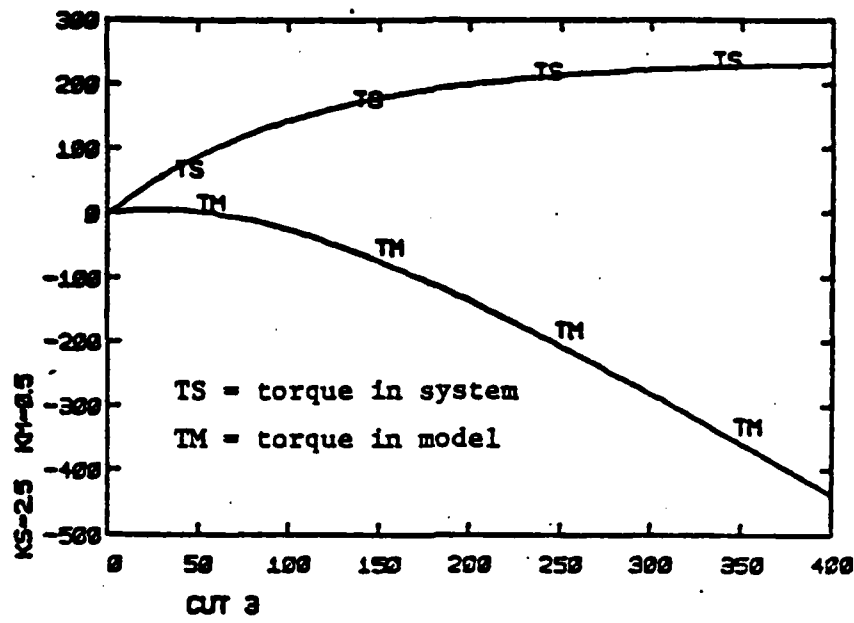


Figure 2.17c FDLM test 3. Torque and angular velocity measured at point 3 in the system compared with the values predicted by the model. Since TS and TM are different the failure is in the left subsystem.

CHAPTER 3

ADVANTAGES AND LIMITATIONS OF FDLM

3.1 System/Model Comparison

An advantage of FDLM is that it utilizes a single model of the system's normal operational mode, and eliminates the necessity to preprogram the system's possible failure modes. FDLM is capable of detecting and locating all system failures which result in significant output deviations. However, in order to apply the method successfully the location task has to be completed before the variables of the failed system wander too far from the normal range such that the model of the system's normal operational mode is no longer valid. This can be achieved by two means: (1) early failure detection (2) efficient failure location.

3.1.1 Early Failure Detection

FDLM is proposed to be applied to systems which are continuously monitored by human operators or computers during the operation. By continuously comparing the outputs of the system, x_s , with their corresponding model variables, x_m , system failures can be detected sooner than would have been possible by observing x_s crossing its preset safety limits. To clarify this statement consider the simulated system and model outputs shown in Figure 3.1. Here, the system failed at time t_0 . This failure causes x_s to deviate from x_m and at time t_1 , the system-model difference ($x_s - x_m$) exceeds the preset allowable threshold, δ^n , indicating a system failure. Here, the failure is detected

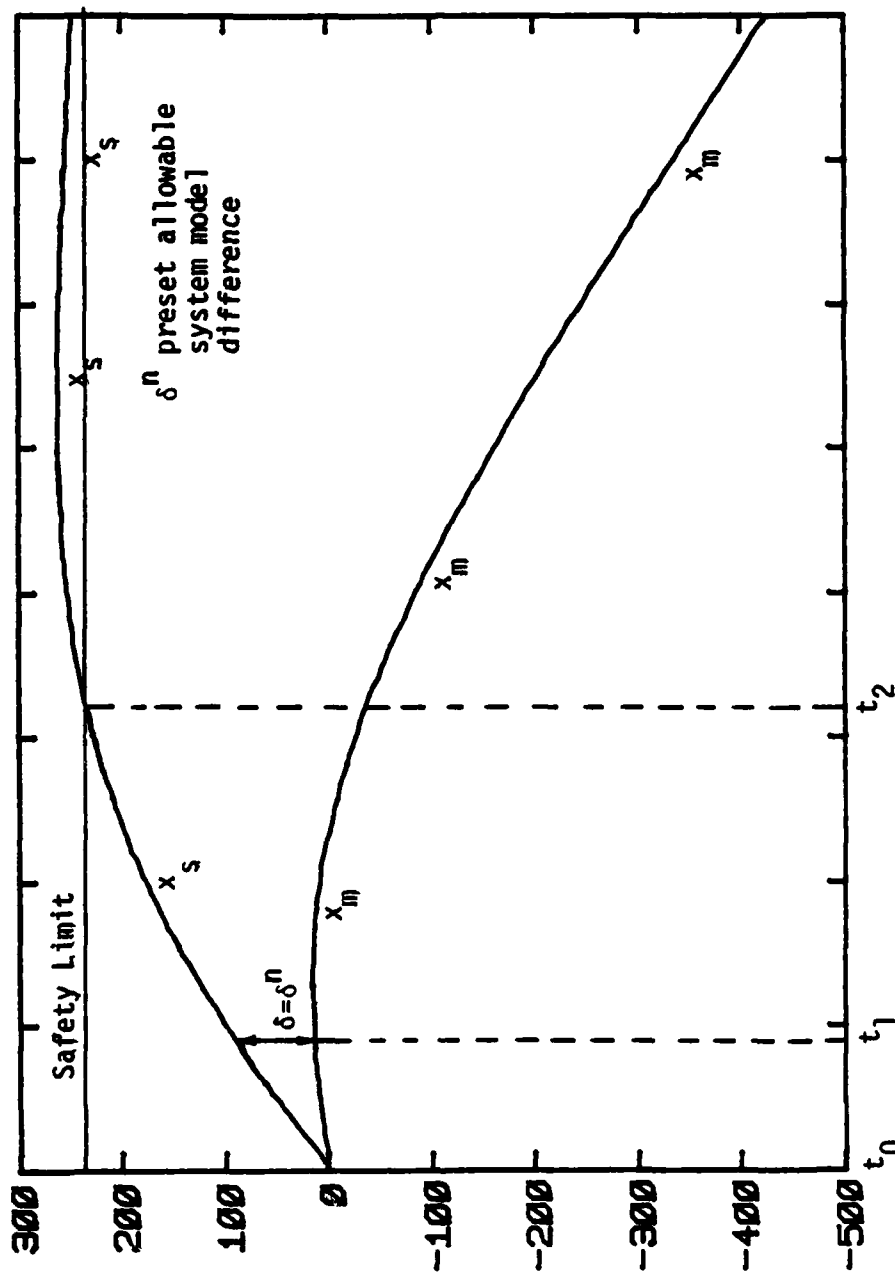


Figure 3.1 The system output x_s crosses its safety limit at time t_2 , whereas the system model deviation ($|x_s - x_m|$) exceeds its allowable threshold, δ , at time t_1 .

while x_s is still in its normal range. x_s crosses its safety limit only at time t_2 . Hence, a system-model comparison can result in early failure detection which has to be followed by an efficient location procedure to obtain a successful FDLM application.

3.1.2 Efficient Failure Location Procedure

The simultaneous mode of FDLM, depicted for the bilateral energy bond case in Figure 2.12, results in locating the system failures while the detection task is performed. In this mode, failures are detected and defective subsystems are located simultaneously. However, this mode requires scanning of many system and model outputs. In large scale systems there may be thousands of outputs which have to be tested. These tests cannot be performed simultaneously unless it is done automatically by computer.

The sequential mode of FDLM requires testing of only a few system and model outputs simultaneously, so that the cognitive load applied to the human operator is minimized. In this mode, it is important to apply an efficient failure location procedure which will identify the defective subsystems soon after a system failure has been detected.

The model state variables turn out to be an important factor in obtaining an efficient location procedure. State variables are associated with storing energy components which introduce time delays and dynamic effects into the model's performance. In order to obtain an efficient location procedure, the relative position of the model's state variables should not change. In the simplest case, this can be obtained by disaggregating the model into at least n submodels, such that each submodel contains a single state variable at the most. This statement is clarified subsequently.

Consider a third order system, as shown in Figure 3.2. Three single sequential FDLM tests (tests 1-3) are applied utilizing the measured outputs of points 1-3. The state variables are marked as S_1-S_3 , and it is assumed that one of the system components has failed. The defective component is marked by an X in Figure 3.2. The outputs of test 1, shown in Figure 3.4, indicate that the failure is located in the right subsystem. These outputs are obtained using the electric network shown in Figure 3.3. To locate the failure one can apply the FDLM tests 2 or 3, shown in Figure 3.2. In test 2, the relative positions of the model state variables are the same as in test 1; S_1 is in the left submodel and S_2 and S_3 are in the right submodel. The outputs of test 2, shown in Figure 3.5, indicate immediately that the failure is still in the right subsystem. However, in test 3 the relative positions of the model state variables are changed; S_1 and S_2 are in the left submodel and S_3 is the right submodel. The outputs of test 3, shown in Figure 3.6, indicate that the failure is still in the right subsystem only after the left system and model outputs coincide.

Thus, transferring of energy-storing components from one submodel to the next introduces transient modes into the model performance and results in a long failure location procedure; whereas by transferring components which do not store energy, immediate results are obtained and the location procedure is efficient.

To avoid the necessity to transfer energy-storing components from one submodel to the next, FDLM should be applied by cutting the aggregated model into at least n submodels, such that each submodel

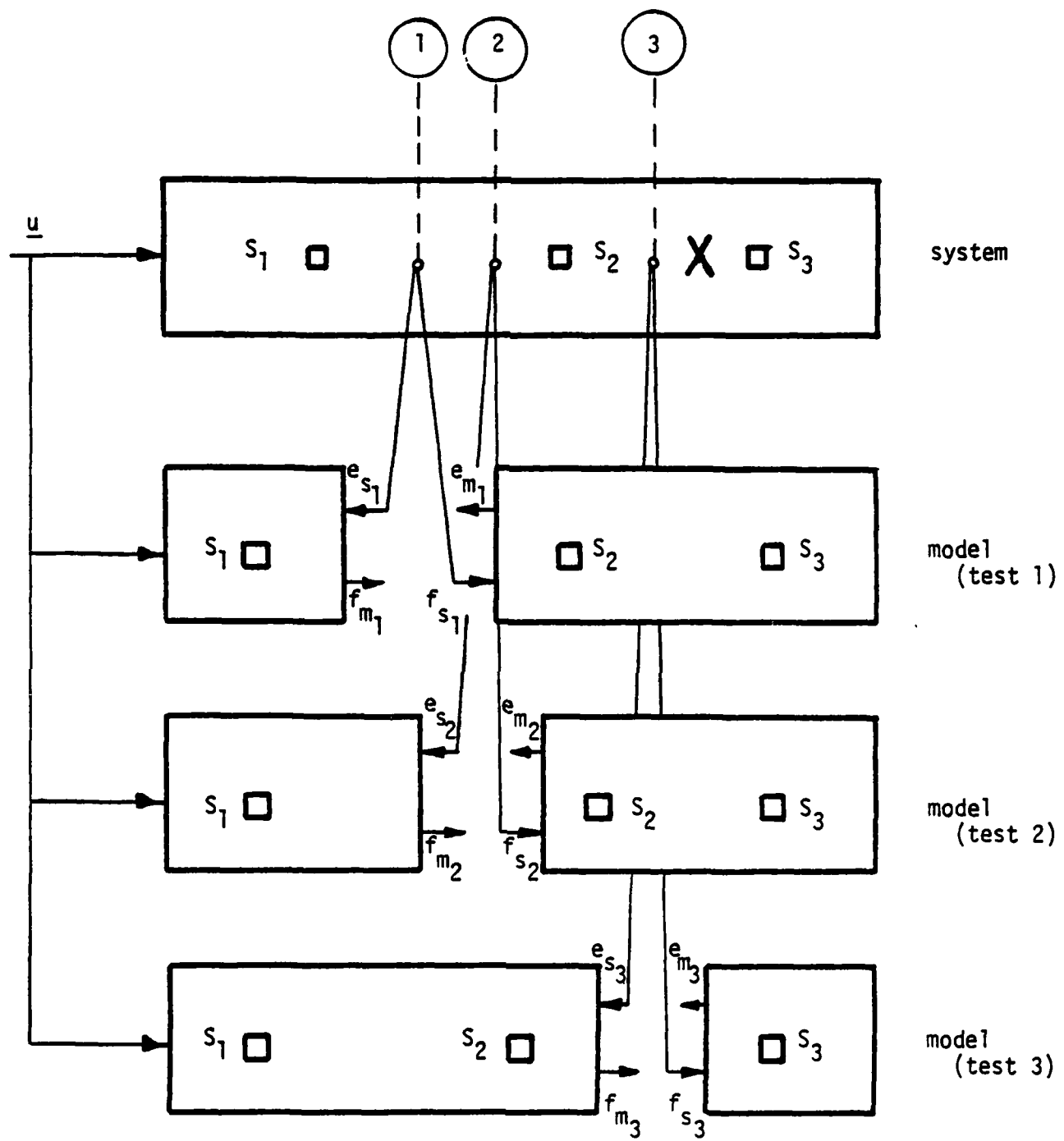


Figure 3.2 A sequence of three single FDLM tests applied to a third order model. s_1 - s_3 are the state variables, and X is a defective system component.

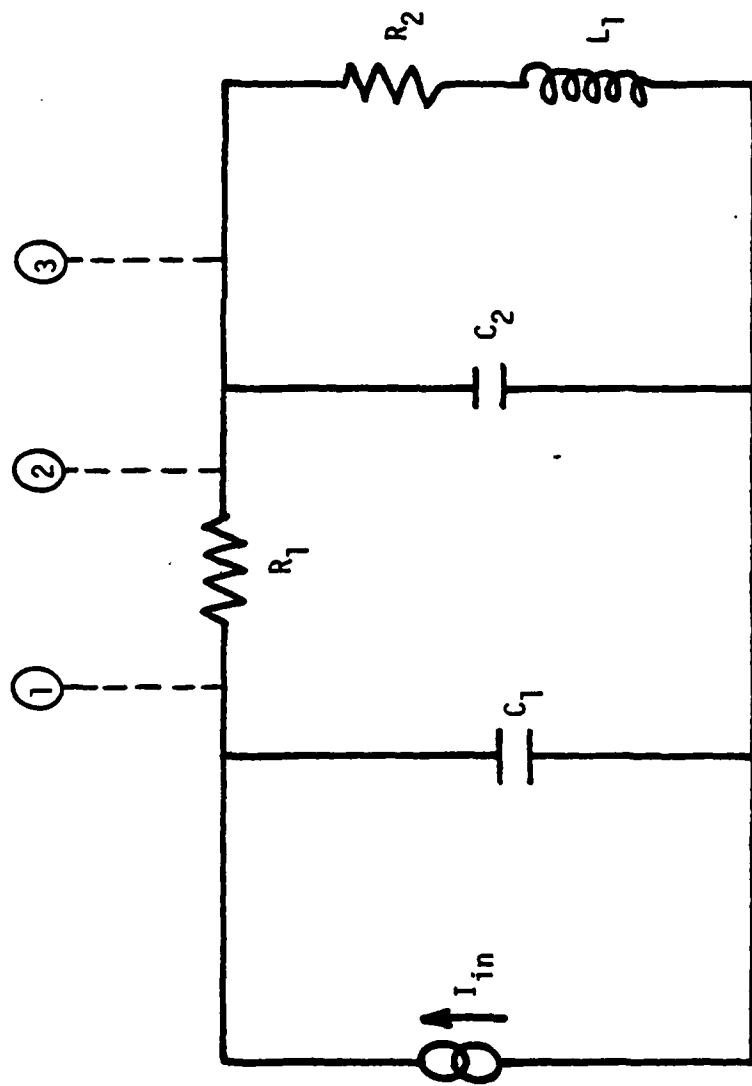


Figure 3.3 A third order electric network utilized to generate the outputs depicted in Figures 3.4-3.6. The three measurement point (points 1-3) correspond to the measurement points shown in Figure 3.2.

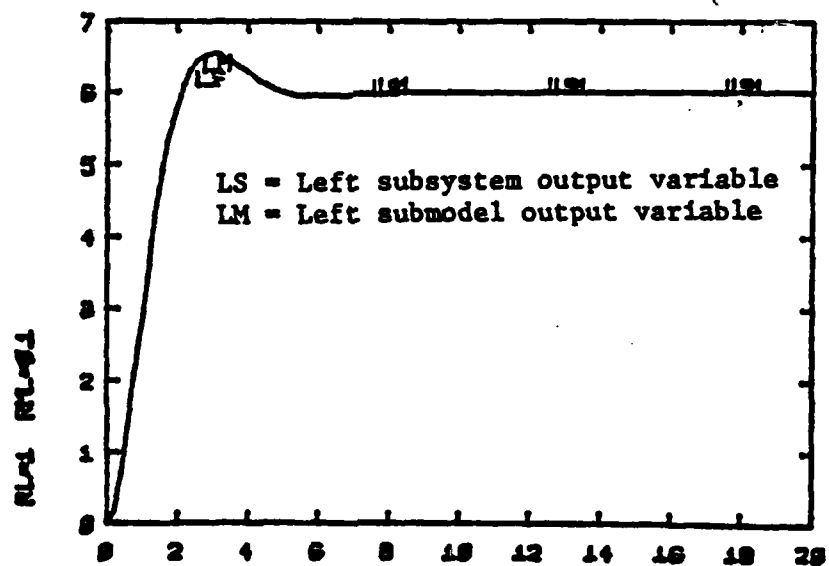
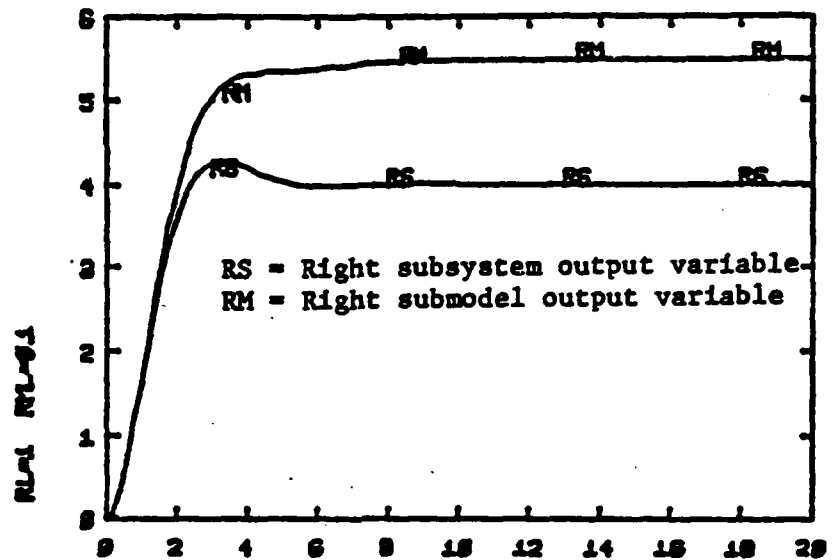


Figure 3.4 The system and model outputs of the left and right submodels. These outputs are obtained by applying the FDLM test 1 and indicate that the failure is in the right subsystem.

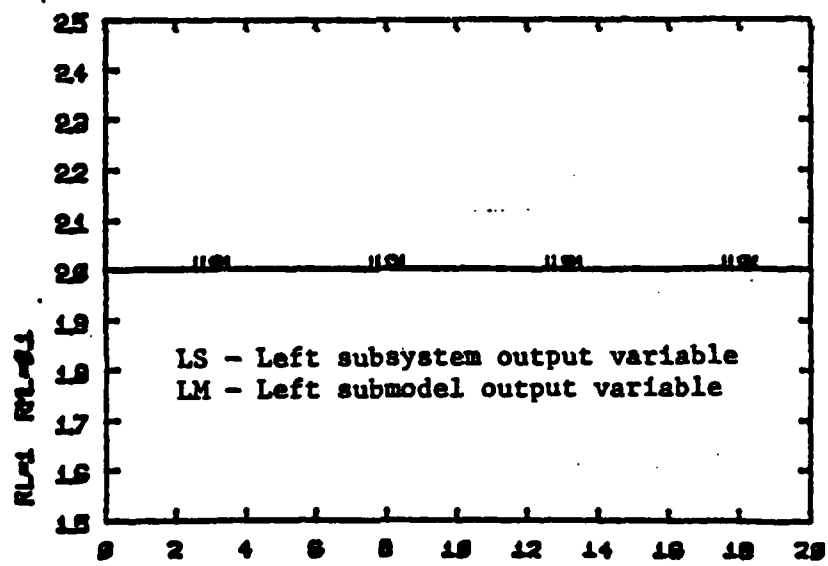
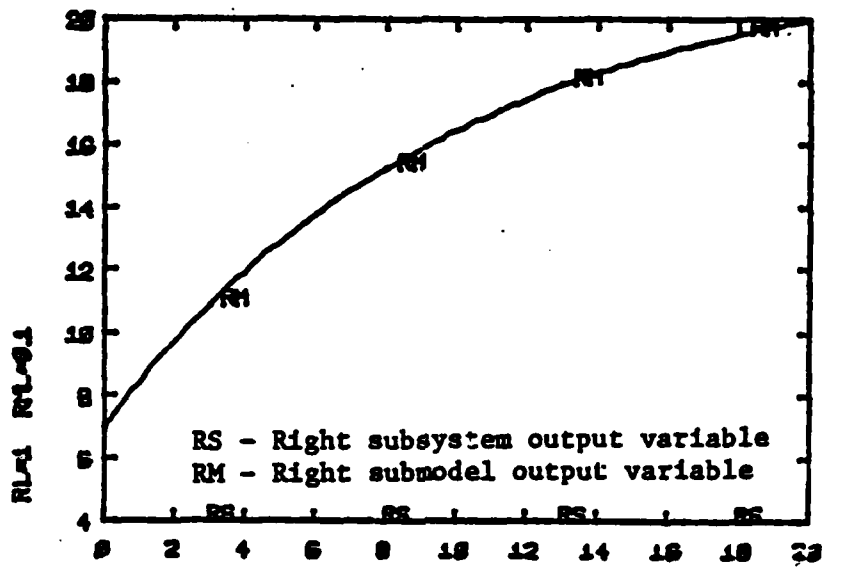


Figure 3.5 The system and model outputs of the left and right submodels. These outputs are obtained by applying the FDLM test 2 and indicate immediately that the failure is still in the right subsystem.

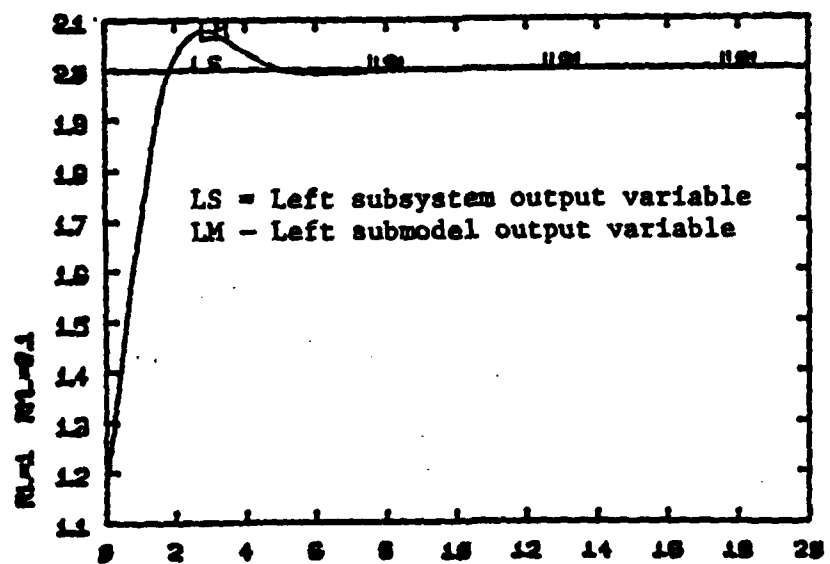
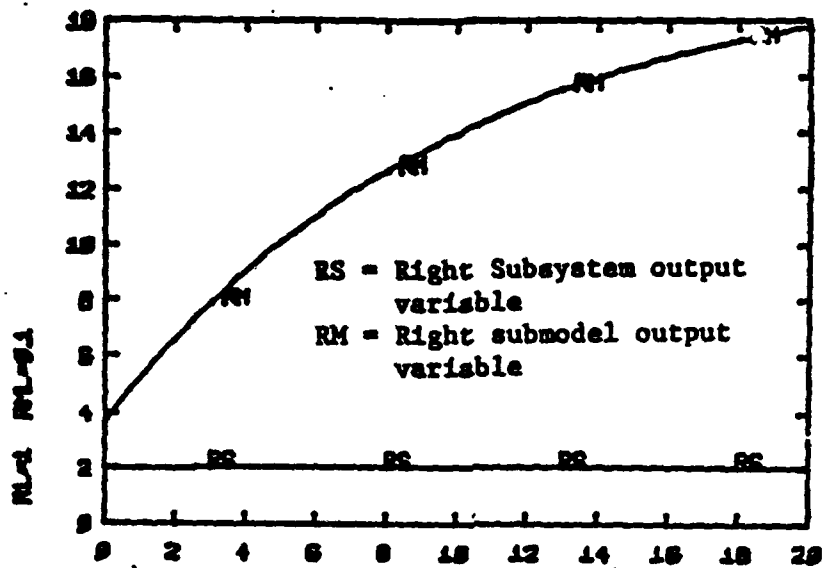


Figure 3.6 The system and model outputs of the left and right submodels. These outputs are obtained by applying the FDLM test 3 and indicate that the failure is in the right subsystem only, after the left system and model outputs coincide.

contains one energy-storing component at most. This will result in an efficient failure location procedure.

3.2 FDLM and the Disaggregated Model Technique

The idea of detecting and locating system failures by cutting the aggregated model into submodels, and comparing the outputs of the system with their corresponding submodels' values is not novel. It has been utilized in the disaggregated model technique discussed in [17]. However, FDLM is distinguished from the disaggregated model technique by specifying the compared system model outputs. In general, there are many system outputs which could have been compared with their model values. It turns out that a system failure does not necessarily cause all of these outputs to deviate from their normal values. Since the number of outputs of a system is usually large, the disaggregated model technique has to be applied by comparing only some of the system and model outputs. This may lead to a situation where a failure has occurred, but the compared system and model outputs will not reflect it.

The following example demonstrates the situation described. Consider the system shown in Figure 2.14, where its model is disaggregated at point 4, and the right submodel is shown in Figure 3.7. The right submodel input is ω_{s4} and its outputs are τ_4 , ω_5 , τ_5 , E_6 and I_6 as shown in Figure 3.7. The mathematical transfer functions of these variables relative to input ω_{s4} are summarized in Table 3.1. These functions show that τ_5 and I_6 do not depend on the bearing friction coefficient, b , that E_6 is not a function of the resistor R_L or b , and

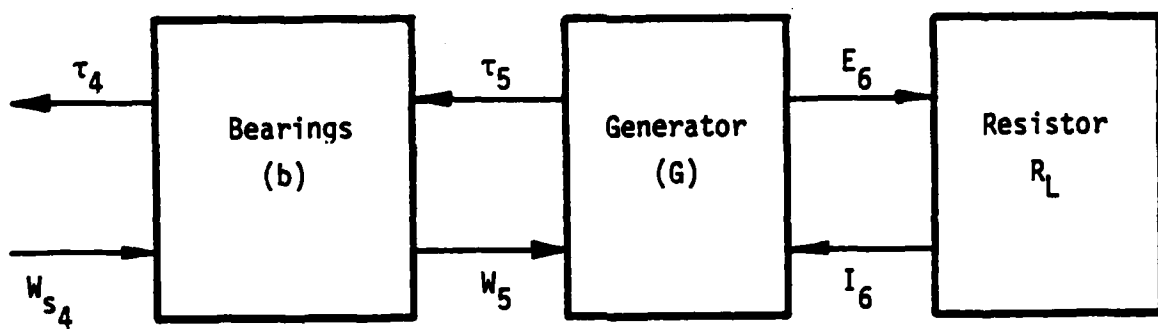


Figure 3.7 The right submodel obtained by applying FDLM to the system shown in Figure 2.12 utilizing measurement point 4. The submodel input is w_{s4} and outputs are τ_4 , τ_5 , w_5 , E_6 , I_6 . The subsystem components are the bearings (b), generator (G), and resistor (R_L).

TABLE 3.1: THE TRANSFER FUNCTIONS OF THE OUTPUTS
OF THE SUBMODEL SHOWN IN FIGURE 3.7

OUTPUTS	TRANSFER FUNCTIONS
τ_5/w_{s_4}	$\frac{G^2}{R_L}$
w_5/w_{s_4}	1
E_6/w_{s_4}	G
I_6/w_{s_4}	$\frac{G}{R_L}$
τ_4/w_{s_4}	$(b + \frac{G^2}{R_L})$

that ω_5 equals the input variable, ω_{s_4} , and does not depend on b , R_L or the generator coefficient, G . Thus, these outputs will not reflect failures located in the named components.

FDLM, on the other hand, compares the power variables of the cut submodels. These variables reflect all system failures as defined in Section 2.3. The power of the right submodel, shown in Figure 3.7, is $\tau_4 \cdot \omega_{s_4}$ and this variable depends on the bearing friction coefficient, b , the generator constant, G , and the resistor, R_L , which are all the submodel components. Thus, comparison of the power variables at the measurement point is sensitive to failures located anywhere within the system.

3.3 Sensitivity Analysis

Sensitivity analysis is performed by measuring the resultant deviations of the system outputs due to a known change in one of its parameters. The sensitivity of the system shown in Figure 2.14 is analyzed as follows.

The values of the seven parameters of this system have been increased by 20%, and the deviations of the steady-state outputs have been observed. This analysis has been performed while applying FDLM using measurement points 1-5. The results of this analysis, summarized in Table 3.2, indicate that:

1. The steady state deviation of the different outputs, due to a change in the inertia, J , is zero. A change in J influences the outputs' transient responses, but does not affect their steady state values. As a result, failures of the shaft's inertia values are difficult to detect, unless it is fatal failure like a broken shaft.

TABLE 3.2: THE RESULTS OF SENSITIVITY ANALYSIS APPLIED
TO THE SYSTEM SHOWN IN FIGURE 2.12

A 20% increase in system para- meters	Deviations FDLM Steady-State Outputs in Percentage				
	Measurement Point 1	Measurement Point 2	Measurement Point 3	Measurement Point 4	Measurement Point 5
Tank Capacitance C	17	18.5	18.5	0	0
Hydraulic Motor Constant k	28	30.6	∞	20	17
Bearings Friction Coefficient b	15	16.6	26.6	19.9	0
Shaft inertia J	0	0	0	0	0
Generator Constant G	0.3	0.3	0.3	0.3	30.6
Resistive Load R_L	0.1	0.1	0.1	0.1	17
Valve Resistance R_V	2.3	2.6	2.6	0	0

2. The deviation of the outputs at measurement point 3 due to a change in the constant of the hydraulic motor, k , in steady-state conditions is infinity. This is due to integration effects of the deviations of the system model outputs with respect to time. This integration phenomenon may cause false alarms, because any small imperfections of the hydraulic motor coefficient, k , will result in large output deviations. Therefore, measurement point 3 should not be used to apply FDLM.
3. FDLM will not detect all system component failures when the outputs of a single measurement point are used. By using measurement point 1 or 2, failures of the tank, hydraulic motor and the bearings can be detected. Measurement point 5 detects failures of the generator and the load resistor. Thus, one can apply the FDLM using measurement points 1 and 5 or 2 and 5, simultaneously. In this way, failures located in the tank, hydraulic motor, bearings, generator and load resistor are to be detected, where malfunction of the valve, R_v , and the shaft, J , are not easily detectable using this method. However, these two components may be tested using fault/event tree analysis, or other available methods.

Thus the system's sensitivity can limit the performance of FDLM in detecting system failures. It has been shown that the sensitivity of some system components may be low or even zero, and as a result failures located in these components are very difficult to detect. On the other hand, there are over-sensitive components, imperfections of which will cause large deviations in some of the FDLM outputs. This over-sensitivity results in false alarms, and therefore measurement points which cause this phenomenon should not be used. It seems that

FDLM best results are obtained by utilizing few of the system measurement points simultaneously. This results in a fast location procedure (Section 3.1.2) as well as in overcoming low components' sensitivity.

3.4 Sensor Failures

FDLM is designed to detect and locate system failures based on a real-time simulation and measured system outputs. The measured outputs are assumed to be validated, and sensors' malfunctions are assumed to be detected separately using the available techniques discussed in [9] and [14]. However, the FDLM sequential mode can detect sensor failures and distinguish them from the system's failures.

A sensor failure causes FDLM to provide inconsistent results when it is applied to two different measurement points. Consider two single FDLM tests, shown in Figure 2.13. Assume that one of the sensors measuring the outputs of point 1 has failed, and as a result, test 1 indicates that the right subsystem is defective. To locate this failure, test 2 is applied, and assuming that there are no sensor failures at point 2, it indicates that the system is operating normally. This inconsistency between the results of point 1 and 2 implies that there is a failure in the sensors of point 1.

Thus, inconsistent results of FDLM sequential tests indicate a sensor failure.

CHAPTER 4

MORE COMPLEX APPLICATIONS OF FDLM

4.1 Applications of FDLM to Non-Linear Systems

So far, FDLM applications included simple, linear and deterministic applications. Here, the method is extended to non-linear applications and it will be shown that the non-linear dynamic systems can be modeled by a set of linear differential equations if certain system outputs are measured and used as the model inputs.

The mathematical description of a non-linear system can be expressed as:

$$\dot{\underline{x}} = [A(\underline{x})]\underline{x} + [B]\underline{u} \quad (4.1)$$

where \underline{x} is an n -dimensional vector of state variables, \underline{u} an r -dimensional vector of input and, $[A(\underline{x})]$ and $[B]$ are $n \times n$ and $n \times r$ matrices, respectively. This set of n non-linear differential equations can be solved numerically using the Trapezoid rule, Runge-Kutta, or any other available method discussed in [20].

However, in order to obtain a stable solution, the integration time-step of the non-linear differential equations has to be significantly reduced, compared to the linearized one [20]. This may result in a non-linear simulation which cannot be implemented in real-time. Therefore, the following transformation, which enables one to apply FDLM to non-linear systems by solving a linear set of differential equations is useful.

Equation (4.1) can be transformed into

$$\dot{\underline{x}} = [\underline{A}']\underline{x} + [\underline{B}]\underline{u} + [\underline{B}']\underline{x}_s \quad (4.2)$$

where $[\underline{A}']$ is an $n \times n$ matrix, \underline{x}_s is an r' dimensional vector of measured system outputs, and $[\underline{B}']$ is an $n \times r'$ matrix.

Since $[\underline{A}']$ does not contain state dependent terms, equation 4.2 is a linear state-space description, where the non-linear system characteristics are introduced through the measured outputs, \underline{x}_s . Thus, FDLM computer simulation is supported by selected measured outputs of the system, which enables one to model the non-linear system using a linear set of differential equations. This is illustrated in the following example.

Consider the fifth-order electric network shown in Figure 4.1, where the transformer coefficient G is a non-linear function of the current, I_1 . G can be expressed as

$$G = k \cos(I_1) \quad (4.3)$$

where k is a constant. The non-linear $[\underline{A}]$ matrix can be written as:

$$[\underline{A}] = \begin{bmatrix} a_{11} & a_{12} & a_{13} & a_{14}(I_1) & a_{15}(I_1) \\ a_{21} & a_{22} & a_{23} & a_{24}(I_1) & a_{25}(I_1) \\ a_{31} & a_{32} & a_{33} & a_{34}(I_1) & a_{35}(I_1) \\ a_{41}(I_1) & a_{42}(I_1) & a_{43}(I_1) & a_{44} & 0 \\ 0 & 0 & 0 & a_{54} & a_{55} \end{bmatrix} \quad (4.4)$$

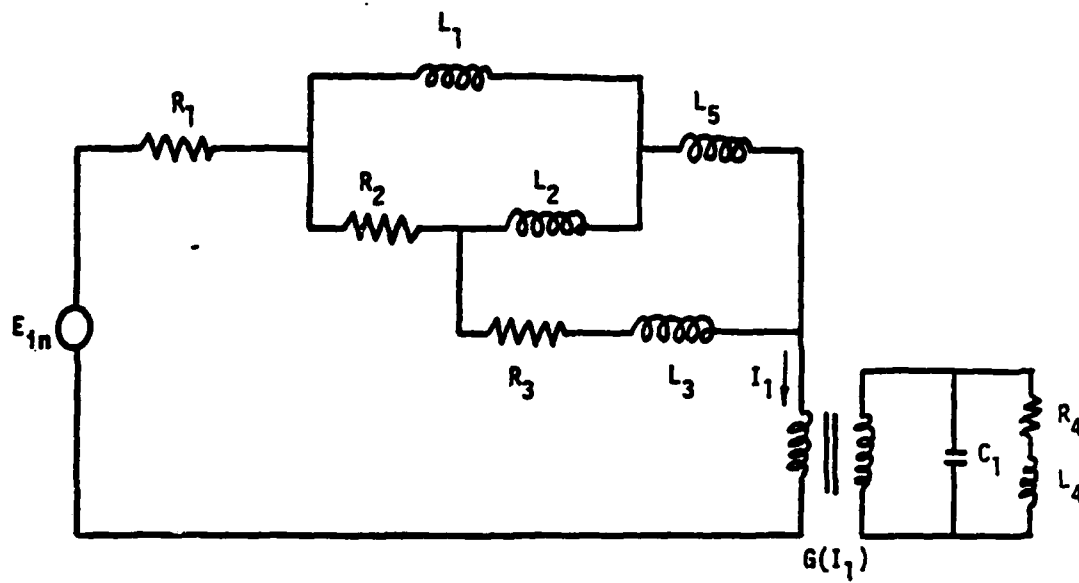


Figure 4.1 A non-linear fifth order electric network. The transformer coefficient G is a function of the current I_1 .

where the states are the voltages of the solenoids L_1 , L_2 , L_3 , and L_4 and the current of the capacitor C_1 . By measuring the system voltage E_{s_1} and current I_{s_1} , one can transform the non-linear differential equations into a linear set where:

$$[A'] = \begin{bmatrix} a_{11} & a_{12} & a_{13} & 0 & 0 \\ a_{21} & a_{22} & a_{23} & 0 & 0 \\ a_{31} & a_{32} & a_{33} & 0 & 0 \\ 0 & 0 & 0 & a_{44} & 0 \\ 0 & 0 & 0 & a_{54} & a_{55} \end{bmatrix} \quad (4.5)$$

and

$$[B'] \underline{x}_s = \begin{bmatrix} b'_{11} & 0 \\ b'_{21} & 0 \\ b'_{31} & 0 \\ 0 & b'_{42} \\ 0 & b'_{52} \end{bmatrix} \begin{bmatrix} E_{s_1} \\ I_{s_1} \end{bmatrix} \quad (4.6)$$

The linear and non-linear simulations have been implemented and their performances are depicted in Figure 4.2-4.4. In Figure 4.2 the integration time step is 0.05 seconds. The third and the fourth state variables of the non-linear simulation (s_3 and s_4) diverge from their system values, where, in Figure 4.3 the simulation is linear and for the same integration time step, these state variables (s_3 and s_4) follow their system values. Figure 4.4 demonstrates that by reducing the integration time step to 0.005 sec,

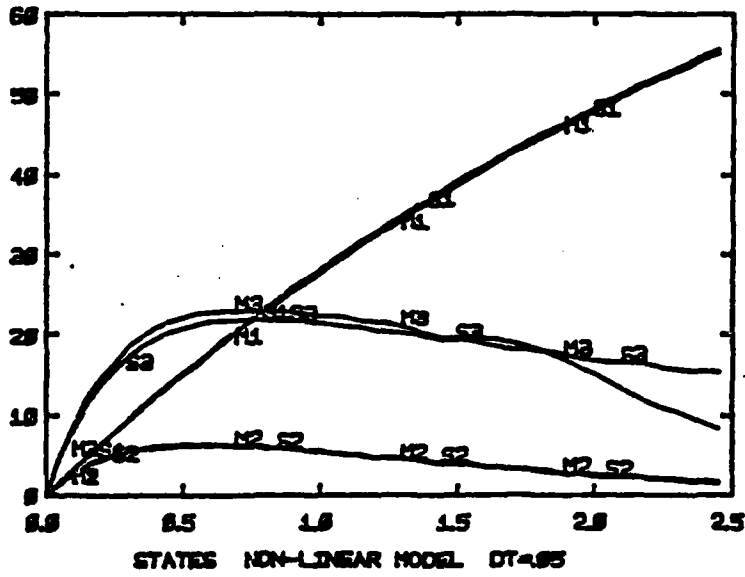
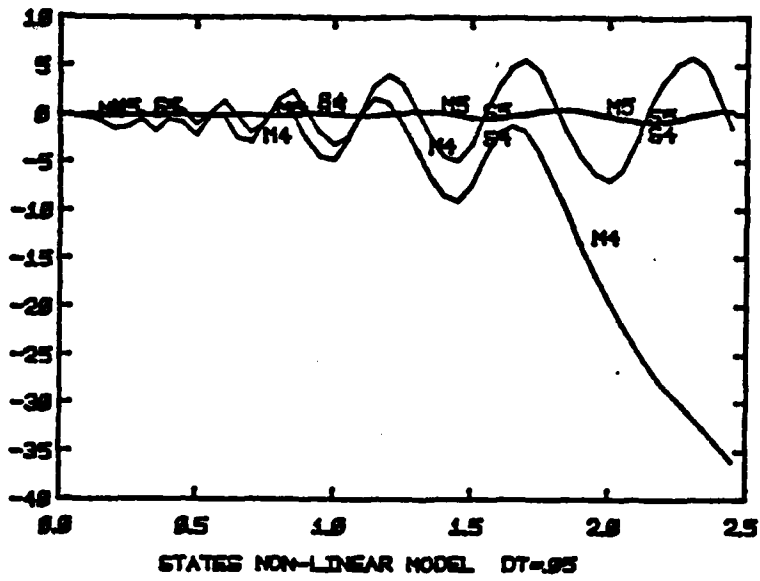


Figure 4.2 The system and model state variables of the electric network shown in Figure 4.1. The model state variables M_3 and M_4 do not follow their corresponding system state variables S_3 and S_4 . The integration time step is 0.05 seconds.

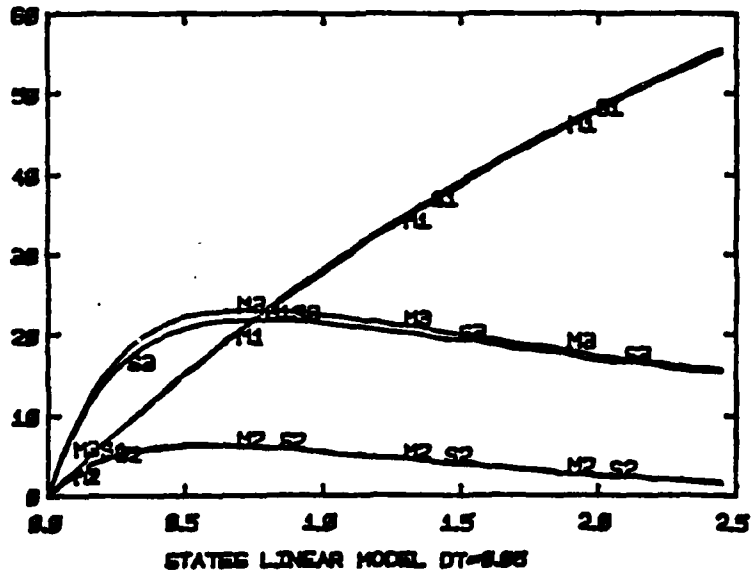
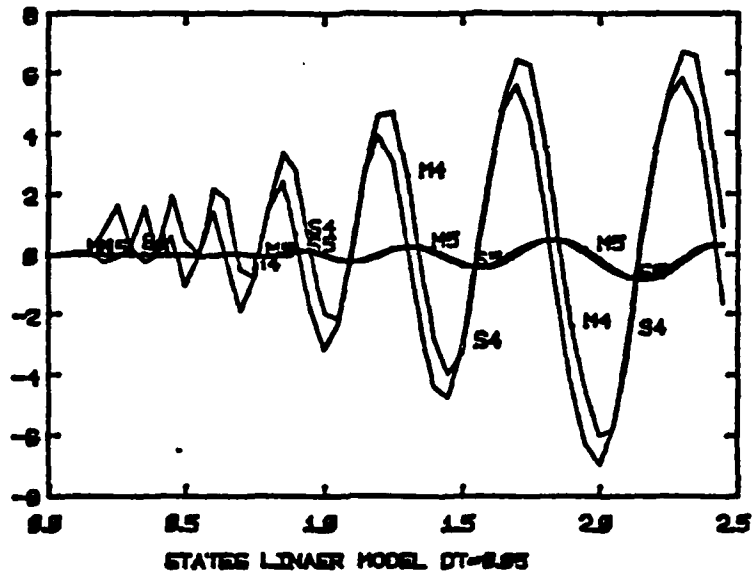


Figure 4.3 The system and model state variables of the electric network shown in Figure 4.1. The model state variables follow their corresponding system state variables. FDLM linear transformation is applied and the integration time step is 0.05 seconds.

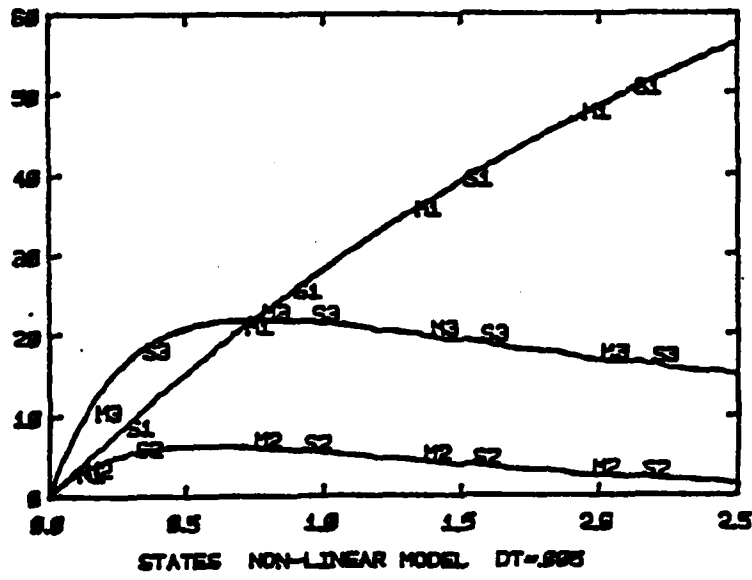
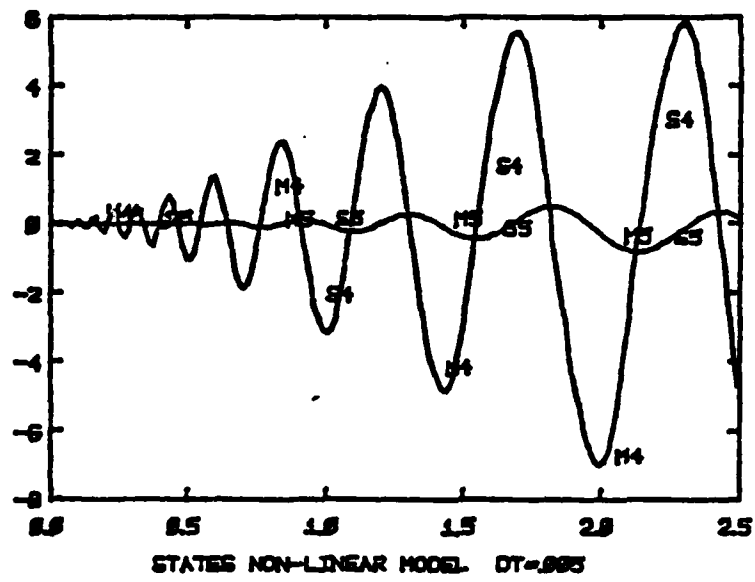


Figure 4.4 The system and model state variables of the electric network shown in Figure 4.1. The model state variables follow their corresponding system state variables. The integration time step is 0.005 seconds.

the unstable characteristics of the non-linear simulation are eliminated.

4.2 Multi-Connected Systems

Systems that their power flow descriptions contain closed loop are multi-connected systems. An example of such a system is depicted in Figure 4.5. In Figure 4.6 FDLM is applied to this system utilizing the measured outputs of a single measurement point.

By using a single measurement point, the aggregated model is not fully partitioned. As a result, the location capability of FDLM is eliminated. However, by utilizing the outputs of two measurement points simultaneously, the multi-connected model is partitioned into two submodels, as shown in Figure 4.7. By comparing the outputs of these submodels with their corresponding system variables FDLM is able to detect and locate failures of multi-connected systems.

4.3 Dependent Energy Storing Components

When the model of a physical system contains dependent energy storing components, applying FDLM may result in calculated model outputs which are functions of the inputs' time derivatives. When the system includes stochastic processes the model inputs are fast changing signals that cannot be differentiated.

To clarify this statement, consider the submodel shown in Figure 4.8. The model output E_m , can be written as:

$$E_{m_1} = L I_{s_1} + R I_{s_1} \quad (4.7)$$

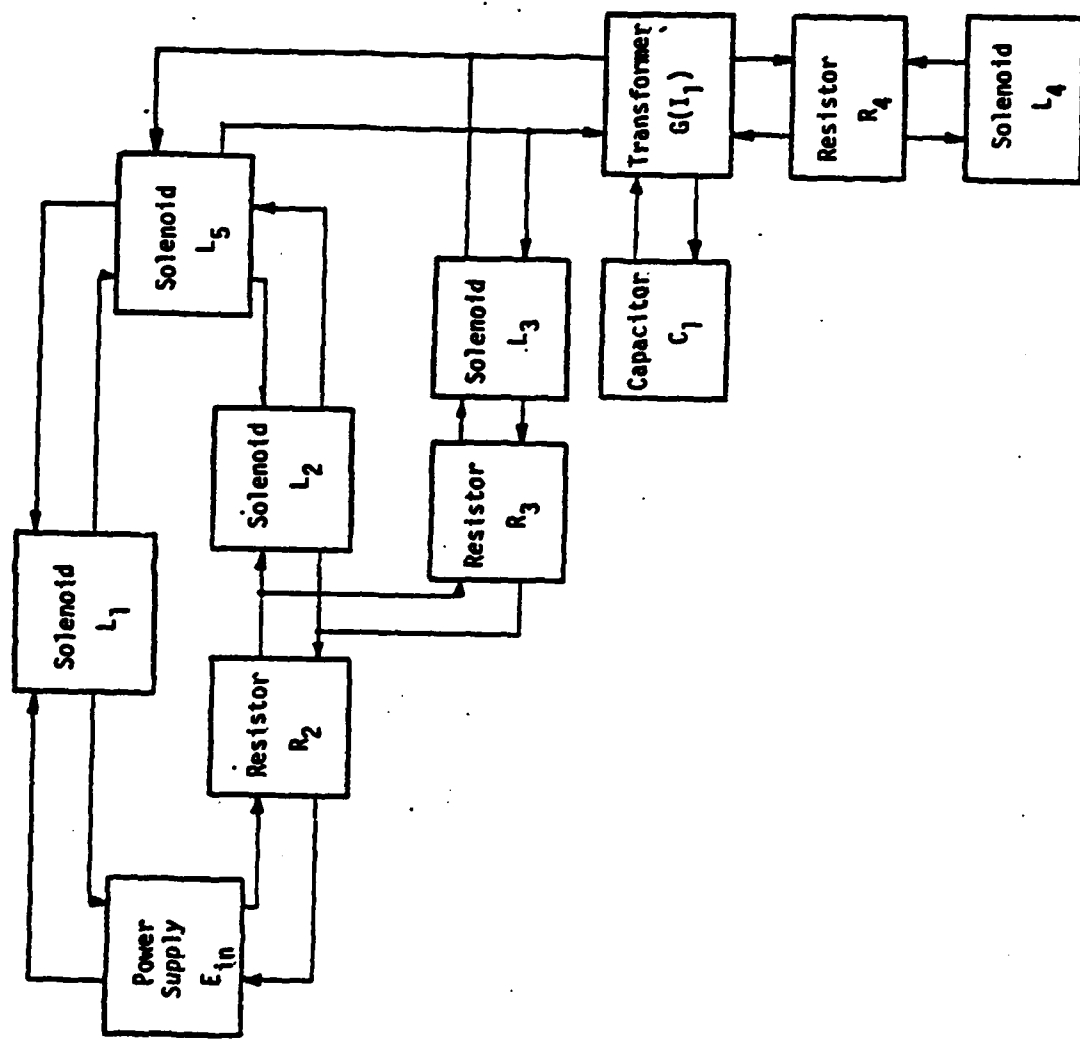


Figure 4.5 Causal description of the electric network shown in Figure 4.1. This system is multiconnected.

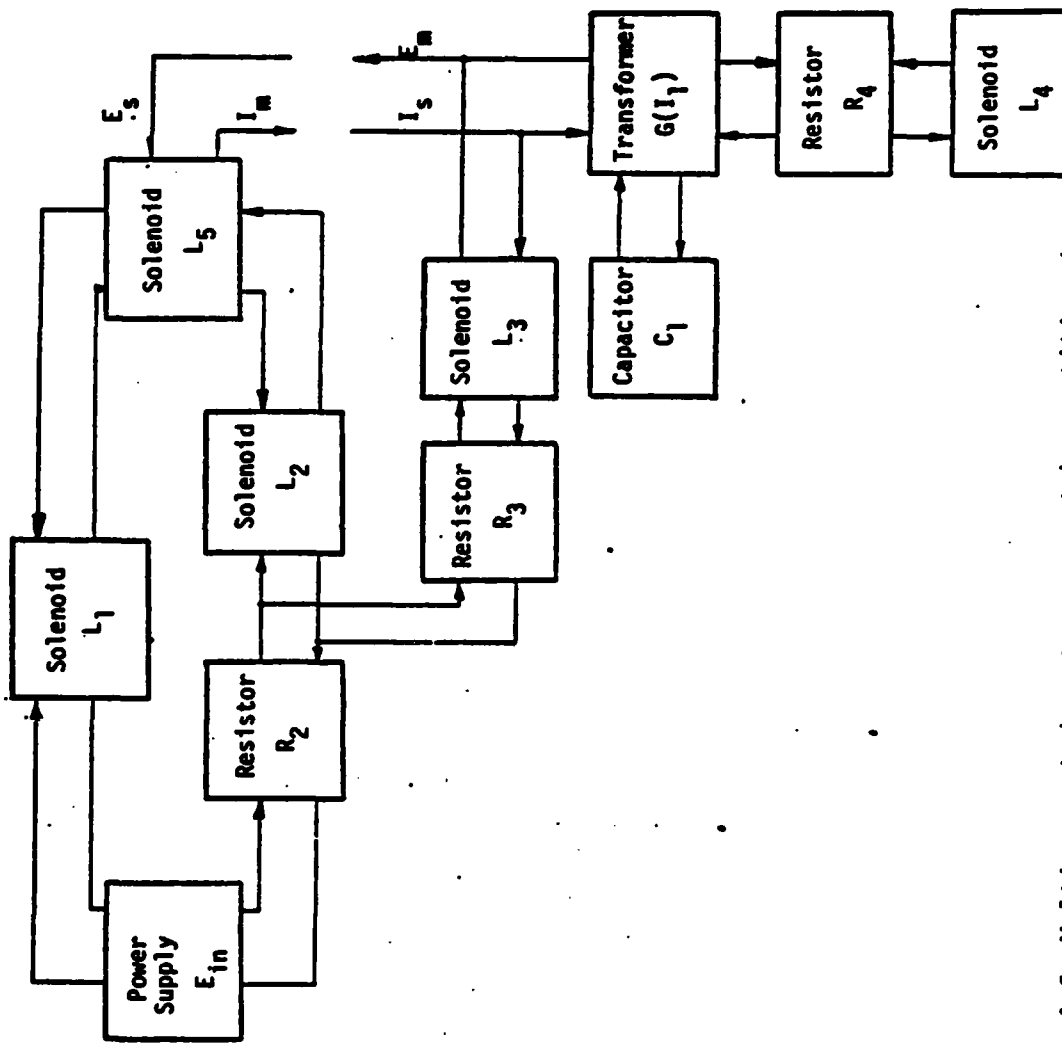


Figure 4.6 Multiconnected systems cannot be partitioned into two subsystems by applying a single cut.

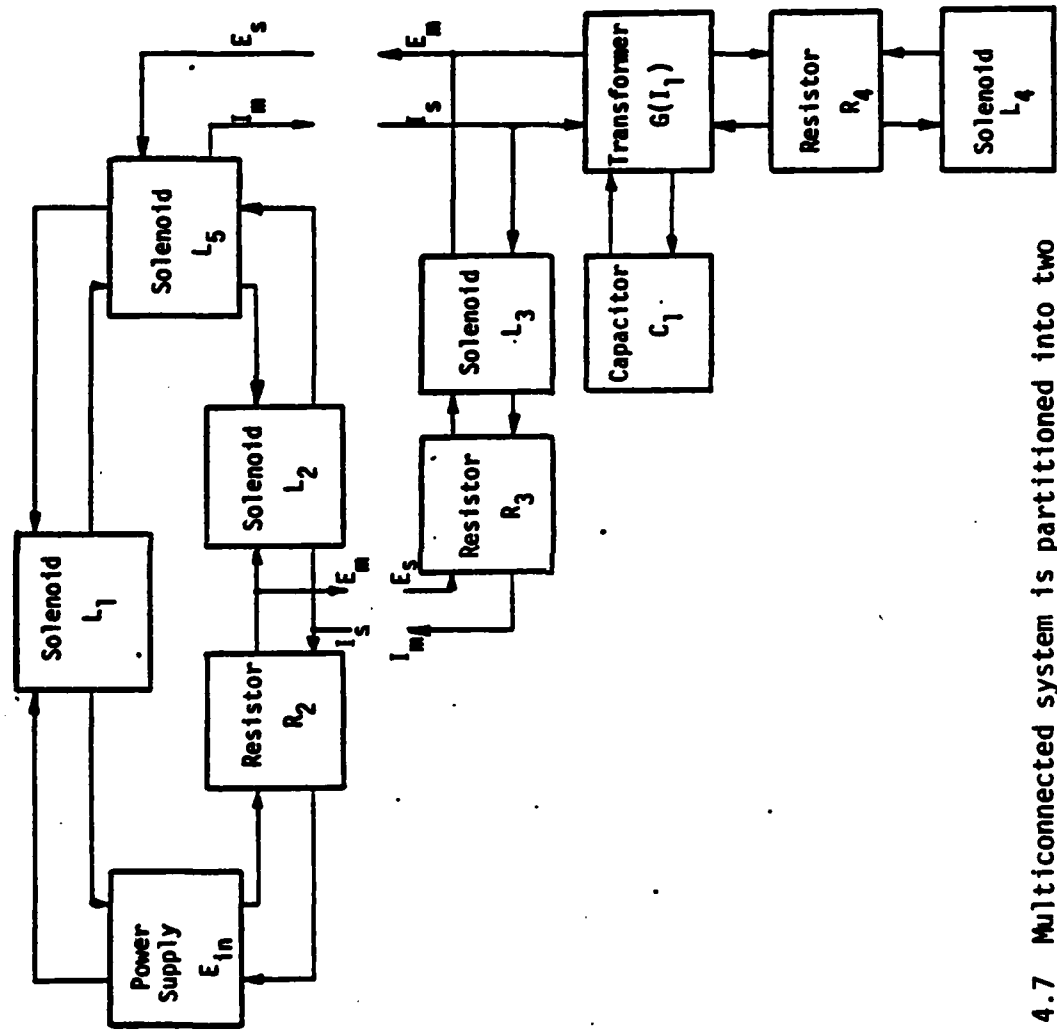


Figure 4.7 Multiconnected system is partitioned into two subsystems by cutting multi energy bonds.

When the system involves stochastic processes, the measured current I_{s_1} is not a smooth function and therefore it cannot be differentiated. As a result, the voltage E_{m_1} cannot be calculated, and FDLM is not applicable.

This problem can be overcome by changing the submodel's causality, which results, on one hand, in adding state variables to the simulation, and on the other hand, in eliminating the necessity of calculating derivatives. In Figure 4.9 the causality of the submodel shown in Figure 4.8 is changed, and the model output, I_{m_1} , can be expressed as:

$$I_{m_1} = \frac{\int (E_{s_1} - E_2) dt}{L} \quad (4.8)$$

where E_{s_1} is the model input and E_2 and L are defined in Figure 4.9.

Thus, in order to detect failure in a system which contains dependent energy storing components, the model causality must be set such that the model outputs are not functions of the inputs' derivatives. This requirement may add state variables to the existing simulation.

4.4 Thermofluidic Systems

Consider a general thermofluidic component, shown in Figure 4.10. The volume, V , of this component is a constant. Fluid is assumed to flow in and out with mass flow rates F_1 and F_2 , respectively. This component is subjected to heat flow \dot{Q} and rate of work \dot{W} . It is assumed that the well-stirred tank and the ideal gas assumptions are valid.

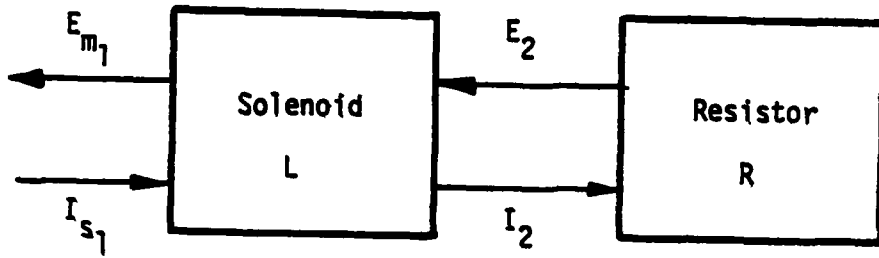


Figure 4.8 The causality of the submodel is such that I_{m1} is the submodel input and E_{m1} is its output.

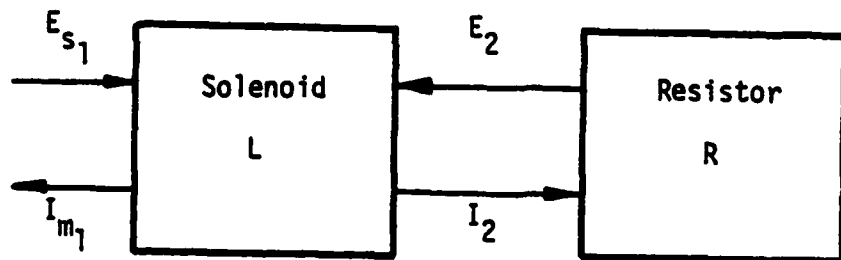


Figure 4.9 The causality of the submodel is such that E_{m1} is the submodel input and I_{m1} is its output.

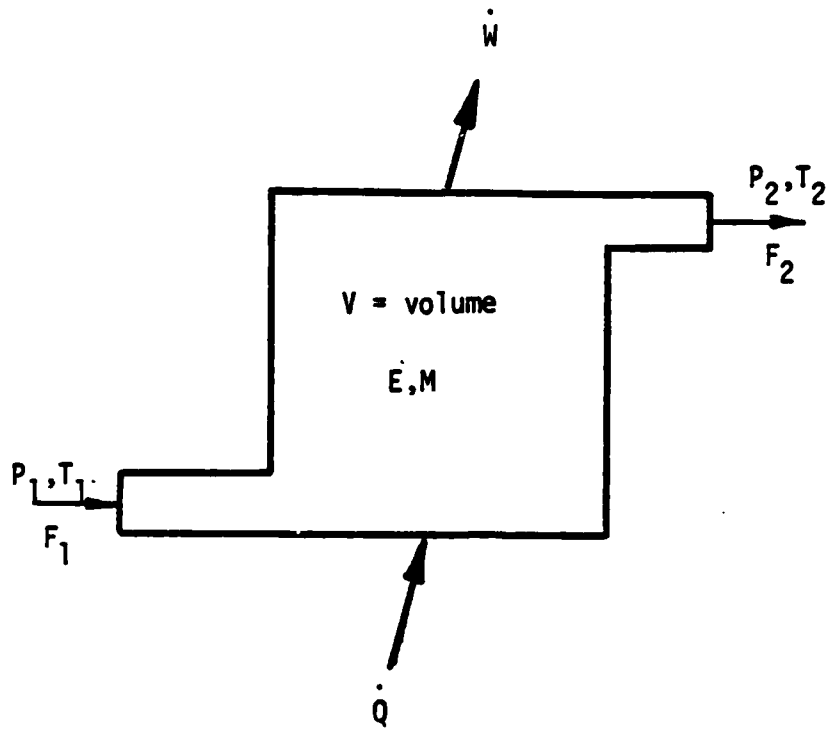


Figure 4.10 A general thermofluidic component. Fluid flows in and out with mass flow F_1 and F_2 . E is the energy and M is the mass of fluid in the component. Q and W are the heat and work rates, respectively.

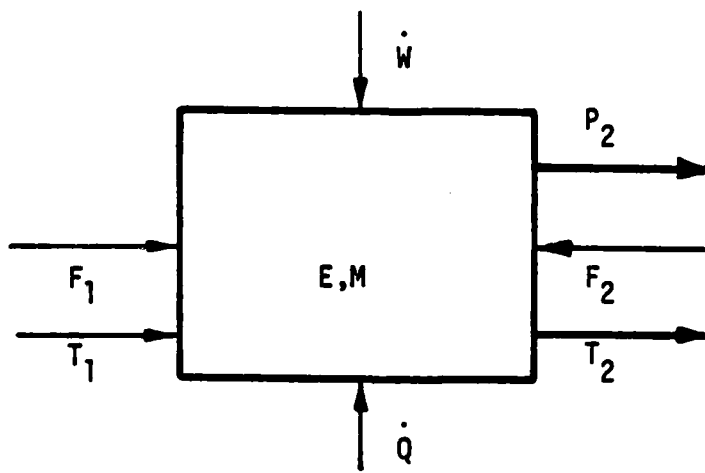


Figure 4.11 The input and output variables of the system shown in Figure 4.10. E and M are the system state variables.

The mass and energy conservation laws applied to this component can be written as:

$$\frac{dM}{dt} = F_1 - F_2 \quad (4.9)$$

$$\frac{dE}{dt} = F_1 h_1 - F_2 h_2 + \dot{Q} - \dot{W} \quad (4.10)$$

where M is the mass and E is the internal energy stored in the component.

Using the well stirred tank assumption, the pressure and temperature at the outlet P_2 and T_2 , respectively, can be related to the pressure and temperature inside the component, P and T [20]. This can be written mathematically as:

$$P_2 = \psi_p(P) \quad (4.11)$$

$$T_2 = \psi_T(T) \quad (4.12)$$

where ψ_p and ψ_T are some known functions. Here, to simplify the analysis, it is assumed that

$$T_2 = T \quad (4.13)$$

$$P_2 = P \quad (4.14)$$

Modeling the fluid inside the component as an ideal gas, its state equation can be written as:

$$P = \rho R T \quad (4.15)$$

where R is the gas constant. The internal energy, E , and the specific enthalpy can be expressed as:

$$E = C_V M T \quad (4.16)$$

$$h = C_p T \quad (4.17)$$

By substituting equations (4.15) - (4.17) into equation (4.10) the energy conservation law can be recast as:

$$\frac{dE}{dt} = F_1 C_p T_1 - F_2 \frac{C_p}{C_V} \left(\frac{E}{M} \right) + \dot{Q} - \dot{W} \quad (4.18)$$

where C_p is the specific heat at constant pressure. Thus the two state variables of the general thermofluidic component are E and M , the values of which are obtained by solving equations (4.9) and (4.18). In order to solve these equations, the following variables must be measured: F_1 , F_2 , T_1 , \dot{Q} , and \dot{W} . The calculated model outputs are P_2 , and T_2 , which can be expressed as:

$$P_2 = \frac{R}{V C_V} E \quad (4.19)$$

$$T_2 = \frac{1}{C_V} \frac{E}{M} \quad (4.20)$$

where V is the volume of the component. These model inputs and outputs are depicted in Figure 4.11.

Another useful element is the choke flow resistor, shown in Figure 4.12. The flow, F , can be expressed as:

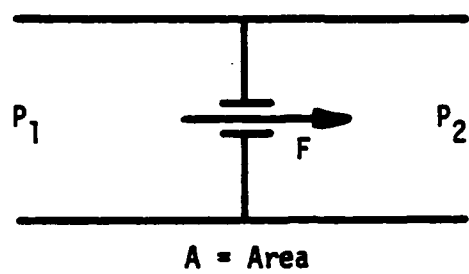


Figure 4.12 Choke flow resistor. F is the flow, P_1 and P_2 are the input and output pressures, A is the nozzle area.

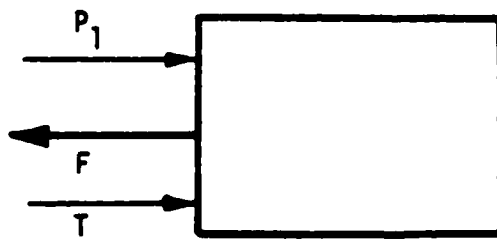


Figure 4.13 The input and output variables of the choke flow resistor.

$$F = \sqrt{A 2\rho |\Delta P|} \operatorname{sgn}(P_1 - P_2) \quad (4.21)$$

where ΔP is the pressure drop $P_1 - P_2$. Utilizing the ideal gas assumption equation (4.21) can be recast as:

$$F = \frac{A}{\sqrt{RT}} \operatorname{sgn}(P_1 - P_2) \sqrt{|P_1^2 - P_2^2|} \quad (4.22)$$

where T is the average temperature and R is the gas constant. In the case where $P_1 \gg P_2$, the flow F can be expressed as:

$$F = \frac{A}{\sqrt{RT}} P_1 \quad (4.23)$$

Thus, by measuring the pressure, P_1 , and the average temperature, T , the flow, F , can be calculated using equation (4.23). This is depicted in Figure 4.13.

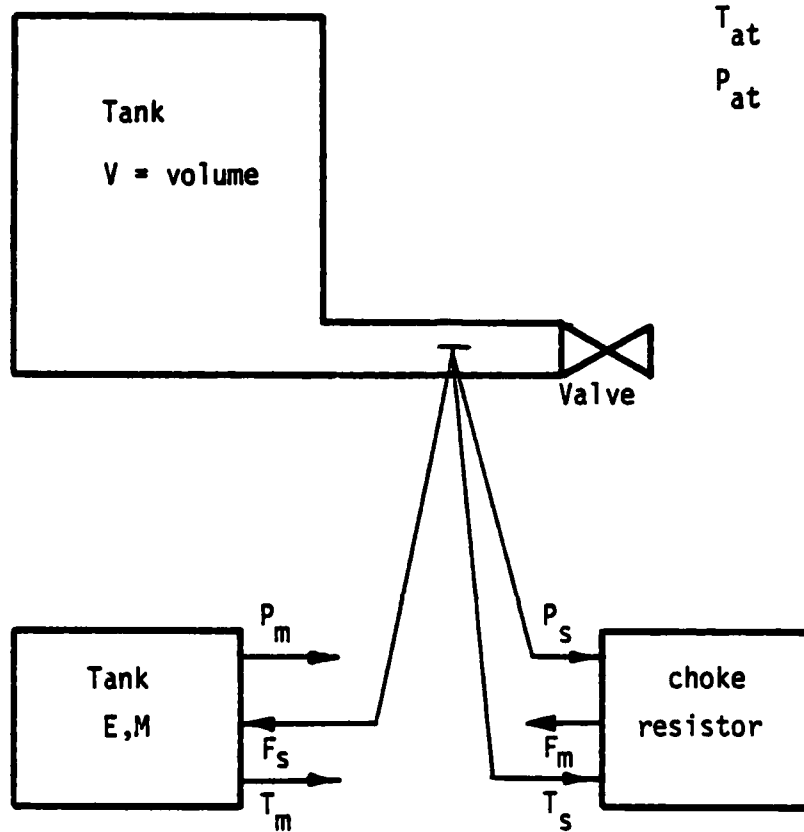


Figure 4.14 FDLM method applied to a simple thermofluidic system. Deviations of P_s from P_m and T_s from T_m indicate that the tank has failed, and deviations of F_s from F_m indicate that the valve has failed.

The following example demonstrates how the models of the general thermodfluidic system and the choke flow resistor can be used to detect and locate system failures. Consider the pressurized tank, shown in Figure 4.14, where gas flows out to the atmosphere through a valve. The pressure, flow, and temperature (P_s , F_s , and T_s , respectively) are measured, and the system's model equations are constructed as follows:

$$\frac{dM}{dt} = -F_s \quad (4.24)$$

$$\frac{dE}{dt} = -F_s \frac{C_p}{C_v} \left(\frac{E}{M} \right) \quad (4.25)$$

where E and M are the two model state variables. Assuming that $P_s \gg P_{at}$ and $T_s \gg T_{at}$, the mass flow, F_m , can be calculated as follows:

$$F_m = \frac{A}{\sqrt{RT_s}} P_s \quad (4.26)$$

The model pressure and temperature can be calculated using equations (4.19) and (4.20). This system model setup is depicted in Figure 4.14. By comparing the measured pressure, flow, and temperature with their corresponding model values system failures can be detected and located. If, for example, P_s deviates from P_m or T_s deviates from T_m , the tank has failed. On the other hand deviations of F_s and F_m indicate that the valve has failed.

Thus, the causal description of systems is utilized by FDLM to locate system defective components.

CHAPTER 5

HUMAN FACTOR CONSIDERATIONS

5.1 Aiding the Operator Detecting System Failures

FDLM is designed to aid the human operator to detect and locate system failures. The operator decides whether or not the system has failed based on:

- (1) the size of the discrepancies between the system and model outputs, and
- (2) the length of time during which these discrepancies have exceeded the allowable thresholds.

To determine whether criteria 1 and/or 2 are violated, the time history of the system and model outputs are displayed to the operator. In most applications the compared system and model outputs are noisy. This fact complicates the comparison task, since it involves checking the expected value of the difference between the system and the model outputs and the variance of the system output. This comparison can be expressed mathematically as:

$$|\bar{x}_s - \bar{x}_m| = |\bar{x}_s - \bar{x}_m| < \Delta \quad (5.1)$$

$$\text{Var}(x_s) < \sigma_n^2 \quad (5.2)$$

where \bar{x}_s and \bar{x}_m are the expected values of the system and model outputs over time, respectively, Δ an allowable threshold, $\text{Var}(x_s)$ and σ_n^2 the variance of the system output and its normal value, respectively. The expected values should be evaluated over a fraction of the system's smallest time constant based on at least 10-15 samples.

One way to perform the monitoring task is to display to the human-operator the time history of the values of x_s and x_m , as shown in Figure 5-1. The length of time viewed in this display is Δt , and the current values of x_s and x_m are displayed on the right hand of the window, as shown in Figure 5.1. It is desired to set Δt to be three times the system associated time constant, such that the system dynamics are captured in the display.

The performance of the human operator, monitoring the system and model outputs and using the display shown in Figure 5.1 turns out to be poor. In an experiment conducted in the M.I.T. Man-Machine Systems Laboratory and discussed in Chapter 6 using the display shown in Figure 5.1 the human operator had 13.75% false alarms and 11.25% misses. To improve the operator's performance, various analog and digital (numerical) displays were considered. These displays, included Raw and Averaged Variables, Percentage Error, Standard Score and Probability Display. These displays are discussed and evaluated below:

5.1.1 Raw Variables Display

To demonstrate the difficulties involved in the monitoring task using the display shown in Figure 5.1, outputs having different noise levels are shown in Figures 5.2 and 5.3. In these displays the measured and modelled output variables are displayed in their raw form. The signals of Figure 5.2 and 5.3 are generated by simulating the outputs of point 4 of the system shown in Figure 2.12, and superimposing on them a random signal which represents the measurements' noise. The standard deviation of the noise in Figures 5.2 and 5.3 is 0.15 and 0.55, respectively.

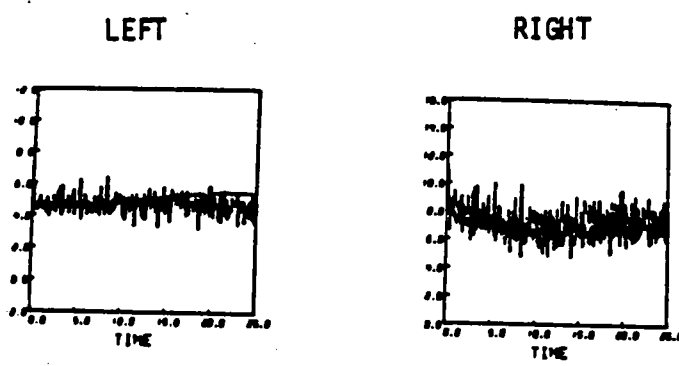
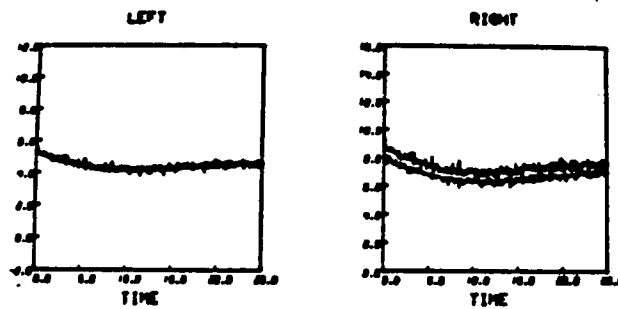


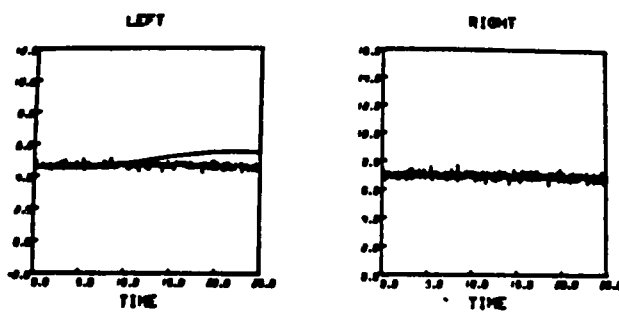
Figure 5.1 FDLM system and model outputs for a single measurement point. The system output is noisy. The left submodel output is smooth, whereas the right submodel output is noisy.

RAW VARIABLES



(a)

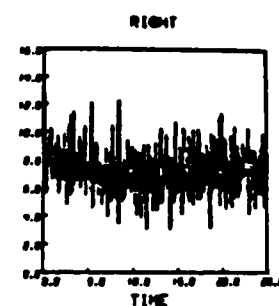
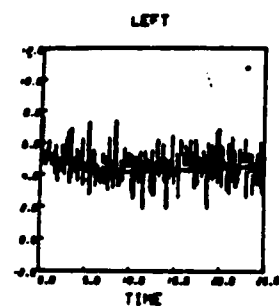
RAW VARIABLES



(b)

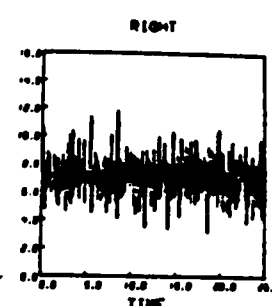
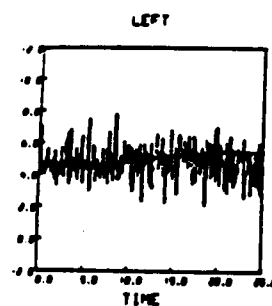
Figure 5.2 Raw variables display. The standard derivation of the noise is 0.15 in the output units. In 5.2a the failure located in the right subsystem and in 5.2b in the left subsystem.

RAW VARIABLES



(a)

RAW VARIABLES



(b)

Figure 5.3 Raw variables display. The standard deviation of the noise is 0.55 in the output units. In 5.3a the failure located in the right subsystem and in 5.3b in the left subsystem.

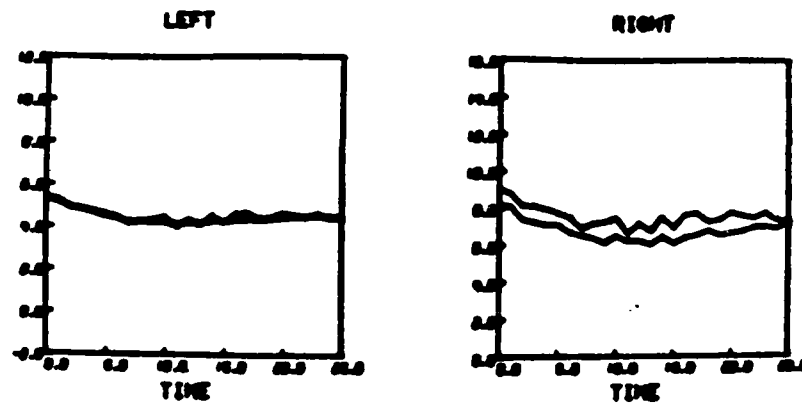
In the side-by-side windows viewed in Figures 5.2 and 5.3 the system and model flows (f_s , f_m) are displayed in the left window, and system and model efforts (e_s , e_m) in the right. Since the left subsystem contains state variables and the right does not, the left model output is smooth and the right is noisy. Furthermore, in case of a failure the left submodel output diverges from its corresponding system variable only after a time delay of δ_t (12 sec in Figure 5.2b and 5.3b), whereas the right submodel output diverges almost immediately (Figure 5.2a). When the noise level is low, the Raw Variables Display can be used for detecting system failures quite successfully (Figure 5.2). However, with a high noise level (Figure 5.3) the Raw Variables display does not seem to be helpful. In the case where the submodel does not contain state variables, failures are not detectable, as shown in Figure 5.3a.

As noted earlier, one way to enable the operator to detect failures of noisy systems is to smooth the output variables. A simple smoothing technique used in this work is averaging the system and model outputs, as discussed below.

5.1.2 Averaged Variables Display

By averaging the raw system and model outputs one smooths the noisy signals. This enables the operator to detect discrepancies between the system and model outputs. The failure of Figure 5.3 is resimulated and the corresponding Averaged Variables Display is shown in Figure 5.4. Averaging the system and model outputs has been suggested by Shackel [21]. The averaging technique enables one to detect fail-

RAW VARIABLES



RAW VARIABLES

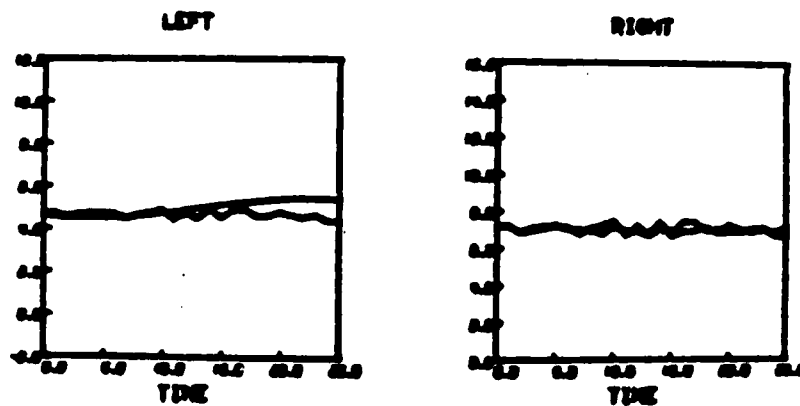


Figure 5.4 Averaged raw variables display. The standard deviation of the noise is 0.55 in the output units as 5.4a the failure is in the right subsystem and in 5.4b in the left subsystem.

ures of a noisy system, but the information of the system noise level is lost. To retain the noise level information and still enable detecting system failures is proposed to average the model outputs only. This will result in a display where the system output is noisy and the model output is smooth, as shown in Figure 5.5. In the experiment discussed in Chapter 6, the effects of the Raw Averaged and model Averaged Variables displays were examined.

Instead of displaying the time history of the system and model outputs in their raw or averaged forms, one can display some of their related functions, which might help the operator in his monitoring task. These functions can be some statistical measures which might reduce the operator's cognitive load and help him perform the comparison task expressed in equations (5.1) and (5.2). The measure of Percentage Error is one candidate index, and its display is discussed in the next section.

5.1.3 Percentage Error Display (PED)

The Percentage Error is defined as the difference between the averaged system (\bar{x}_s) and model (\bar{x}_m) outputs divided by \bar{x}_m , i.e.,

$$PE = \frac{\bar{x}_s - \bar{x}_m}{\bar{x}_m} \quad (5.3)$$

Equation (5.3) and the comparison test of equation (5.1) are directly related. The threshold Δ (equation 5.1) can be expressed as: $|PE \cdot \bar{x}_m| < \Delta$.

Thus, Percentage Error Display seems to be helpful in applying the test of equation (5.1). However, it eliminates the possibility of checking the noise level of the system outputs. Furthermore, PED does

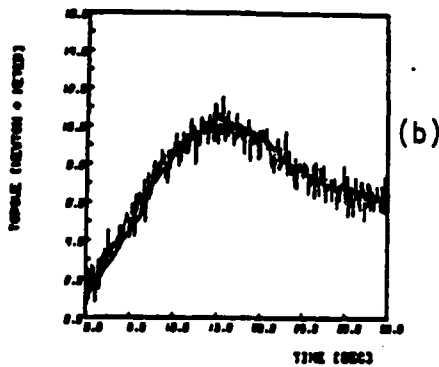
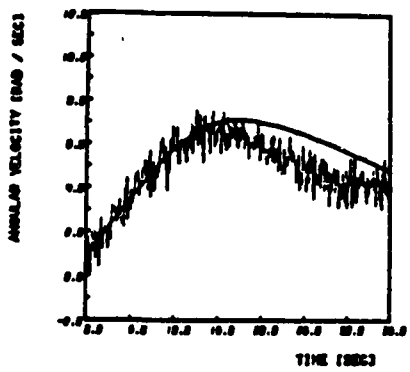
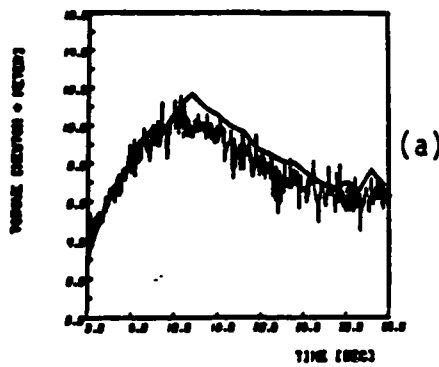
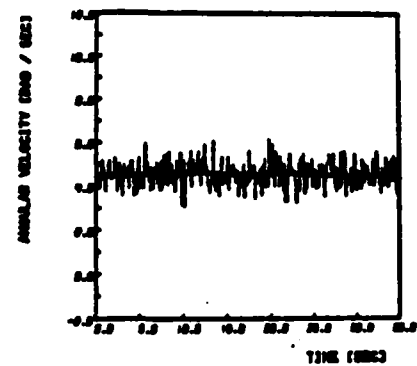


Figure 5.5 Raw system and averaged model outputs display.

not show the values of the system and model variables. Therefore it is coupled with the Raw Variables Display as shown in Figures 5.6 and 5.7. The standard deviation of the noise in Figures 5.6 and 5.7 is 0.15 and 0.55, respectively.

The Percentage Error is a measure that helps the operator to monitor the differences between the expected values of the model and system outputs but it does not consider the system noise level. A measure that takes into account the difference between \bar{x}_s and \bar{x}_m , as well as the system noise level is the Standard Score Display.

5.1.4 Standard Score Display (SSD)

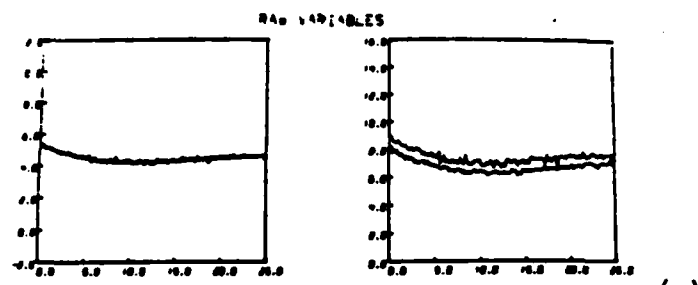
The Standard Score, Z, is defined as the difference between the averaged system and model outputs divided by the value of the standard deviation of their difference Z can be expressed mathematically as:

$$Z = \frac{\bar{x}_s - \bar{x}_m}{\sigma_d / \sqrt{n}} \quad (5.4)$$

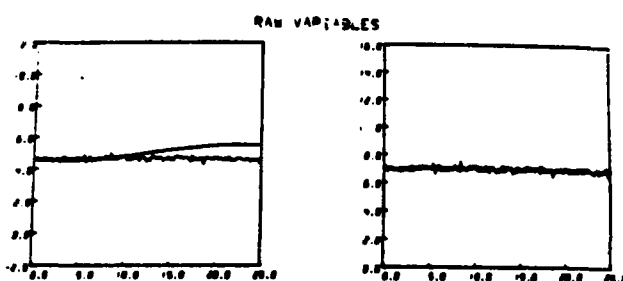
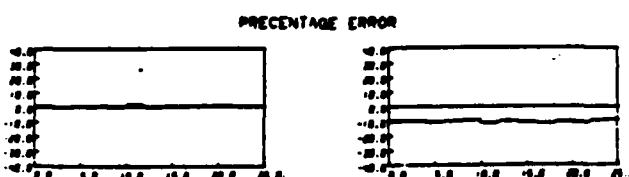
where n is the size of the samples, the averages (\bar{x}_s and \bar{x}_m) of which are calculated, and σ_d / \sqrt{n} is the standard deviation of the difference $\bar{x}_s - \bar{x}_m$, during the system normal operation mode. σ_d can be expressed as:

$$\sigma_d^2 = \sigma_{x_s}^2 + \sigma_{x_m}^2 - 2\sigma_{x_s x_m} \quad (5.5)$$

where σ_{x_s} and σ_{x_m} are the standard deviations of the system and model outputs, respectively, and $\sigma_{x_s x_m}$ is the covariance of the system and model outputs. σ_d is measured for the normal operation of the system off line. This value is used to calculate the Z score value in real-time.



(a)



(b)

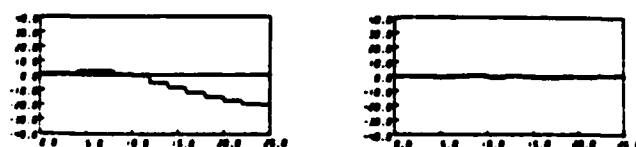


Figure 5.6 Percentage error and raw variables display. The standard deviation of the noise is 0.15 in the output units. In 5.6a the failure is in the right subsystem and in 5.6b is in the left subsystem.

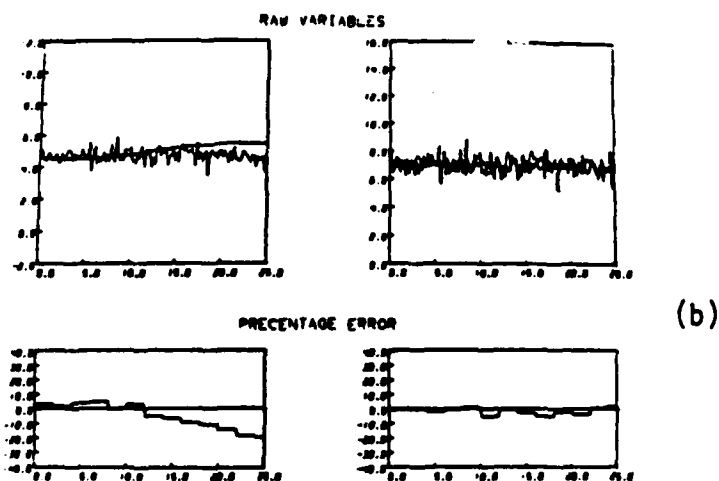
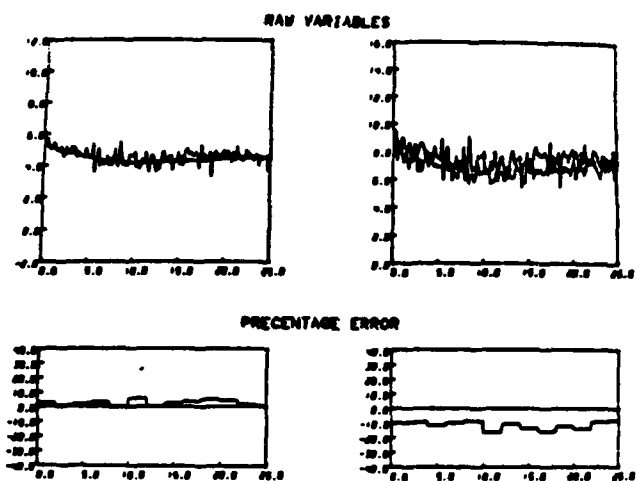


Figure 5.7 Percentage error coupled with the raw variables display. The standard deviation of the noise is 0.55 in the output units. In 5.7a the failure is in the right subsystem and in 5.7b is in the left subsystem.

Similar to PED the Standard Score Display does not show the values of the system and model outputs. Therefore, SSD was coupled with the Raw Variables Display, as shown in Figure 5.8 - 5.10. The standard deviation of the noise in Figure 5.8 - 5.10 is 0.15, 0.55 and 1.0, respectively, and the thick lines in these graphs indicate that the Z score value is beyond the display scale.

The Z score is a function of the sampled values of x_s and x_m , the sample size, n , and the noise level of the system normal operation mode. The Z values for the simulations shown in Figures 5.8 - 5.10 are summarized in Table 5.1.

Thus, the Z score is sensitive to the noise level of the normal operation mode of the system, but it is not directly related to the current system noise level. As a result, this measure does not help the operator perform the variance comparison-test described in equation (5.2).

Another measure appearing useful and of help to the operator performing the comparison test described by equations (5.1) and (5.2) is the probability measure. This measure has been suggested by Moray [23]. In order to estimate the probability that the system has failed, a statistical model has been incorporated into FDLM. This model is discussed in Section 5.2 and a description of the Probabilities Display follows.

TABLE 5.1: Z VALUES FOR DIFFERENT NOISE LEVELS OF SYSTEM MEASURED OUTPUTS

NOISE LEVEL	Z VALUES OF UNFAILED SYSTEM	Z VALUES OF FAILED SYSTEM	SAMPLE SIZE
$\sigma = 0.15$	$ Z < 2.0$	$ Z > 5.0$	20
$\sigma = 0.55$	$ Z < 1.8$	$ Z > 3.0$	20
$\sigma = 1.0$	$ Z < 1.5$	$ Z > 2.0$	20

RD-A123 783

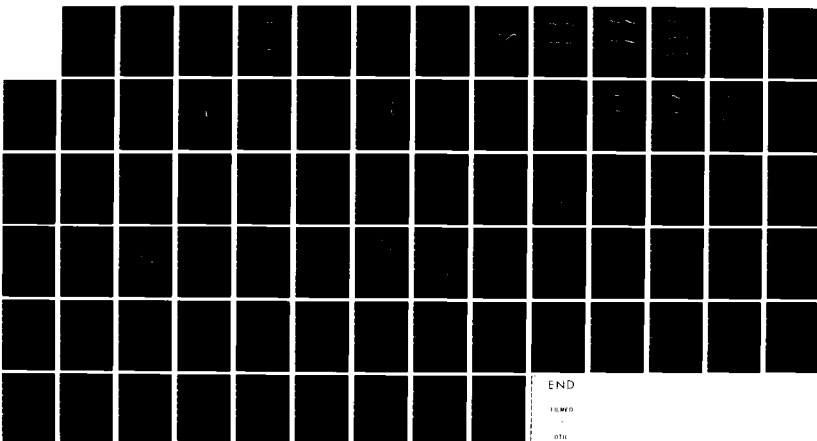
FAILURE DETECTION AND LOCATION METHOD (FDLM) (U)
MASSACHUSETTS INST OF TECH CAMBRIDGE MAN-MACHINE
SYSTEMS LAB U TSACH 30 SEP 82 N00014-77-C-0256

2/2

UNCLASSIFIED

F/G 5/8

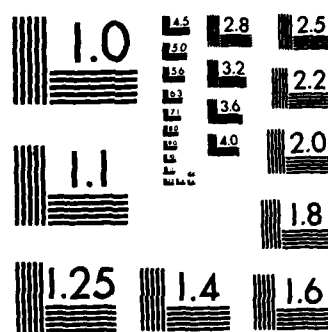
NL



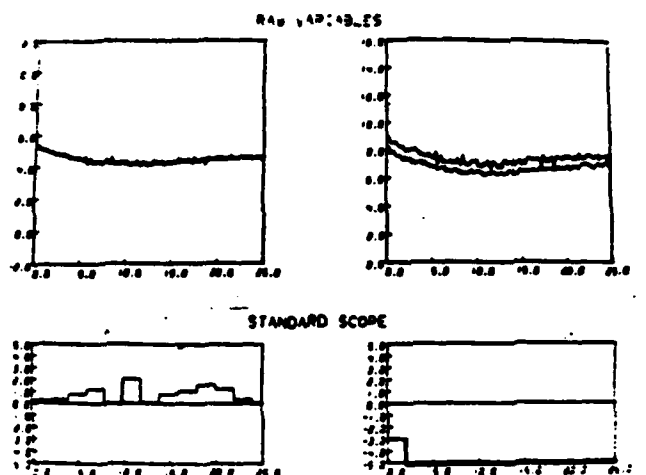
END

END

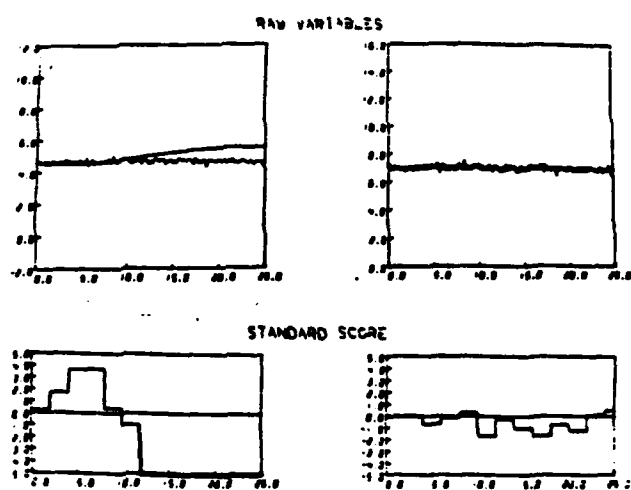
END



MICROCOPY RESOLUTION TEST CHART
NATIONAL BUREAU OF STANDARDS-1963-A

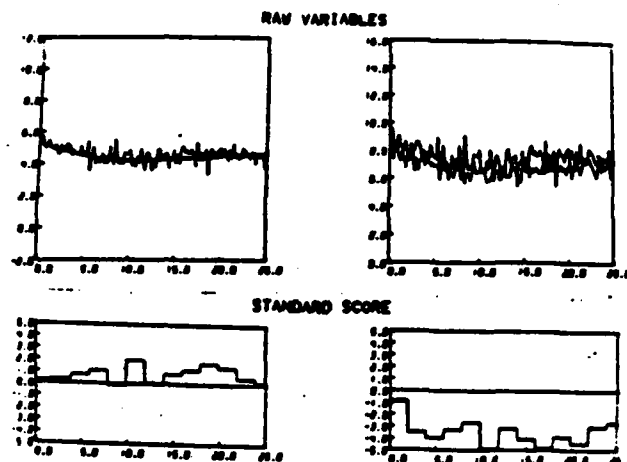


(a)

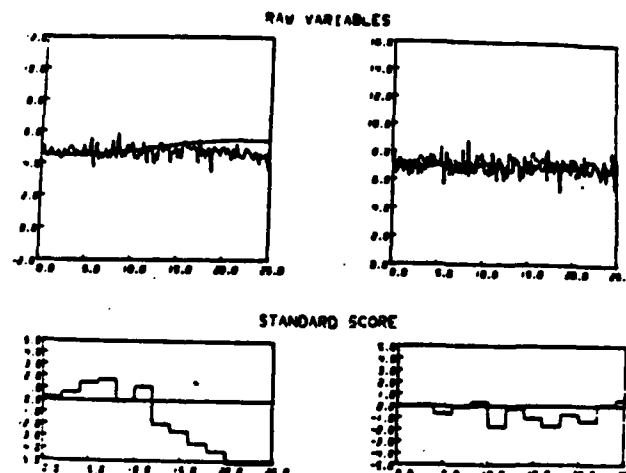


(b)

Figure 5.8 Standard score and raw variables display. The standard deviation of the noise is 0.15 in the output units. In 5.8a the failure is in the right subsystem and in 5.8b is in the left subsystem.



(a)



(b)

Figure 5.9 Standard score and raw variables display.
 The standard deviation of the noise is 0.55
 in the output units. In 5.9a the failure is
 in the right subsystem and 5.9b is in the
 left subsystem.

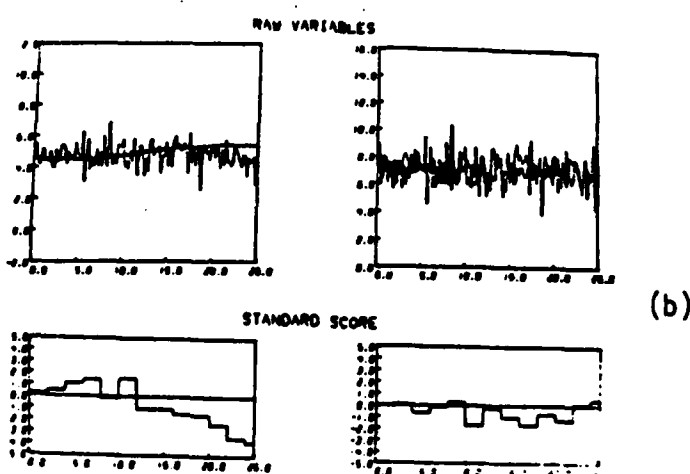
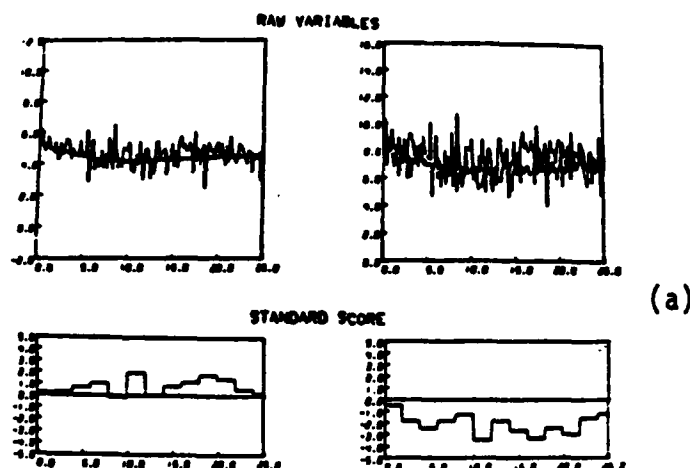


Figure 5.10 Standard score and raw variables display.
 The standard deviation of the noise is 1.0 in the output units. In 5.10a the failure is in the right subsystem and in 5.10b is in the left subsystem.

5.1.5 Probabilities Display

By using the Bayesian Statistical model discussed in Section 5.2.2 one can calculate the probability that the system has failed, based on:

1. A sampled difference between the system and model outputs,

$$\bar{x}'_d = \bar{x}'_s - \bar{x}'_m$$

2. An allowable difference threshold, Δ , of \bar{x}'_d
3. The standard deviation of the sampled difference in normal operation mode.

This probability is denoted as $p(\text{Failure} | \bar{x}'_d)$.

A measure that might be useful in drawing the operator's attention to a possible system failure is the ratio of probabilities of failure to no-failure, or, as it is called in the Bayesian theory, the odds ratio, Ω . Ω can be expressed mathematically as:

$$\Omega = \frac{p(\text{Failure} | \bar{x}'_d)}{p(\text{No Failure} | \bar{x}'_d)} \quad (5.6)$$

The odds ratio seems to be a useful measure because it is a comparative measure that people apply when the probabilities of two events are estimated [22]. In Figure 5.11 it is shown that the values of $p(\text{Failure} | \bar{x}'_d)$ lie between 0 to 1, whereas the corresponding odds ratio varies from 0 to ∞ . By setting a critical odds ratio value, Ω_c , and calculating the current odds values, Ω in real-time an indication of system failure is generated. The system is suspected to be failed when Ω exceeds Ω_c . Therefore, it is proposed to display the current Ω values. In addition, the time it exceeds Ω_c is displayed as well. Because of

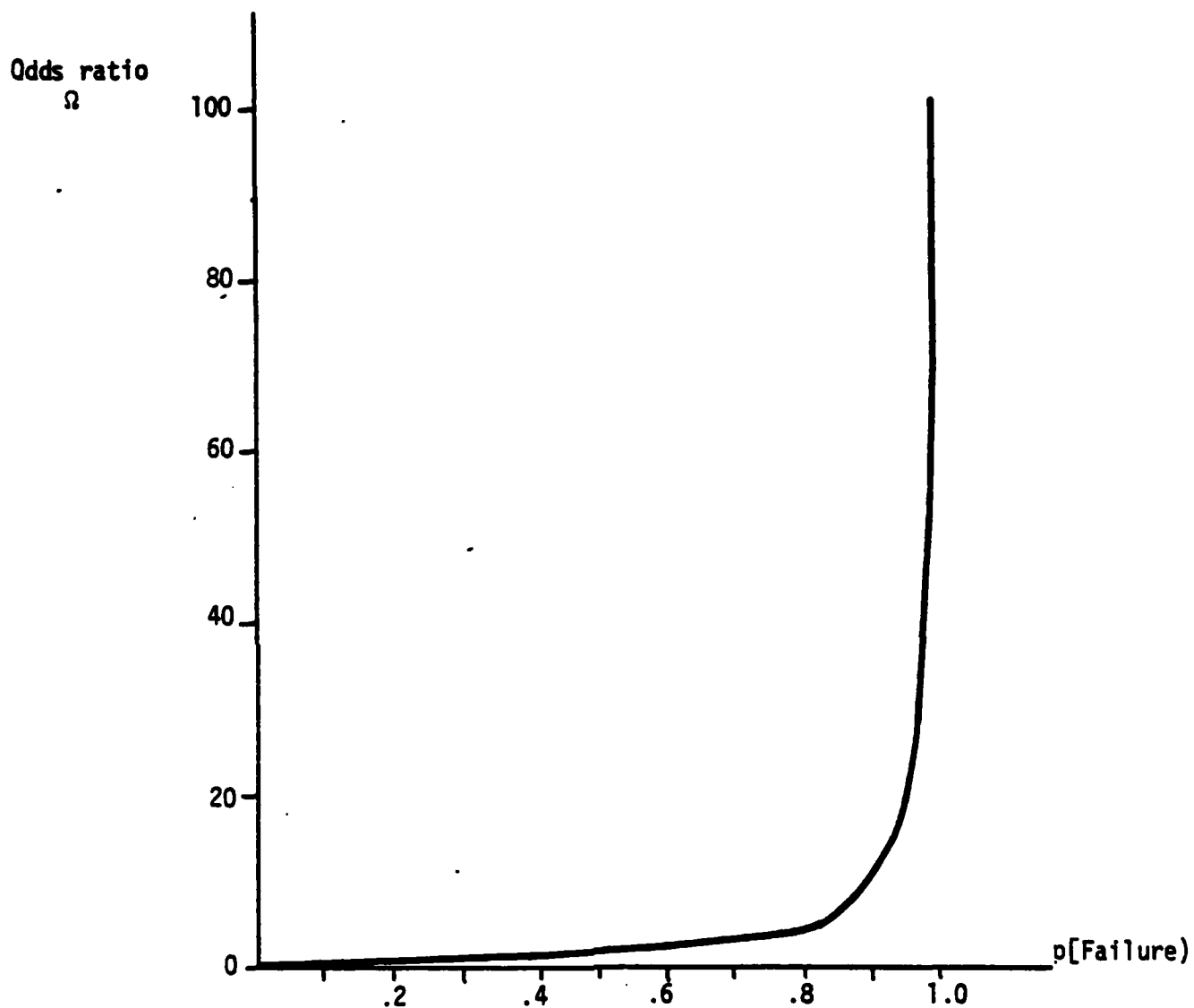


Figure 5.11 The odds ratio, Ω versus the probability of a system failure, $-p[\text{failure}]$.

system dynamics and noise effects Ω might exceed Ω_c for a short period of time. This, however, should not be considered to be a system failure. Thus the combination of the Ω value and the time it exceeds Ω_c indicates whether or not a system failure exists.

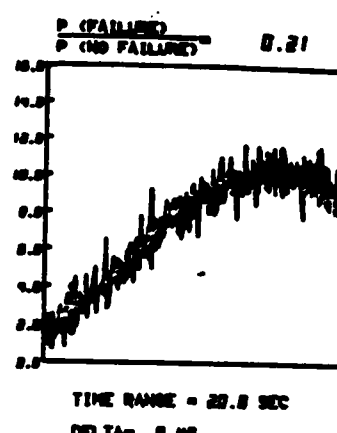
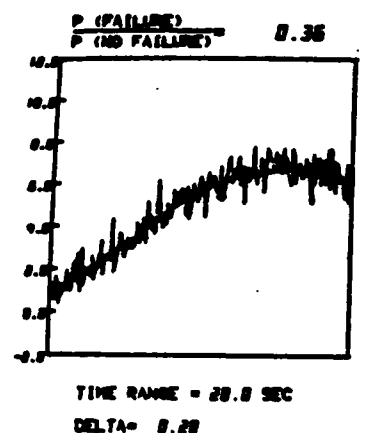
The Probabilities Display coupled with the Model Averaged Variables is shown in Figures 5.12 - 5.15. In this simulation Ω_c was set to be unity.

In these figures the odds ratios are displayed in a digital (numerical) form, and the system and model outputs in an analog form. This display is useful in determining the expected values (equation 5.1) as well as making the variances comparison tests (equation 5.2). In the case where a failure results in increasing the system noise level only the calculated odds ratio, Ω , will swing frequently below and above the critical odds value, Ω_c . In this case it might be useful to display the time history of the odds values. It is the capability to compare the expected values and the variances (equations 5.1 and 5.2) which makes the Probabilities Display very promising.

5.2 Incorporating a Statistical Model within FDLM

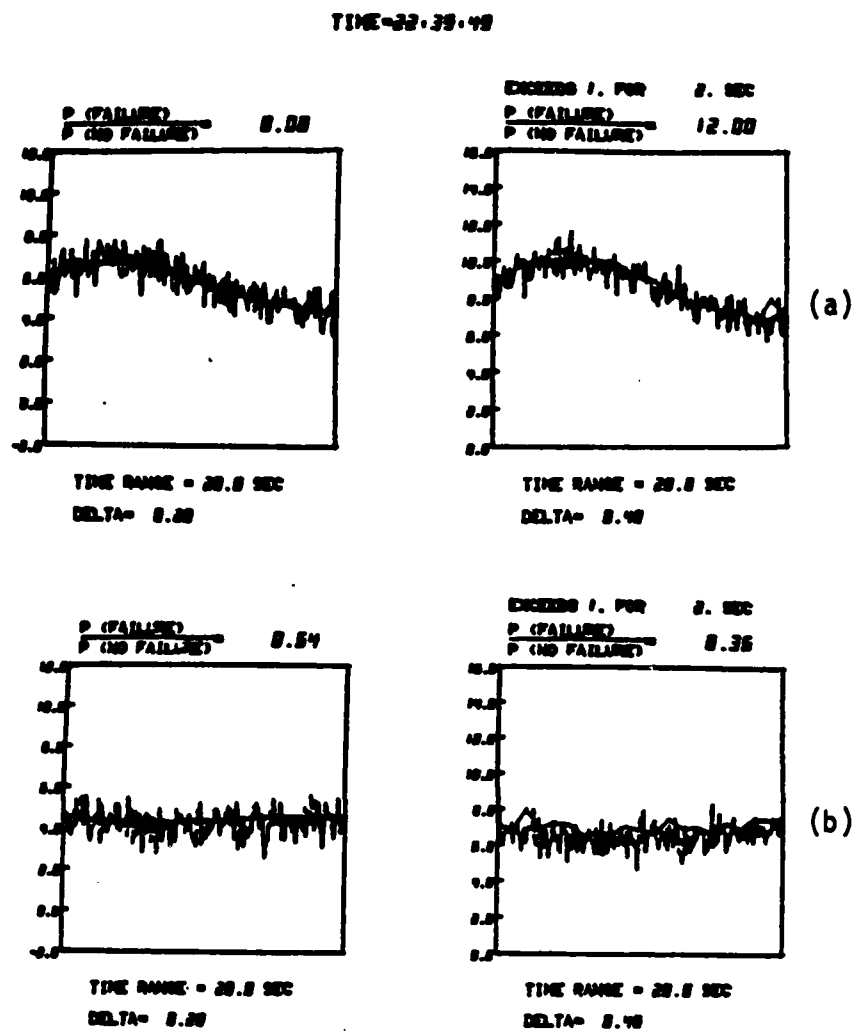
In Chapter 5.1.5 it has been shown that calculating and displaying the probability of a failure might help the operator perform the monitoring task. To calculate these probabilities, a statistical model has to be incorporated into FDLM. To construct this model it is assumed that x_s and x_m are the outputs of the system and the model, respectively. The standard deviation σ_d of the difference, $x_s - x_m$, for the system's normal operation mode can be estimated. For a sample of n

TIME=21.35.34



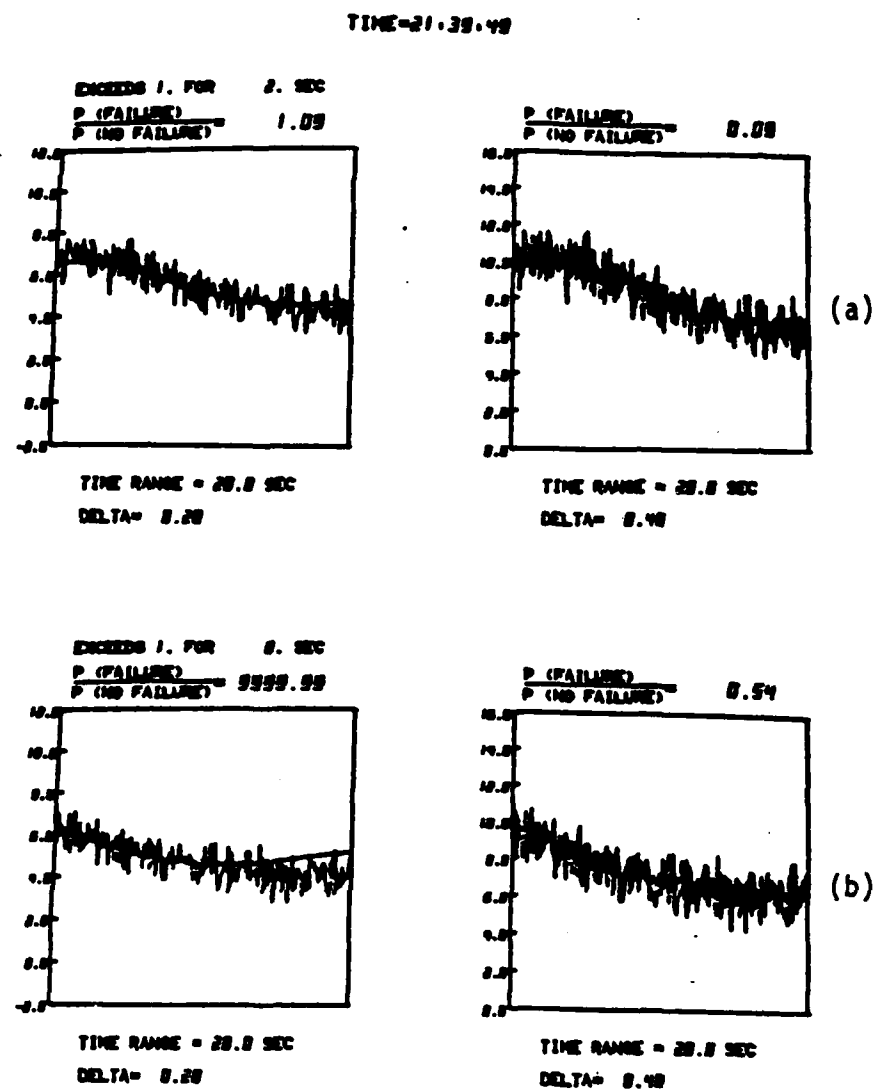
NO DISCREPANCY
MODERATE NOISE LEVEL

Figure 5.12 Raw system averaged model outputs display and the odd calculated by a Bayesian statistical model. The system is under normal conditions.



**RIGHT DISCREPANCY AT 22, 39, 39
MODERATE NOISE LEVEL**

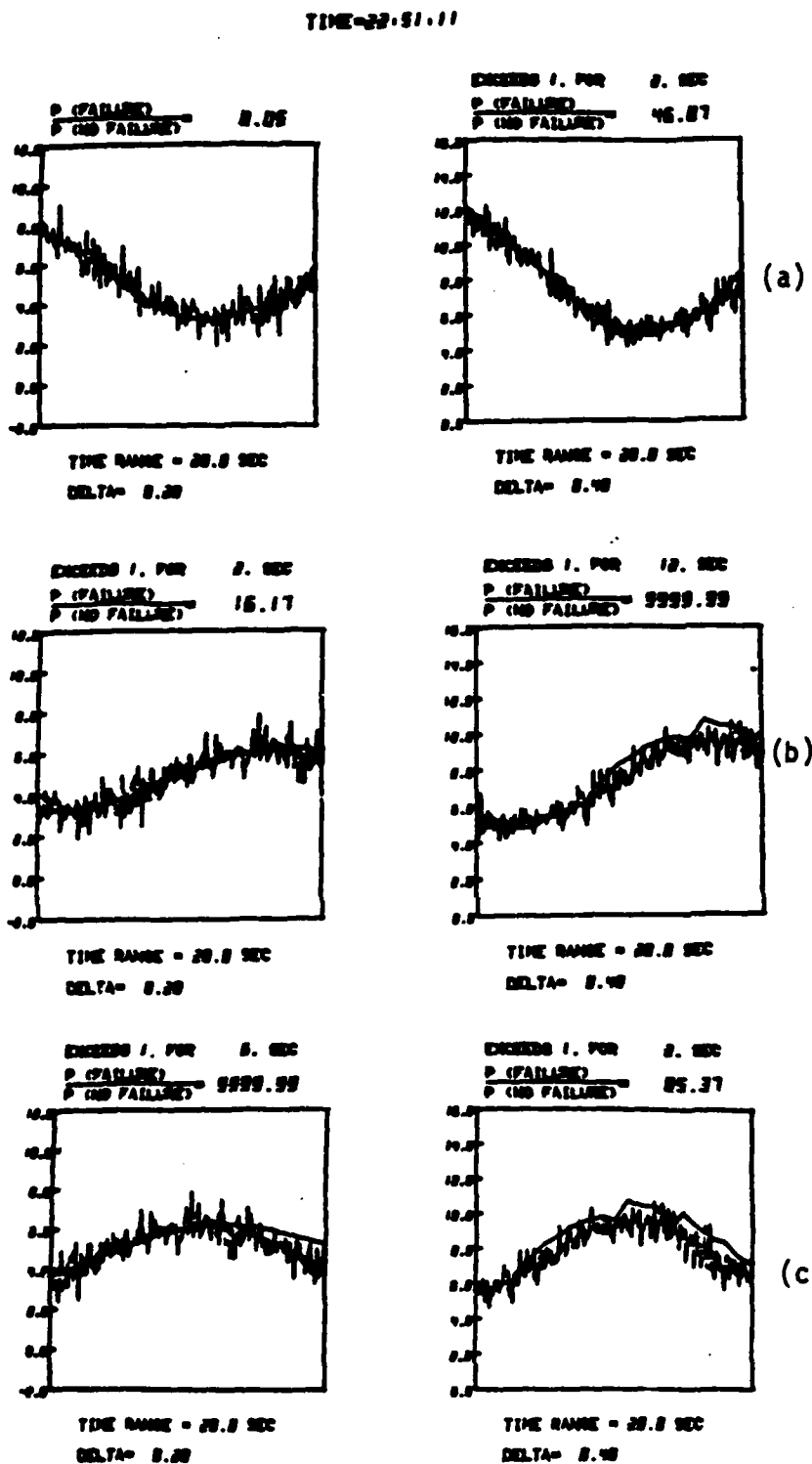
Figure 5.13 Raw system averaged model outputs display and the odds calculated by a Bayesian statistical model. There is a failure in the right subsystem.



LEFT DISCREPANCY AT 21.38.59

MODERATE NOISE LEVEL

Figure 5.14 Raw system averaged model outputs display and the odds calculated by a Bayesian statistical model. There is a failure in the left subsystem.



LEFT DISCREPANCY AT 22.51.81 AND RIGHT AT 22.51.82
MODERATE NOISE LEVEL

Figure 5.15 Raw system averaged model outputs display and the odds calculated by a Bayesian statistical model. There is a multiple failure in the left and the right subsystems.

observations from equation (5.1) the expected value of the sampled difference between the system and model outputs is \bar{x}'_d and its standard deviation is σ_d/\sqrt{n} .

If the sample size, n , is chosen to be large enough, the probability density function of \bar{x}'_d can be approximated as a Gaussian distribution. This is a result of the Central Limit Theorem [23]. The Gaussian assumption is valid if the n sampled system and model outputs are independent, identically distributed random variables with a finite expected value and a finite variance. This is regardless of the form of the probability density function of the individual x_s and x_m variables. In practical applications the probability density function of \bar{x}'_d calculated by 15 observations can be assumed to be Gaussian. There are two mutually exclusive, collectively exhaustive hypotheses one has to consider.

Null Hypothesis H_0 : $\bar{x}'_d = x_0$ no failure exists

Alternative Hypothesis H_1 : $\bar{x}'_d > |x_0|$ failure exists

where x_0 in this application is zero if no prior lies between system and model is assumed. Two basic statistical models can be constructed to test the H_0 and H_1 hypotheses. These two models are discussed as follows.

5.2.1 Classical Hypothesis Testing

Using the Classical Hypothesis Testing one can calculate the rarity of the obtained sampled difference, \bar{x}'_d , assuming that the null hypothesis, H_0 , is true.

The assumption that H_0 is true implies that the probability density function is centered on the x_0 value, as shown in Figure 5.16. The probability that the difference x_d exceeds the absolute sampled value, \bar{x}'_d , is represented by the crossed area shown in Figure 5.16. If \bar{x}'_d is far enough out in either tail meaning $p(\bar{x}'_d > |\bar{x}_d| | H_0)$ is low (less than 0.05 by convention), the null hypothesis, H_0 , is rejected, which implies that the alternative hypothesis, H_1 , is accepted.

Classical Hypothesis Testing does not evaluate the alternative hypothesis directly. H_1 is either accepted or rejected based on testing the H_0 hypothesis. The difficulty to test H_1 directly results from the fact that the value of the population mean of the difference, \bar{x}_d , cannot be specified when H_1 is assumed to be true. In this case \bar{x}'_d can get a range of values. This is in contrast to the H_0 assumption that sets \bar{x}'_d to be a single value, x_0 . The difficulty to apply the Classical approach to test the hypothesis that the system has failed, has been recognized by Gai and Curry [24] who suggested ways to overcome it.

5.2.2 Bayesian Approach

Using the Bayesian statistical model one can calculate the probability that the system has failed based on a sampled averaged difference, \bar{x}'_d . This Probability is denoted as $p(\text{Failure} | \bar{x}'_d)$. The probability density function of \bar{x}_d in this model is centered on the sampled \bar{x}'_d value as shown in Figure 5.17. By setting an allowable difference between the system and the model outputs, the $p(\text{Failure} | \bar{x}'_d)$ can be calculated. This probability is represented as the crossed

Probability
Density
Function

$$N(0, \frac{\sigma_d}{\sqrt{n}})$$

$$\blacksquare p(\bar{x}_d > |x_d'| | H_0)$$

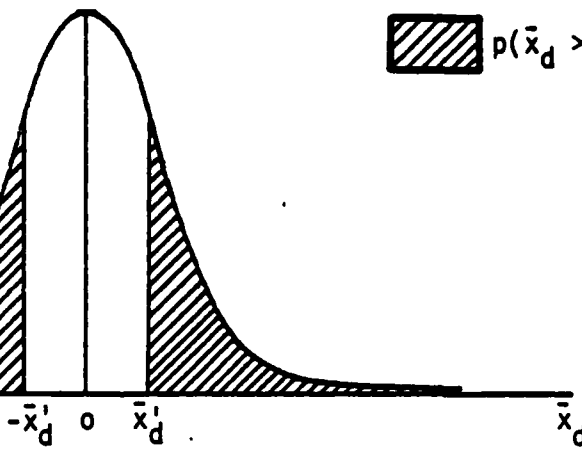


Figure 5.16 The classical hypothesis testing centers the probability density function on zero. The crossed area is the probability that \bar{x}_d exceeds the absolute obtained value, $|x_d'|$.

area in Figure 5.17.

When the system fails, the observed \bar{x}_d' value deviates from the x_0 value and the calculated probability that the system has failed is increased. This is shown in Figure 5.18.

The ratio of the probability that the system has failed to the probability that the system has not failed is the odds ratio, Ω . Ω can be expressed mathematically as:

$$\Omega = \frac{P(\text{Failure}|\bar{x}_d')}{P(\text{No Failure}|\bar{x}_d')} = \frac{P(H_1|\bar{x}_d')}{P(H_0|\bar{x}_d')} \quad (5.7)$$

The advantages of displaying the odds ratio to the operator are discussed in Section 5.1.5. The odds ratio can be calculated based on one or more samples of n system and model outputs. For the case of two samples of size n the expected value of the difference can be expressed as:

$$\bar{x}_d = \frac{1}{n} \sum_{i=1}^n (x_{s_i} - x_{m_i}) + \frac{1}{n} \sum_{i=n+1}^{2n} (x_{s_i} - x_{m_i}) \quad (5.8)$$

and the standard deviation of this \bar{x}_d value is $\sigma_d/\sqrt{2n}$. Combining the information of two samples of size n is described graphically in Figure 5.19. Tzelgov [25] has shown how this property can be used to combine the operator's subjective belief in calculating the probability of a system failure.

In applying the Bayesian statistical model, accumulating sampled information might cause misleading results. Consider the case where a

Probability
Density
Function

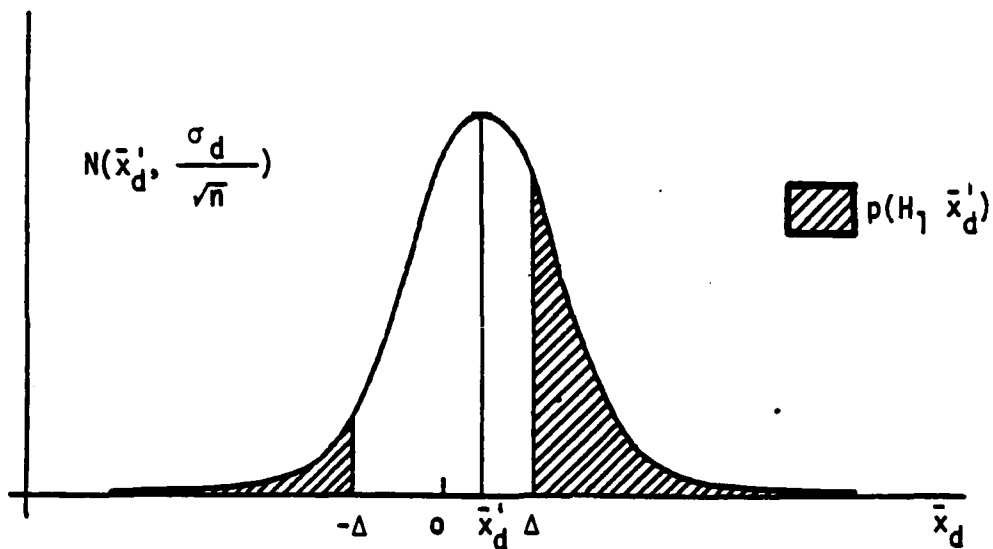


Figure 5.17 The Bayesian model centers the probability density function on \bar{x}_d' . The crossed area is the probability that the system has failed.

Probability
Density
Function

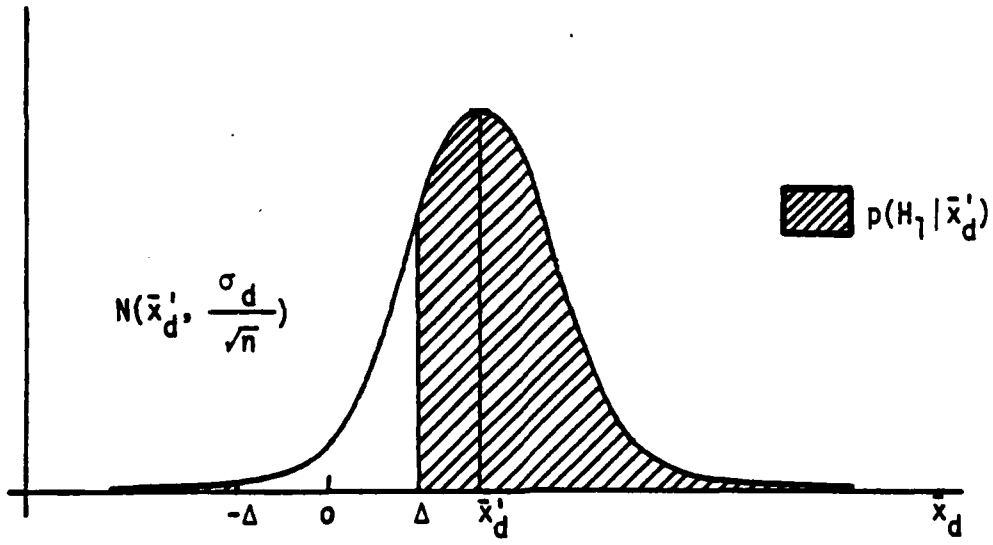


Figure 5.18 The Bayesian model centers the probability density function on \bar{x}_d' . The crossed area is the probability that the system has failed. $p(\text{failure})$ is increased when \bar{x}_d' increases.

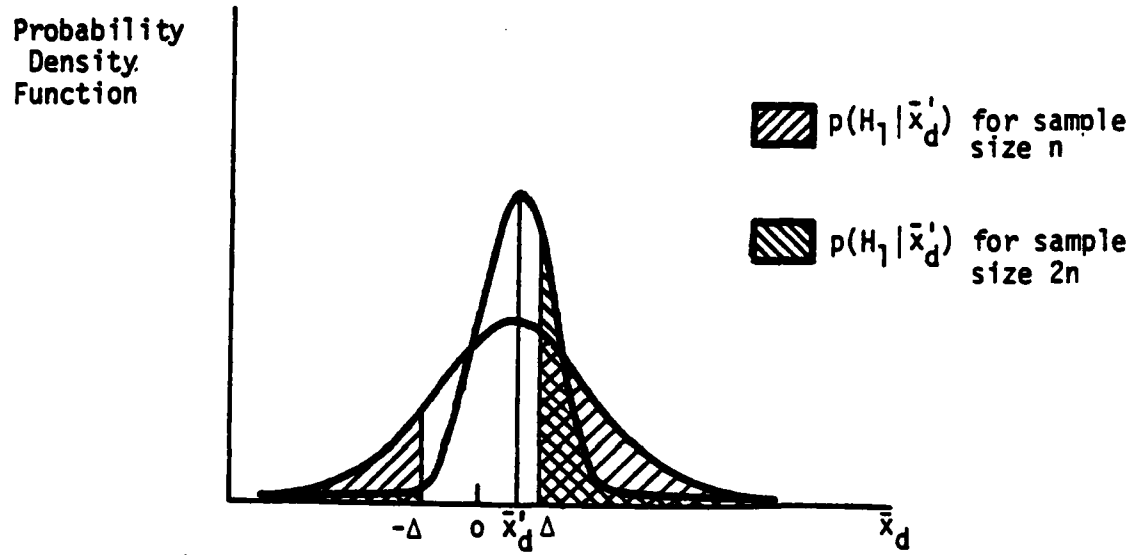


Figure 5.19 The Bayesian model is able to accumulate information. The probability calculation is changed by accumulating the information of two samples of size n .

system failure occurs after a long time of normal operation. By accumulating the non-failure information, the calculated odds ratio and the standard deviation are both small numbers, reflecting the certainty that the model gained by having the system operating normally. As a result, it will be long before the "belief" that the system has not failed is overcome, and the statistical model will indicate that the system has failed only long after it has occurred. Therefore, non-failure information is not accumulated. On the other hand, information which indicates that the system has failed is accumulated. This structure of not accumulating non-failure, and accumulating the failure information, results in minimizing the chances that a failure will not be detected shortly after it has occurred.

5.3 Computer/Human-Operator Interaction in Applying FDLM

FDLM is intended to run continuously during the system operation, waiting for significant discrepancies between actual systems and model outputs. The task of monitoring the system and model outputs, if performed by a human operator, is boring and has high cognitive load. For these reasons the routine monitoring task should be performed by a human operator, is boring and has high cognitive load. For these reasons the routine monitoring task should be performed by computer. The computer would examine all available system measurement points simultaneously, as shown in Figure 2.12. According to this examination the computer, if necessary, will alert the operator and locate the defective subsystems. When the operator is alerted his task then is to confirm the evidence of a system failure and to identify the failed

components of the defective subsystems. These components can be identified either by using the operator's knowledge and experience, or by applying simple fault/event tree analysis to the suspected defective subsystems. By identifying the defective subsystems, the required fault/event trees are drastically simplified. Therefore the combination of FDLM and the fault/event tree analysis seems to be very promising.

A suggested FDLM computer/human operator interface is shown in Figure 5.20. In this interface a schematic description of the system is displayed together with the odds ratio, calculated by the computer. When the odds ratio of a particular point exceeds the critical value, Ω_c , the operator is alerted, and his task then is to confirm the evidence of a failure by checking the corresponding system and model outputs viewed on a separate CRT display.

Five different displays were described and evaluated earlier in this Chapter. To determine the most powerful display, an experiment was conducted in the M.I.T. Man-Machine Systems Laboratory. In this experiment eight subjects were asked to monitor the system and model outputs in real time and to detect possible system failures. The experiment and its results are discussed more fully in Chapter 6.

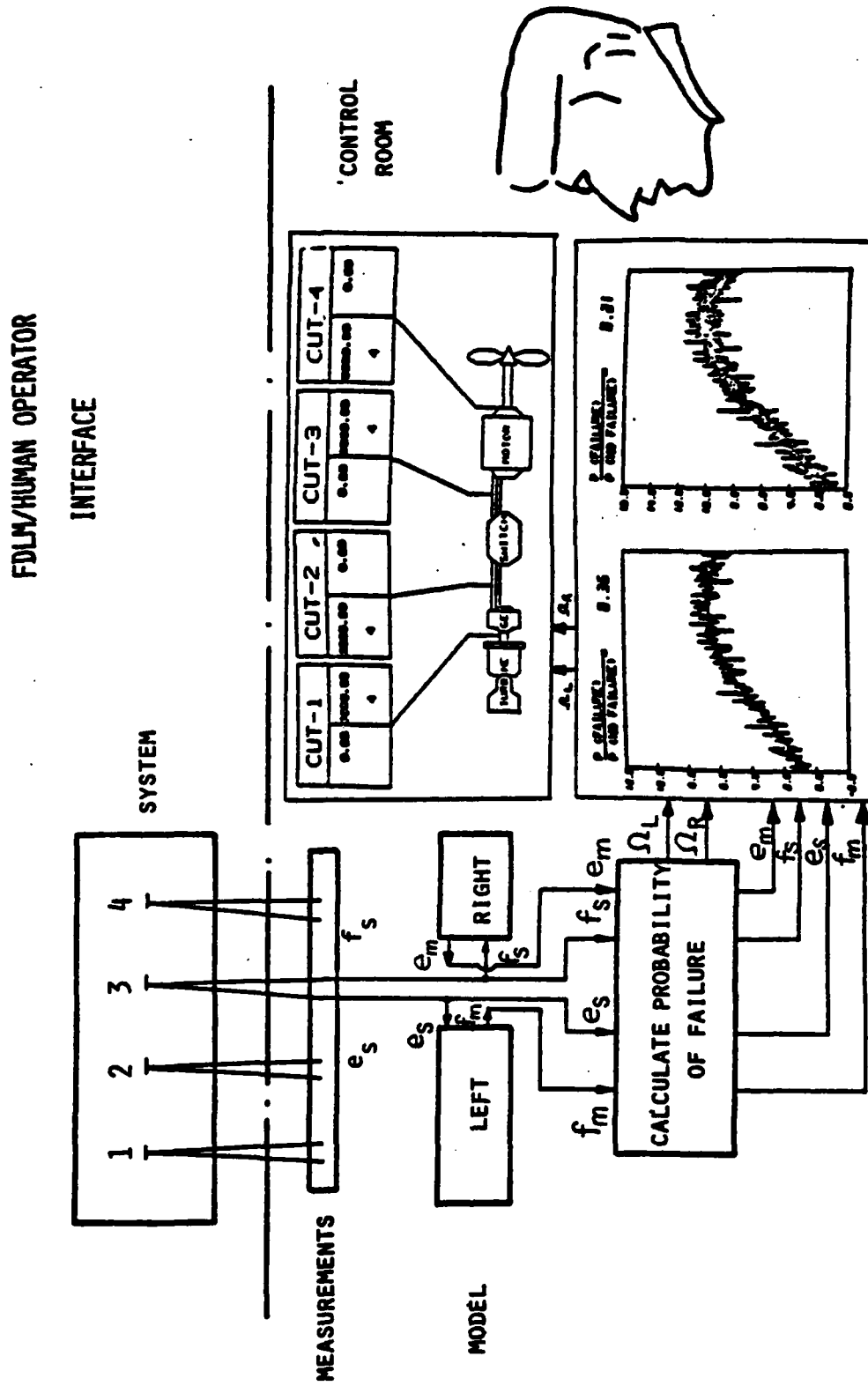


Figure 5.20 Proposed FDLM computer/human operator interface. A schematic description as well as the system and model outputs are displayed to the operator.

CHAPTER 6

EXPERIMENTAL DETERMINATION OF AN OPTIMAL DISPLAY

6.1 Experimental Goals

The display interface between FDLM and the human operator can be constructed in various ways. Five different displays were discussed in Section 5.1. The most useful displays should enable the operator to detect system failures shortly after they have occurred, and to minimize the two possible errors of false alarms and misses. For this reason, the five displays were compared experimentally.

Informal observations have indicated that the probabilities combined with the averaged or raw variables display results in short failure detection time and low miss and false alarms rates. The failure detection, referred to also as the subject's reaction time, was measured from the time a system failure has been introduced to the time the subject has detected it.

The performance of the human operator, monitoring real-time system and model outputs and using the Probabilities Display, was determined experimentally. The experiment was conducted in the Man-Machine Systems Laboratory in M.I.T. The goals of the experiment were to determine how the performance of the human operator is affected by:

1. Including/not including state variables in the referenced sub-models.
2. Displaying raw noisy/averaged system and model outputs.
3. Displaying different digital (numerical) calculated measures in addition to the analog signals of the system and model outputs.

To meet these goals the experiment was designed as follows.

6.2 Experimental Design

To explore the effects of including/not including state variables in the referenced submodels the experiment was performed in two sessions. In one session the referenced submodel contained state variables, and in the other session it did not. There were 240 experimental trials in each session. The types of analog output and digital displayed information in these trials are summarized in Table 6.1. There were 20 experimental trials for each combination of digital and analog information.

TABLE 6.1: THE COMBINATIONS OF ANALOG AND DIGITAL DISPLAYED INFORMATION EACH HAVING 20 EXPERIMENTAL TRAILS

Digital Analog	No digital information	odds ratio Ω	the time Ω exceeds 1, t_{Ω}	Ω & t_{Ω}
Raw system & model outputs	20	20	20	20
Raw system & smooth model outputs	20	20	20	20
Smooth system & model outputs	20	20	20	20

The effects of displaying noisy/smooth system and model outputs were explored by changing the type of the analog information. The analog outputs were generated in three forms:

1. Raw system and model outputs.
2. Raw system and smooth model outputs.
3. Smooth system and model outputs.

These three types of outputs are shown in Figure 6.1 and 6.2 for the state variable and non-state variable cases, respectively. Although the displays of raw system and model outputs and raw system and smooth model outputs in the state variable case are similar, these two types of analog outputs were included in the experiment to balance the non-state variable case.

The effects of displaying different digital (numerical) measures were determined by combining the described analog outputs with the following digital forms:

1. No digital information displayed.
2. The odds ratio, Ω , is displayed.
3. The time Ω exceeds 1 is displayed, t_{Ω} .
4. The odds ratio, Ω , and the time it exceeds 1, t_{Ω} , are displayed.

These four types of digital information combined with the raw variables display are shown in Figure 6.3. Eight subjects participated in this experiment. The subjects were Mechanical Engineering students who had some background in control and modeling. The experiment was performed in two sessions consisting of 240 experimental trials each. The reliability of the simulated system was assumed to be 0.5. That is, in 50% of the experimental trials (for each analog and digital combination), a system failure was introduced early in the trial, by changing one of the system parameters stepwise. The failure occurrences were randomly ordered. Each trial lasted 35 seconds, unless it was interrupted by the subject detecting a failure.

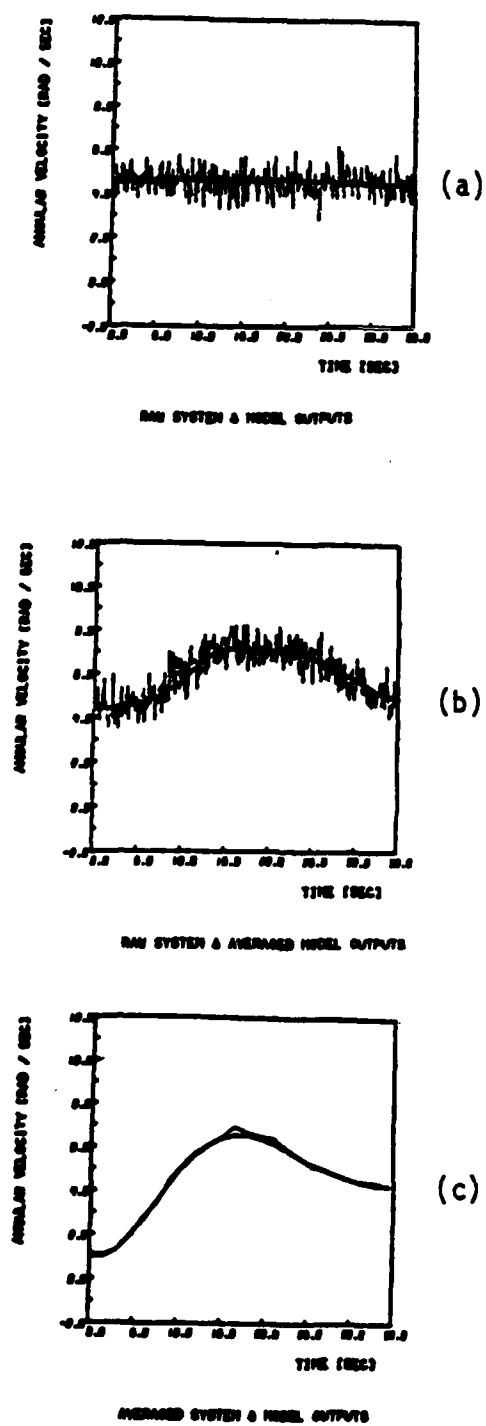


Figure 6.1 Raw system and model outputs in 6.1a, raw system and averaged model outputs in 6.1b, and averaged system and model outputs in 6.1c. The submodels generating these outputs include state variables.

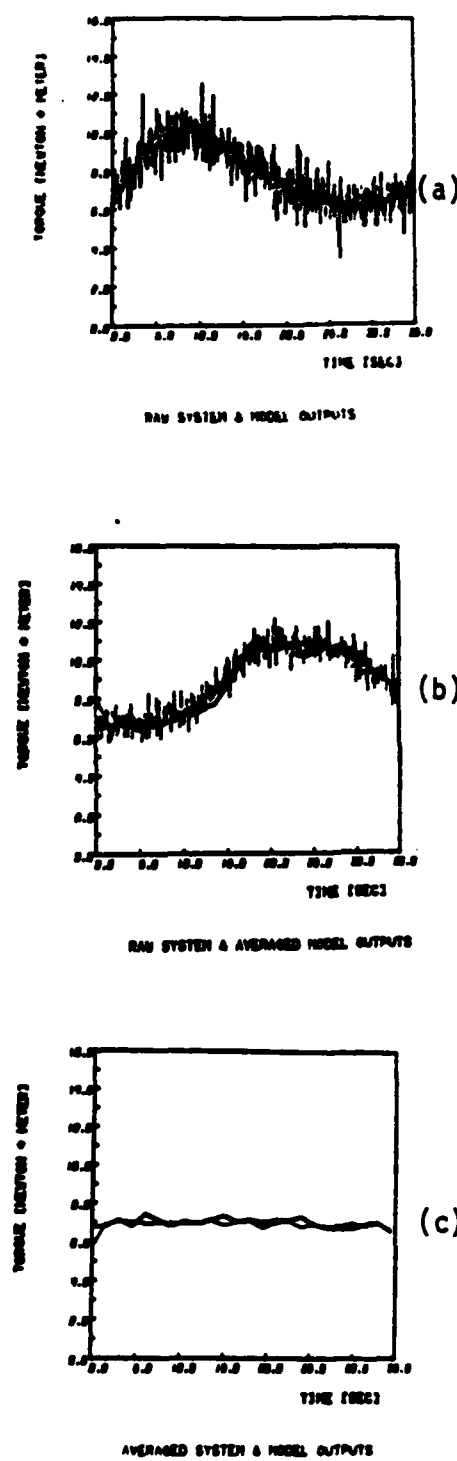
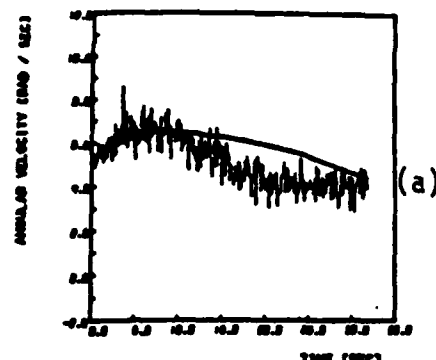
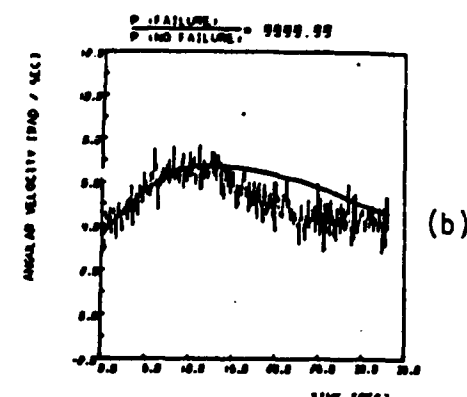


Figure 6.2 Raw system and model outputs in 6.2a, raw system and averaged model outputs in 6.2b, and averaged system and model outputs in 6.2c. The submodels generating these outputs do not include state variables.



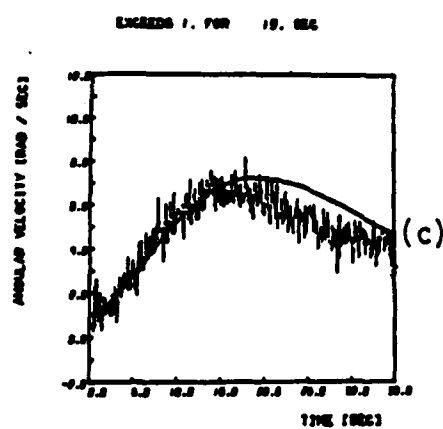
RAW SYSTEM & MODEL OUTPUTS

NO DIGITAL INFORMATION



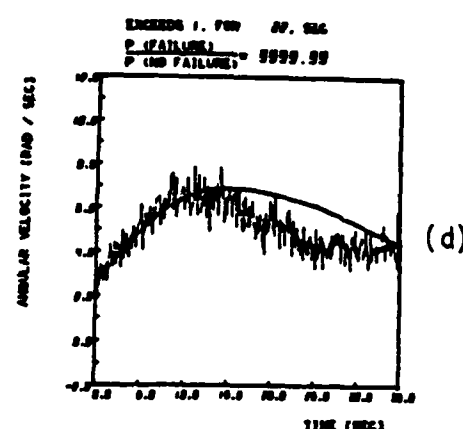
RAW SYSTEM & MODEL OUTPUTS

DIGITAL: PROBABILITY RATIO IS DISPLAYED



RAW SYSTEM & MODEL OUTPUTS

DIGITAL: TIME DURING WHICH THE PROBABILITY RATIO EXCEEDS 1



RAW SYSTEM & MODEL OUTPUTS

DIGITAL: PROBABILITY RATIO AND THE TIME DURING WHICH IT EXCEEDS 1

Figure 6.3 Digital information display. No digital information in 6.3a the odds ratio, Ω , in 6.3b, the time Ω exceeds 1, t_Ω , in 6.3c, and Ω plus t_Ω in 6.3d.

There were four independent variables associated with this experiment:

- A. State-variable-included in model no-state-variable-included. This is an within-subjects variable, where A1 is the case where the compared model output is generated by a submodel which contains a state variable, and A2 is the case where the submodel does not contain a state variable. To balance this effect, a session order variable was introduced.
- B. Sessions order. This is a between-subjects variable where, B1 is starting with the state-variables session and proceeding with the no-state-variable-session, and B2 is starting with the no-state-variable session and proceeding with the state-variable one. This variable was balanced by assigning B1 to the first four subjects, and B2 to the second four.

- C. The type of analog outputs.

- C1 = Raw system and model outputs.
- C2 = Raw system smooth model outputs.
- C3 = Smooth system and model outputs.

- D. The type of the displayed digital measure.

- D1 = No digital information is displayed.
- D2 = The odds ratio, Ω , is displayed.
- D3 = The time, t_{Ω} , the odds exceeds 1 is displayed.
- D4 = The odds ratio, Ω , and the time t_{Ω} , it exceeds 1 are displayed.

Each experimental session contained four blocks, standing for the four digital information displays D1 - D4. The type of the analog outputs changed within each block in a random order, where the digital information was balanced using the latin square technique discussed in [26].

Both C and D are within subjects-variables.

6.3 Experimental Method

The subjects participating in this experiment were asked to monitor in real-time the system and model outputs. The simulated system is described in the experimental instructions in Appendix A. The subject's task was to use all the available information displayed on the CRT screen to decide whether the system in any particular trial was or was not defective. The system time constant as well as the threshold size were specified to the subjects. There were two control buttons:

1. Start
2. Alarm

Each trial was initiated by pressing the Start button. The alarm was to be pressed when a system failure was detected. The subjects were told that their reaction time and accuracy were of equal importance. Therefore, immediately after they were certain that the system had failed, they pushed the Alarm button.

In order to establish a certain level of familiarity with the simulation, the subjects had practice trials in which they were notified whether or not they made the right decision.

6.4 Experimental Results

The effects of the experimental variables described in Section 6.3 can be explored by analyzing the experiment in the light of:

1. The accuracy of the subjects decisions.
2. The subject's reaction times for detecting system failures.

The results of this analysis suggest the "best" digital/analog display combination by which fast and accurate system failure detections are obtained.

6.4.1 Accuracy Analysis

The percentages of false alarms and misses are summarized in Tables 6.1 and 6.2 for the state-variable and no-state-variable-cases, respectively. These values are based on 160 observations for each combination of analog and digital displayed information.

In the no-state-variable case (Table 6.2) the percentage of false alarms and misses was reduced from 13.75 and 11.25 to zero either by displaying smooth analog outputs, or by adding digital information. In the state-variable case (Table 6.3) these percentage values do not exceed 2.5%. This reflects the fact that the model outputs in this case are smooth in their raw form, which makes the detection task easier.

6.4.2 Analysis of the Subjects' Reaction Times

The average reaction times of the subjects are summarized in Tables 6.4 and 6.5 for the state-variable and no-state-variable cases, respectively. These data have been subjected to a four-way analysis of variance. The results of this analysis are:

1. The displayed digital information causes the reaction times to change significantly. Applying the F test results in an $F(2, 18)$ of 5.02 which is significant for probability $P < 0.02$. The averaged reaction times for the different digital displays are shown in Figure 6.4. The Newman-Keuls test [27] indicates insignificant differences between the reaction times for displaying no digital information versus displaying the time

TABLE 6.2: PERCENTAGES OF FALSE ALARMS (FA) AND MISSES (MS)
FOR THE NO-STATE-VARIABLE CASE

Digital Analog	No digital		Ω		t_Ω		$\Omega & t_\Omega$	
	FA	MS	FA	MS	FA	MS	FA	MS
Raw system & model outputs	13.75	11.25	0.0	0.0	3.75	0.0	0.0	0.0
Raw system & smooth model outputs	5.0	1.25	0.0	0.0	1.2	0.0	2.5	1.25
Smooth system & model outputs	0.0	0.0	0.0	0.0	0.0	0.0	0.0	0.0

TABLE 6.3: PERCENTAGES OF FALSE ALARMS (FA) AND MISSES (MS)
FOR THE STATE-VARIABLE CASE

Digital Analog	No digital		Ω		t_Ω		$\Omega & t_\Omega$	
	FA	MS	FA	MS	FA	MS	FA	MS
Raw system & model outputs	0.0	0.0	1.25	0.0	0.0	0.0	0.0	0.0
Raw system & smooth model outputs	1.25	1.25	1.25	0.0	1.25	0.0	1.25	0.0
Smooth system & model outputs	2.5	0.0	0.0	0.0	2.5	0.0	2.5	0.0

TABLE 6.4: SUBJECTS' AVERAGE REACTION TIMES FOR THE STATE-VARIABLE CASE. TIME IN SECONDS

Analog \ Digital	No digital information	Ω	t_Ω	$\Omega & t_\Omega$
Raw system & model outputs	17.12	17.90	16.30	16.15
Raw system & smooth model outputs	17.72	17.90	16.77	16.77
Smooth system & model outputs	17.10	16.8	17.17	16.02

TABLE 6.5: SUBJECTS' AVERAGE REACTION TIME FOR THE NO-STATE VARIABLE CASE. TIME IN SECONDS.

Analog \ Digital	No digital information	Ω	t_Ω	$\Omega & t_\Omega$
Raw system & model outputs	11.72	8.85	7.70	8.70
Raw system & smooth model outputs	11.35	9.22	9.35	8.70
Smooth system & model outputs	8.62	7.25	6.97	8.90

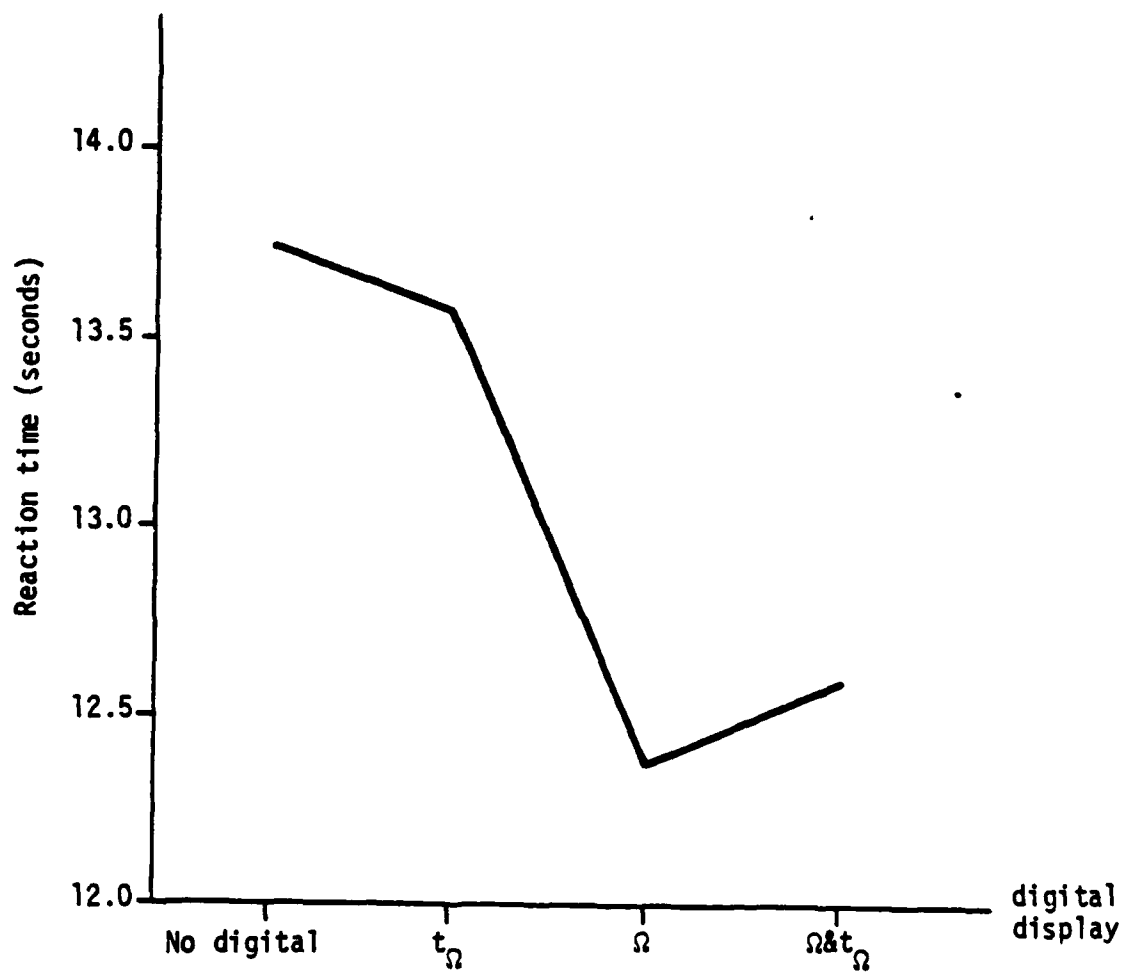


Figure 6.4 The operators' reaction times versus the different digital information displays.

over which Ω exceeds 1, t_{Ω} . Furthermore, the reaction time differences between displaying Ω and Ω plus t_{Ω} are not significant, as well. However, displaying either Ω or the combination of Ω and t_{Ω} is better than displaying t_{Ω} alone or not displaying digital information at all. This is true for both state-variable and no-state-variable cases.

2. Changing the type of the analog outputs results in significant differences of the reaction times. The analog outputs variable turns out to have interactions with the state-variable/no-state-variable. To analyze this relation the Newman-Keuls test was applied and the results are summarized in Table 6.6. The A1-A2 and C1-C3 variables are defined in Section 6.2.

TABLE 6.6: THE INTERACTION BETWEEN THE DIFFERENT ANALOG OUTPUTS AND THE STATE VARIABLE/NO-STATE VARIABLE CASES

	C1 vs C2	C1 vs C3	C2 vs C3
A1	no significant	not significant	not significant
A2	not significant	significant $P < 0.01$	significant $P < 0.01$

These indicate that in the case of a state-variable-included in the model, reaction times are not affected significantly changing the analog outputs display. However, in the no-state-variable case they are affected significantly by changing the analog display. The reaction times for the state-variable and no-state-variable cases, as a function of the types of the analog outputs, are shown in Figure 6.5. The best

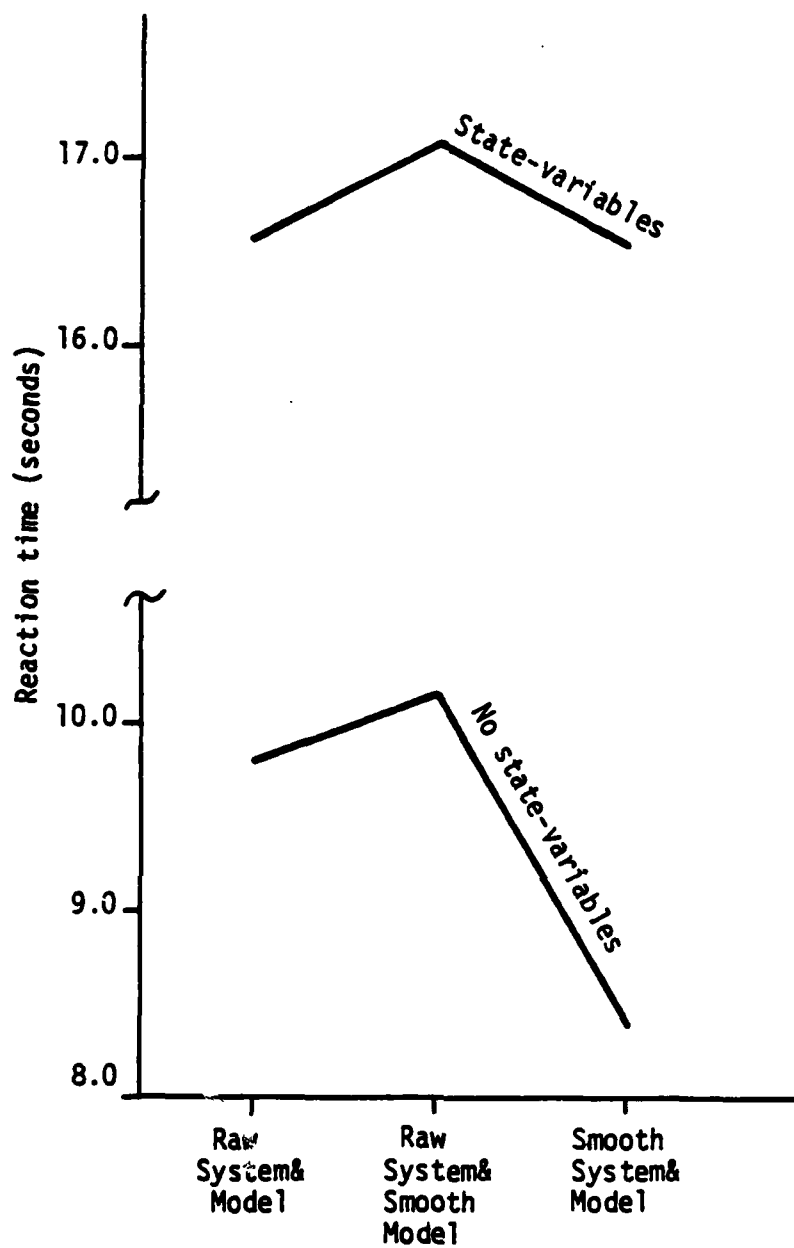


Figure 6.5 The operators' reaction times, versus the different analog outputs for state and no-state variables cases.

results are obtained using the smooth system and model outputs, where the raw and smooth model outputs (C1 and C2) do not differ significantly in their effects on reaction time.

6.5 Summary and Conclusions

The experimental results described in Sections 6.4.1 and 6.4.2 show that:

1. The failure detection task is easier when the calculated model output is generated by a submodel which contains state-variables. In this case, the rates of false alarm and miss are low, regardless of the type of analog output and digital information displayed. For this case, however, failure causes the model-associated output to deviate from its system value only after a time delay as discussed in Section 5.2.1.
2. Displaying additional digital information improves the operator's performance. In particular, the odds ratio, Ω , and the odds combined with the time it exceeds Ω_c , t_Ω , give the best results.
3. Displaying the smooth model and system output results in the best operator performance. In the no-state-variable case, the operator's reaction time is decreased significantly. Since the smooth system and model outputs display eliminates important system noise level information, the raw system and smoothed model output display is preferred. This is used in the Ship's Engine simulation described in Chapter 7.

CHAPTER 7

SHIP'S ENGINE SIMULATION

7.1 A Description of the Ship's Engine Simulation

In the following example, FDLM is applied to part of a ship's engine. The engine's simulation includes a gas turbine, which rotates a three phase ac generator. The generator produces electric power, which forces the ac motor to spin the ship's propeller. This system is depicted in Figure 7.1, and its model is shown in Figure 7.2. It is assumed that the power variables can be measured at four different locations in the system (points 1-4 in Figure 7.2).

The input variables of the simulation are the pressure and the temperature of the gas at the turbine's inlet. The turbine is simulated as a transformer, as constructed by Markunas in [28]. The three phase ac motor and generator are simulated using Paynter's models discussed in [29] and [30].

The model of the ship's engine has been implemented on the PDP11 computer system of the Man-Machine Systems Laboratory in M.I.T. To interface FDLM with the human operator, a schematical description of the engine is displayed on the Lexidata's screen, as shown in Figure 7.3. The four available measurement points and their correspondence calculated probability ratios are displayed, as well. When one of the calculated probability ratios exceeds its critical value (1 in our case), the time in seconds during which it has happened is displayed below the over-critical probability ratio value.

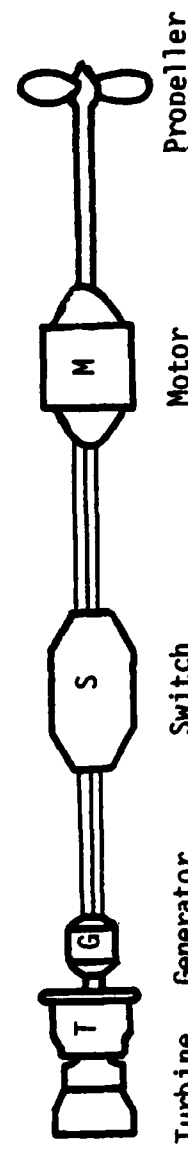


Figure 7.1 The ship's engine simulation consists of a turbine, three phase ac generator, switch, motor and propeller.

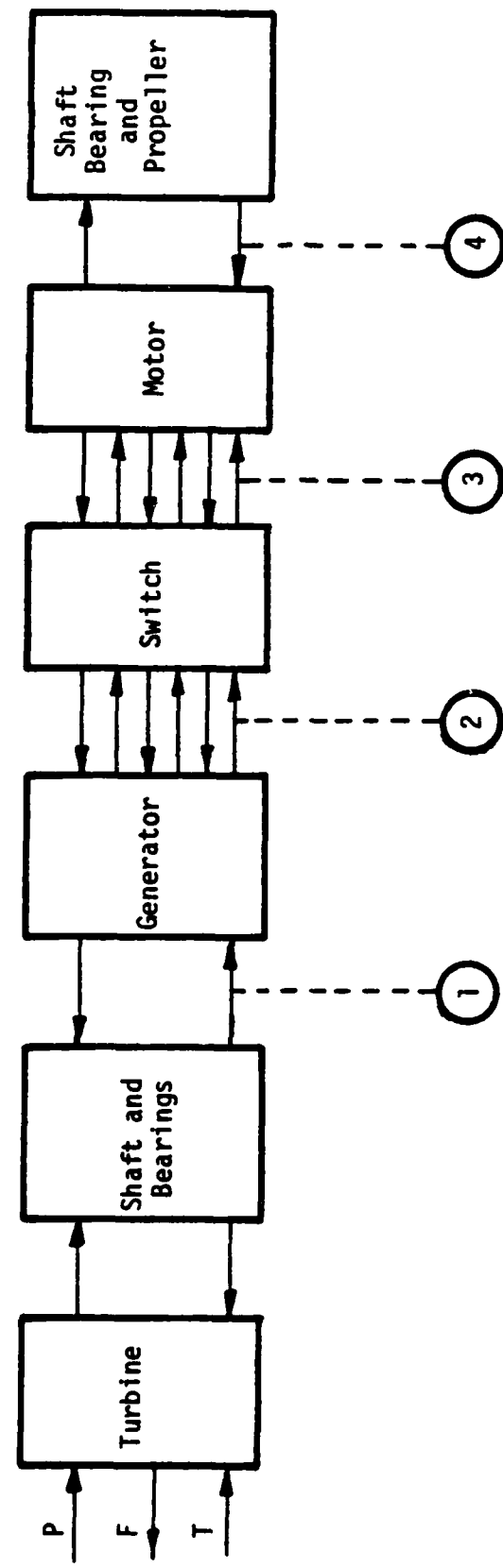


Figure 7.2 Causal description of the ship's engine simulation. There are 4 measurement points (Points 1-4). The pressure and temperature of the gas at the turbine's inlet are input variables.

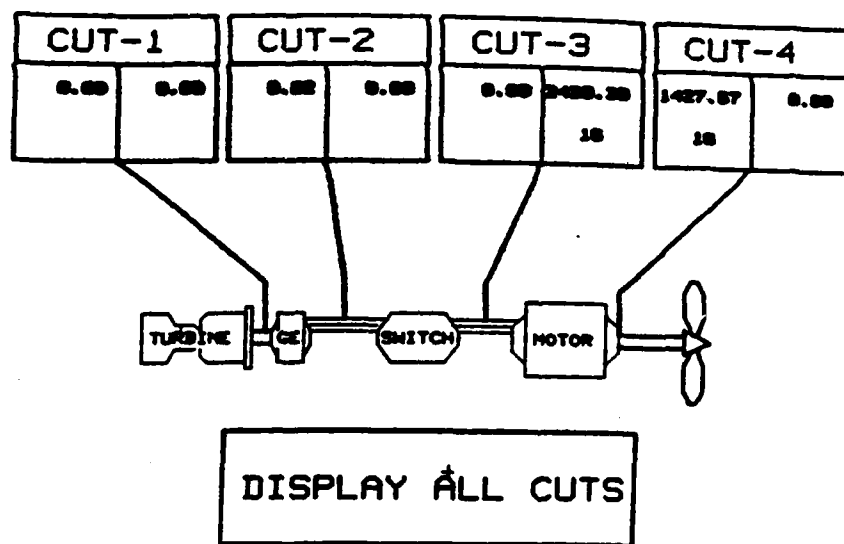


Figure 7.3 Schematic description of the ship's engine. The four measurement points and the calculated probability ratios are displayed. When Ω exceeds 1, the time during which it has happened is displayed as well.

By touching the Lexidata's touch sensitive panel, the operator controls which of the measurement points are utilized by FDLM. The system and model outputs of the activated measurement points are displayed as two side by side graphs on the Megatek's screen.

The ship's engine simulation demonstrates that a non-linear system can be traced solving a linear set of differential equations forced by non-linear inputs. This is discussed in Section 7.2. In Section 7.3 it is shown that, when the model includes dependent energy-storing components, the submodels causalities can be set such that derivative calculations are eliminated at the expense of increasing the model's order.

In Section 7.4 it is shown that the ac system and model power comparison, is advantageous on comparing their corresponding effort or flow values. The sequential and simultaneous failure location procedures are demonstrated and evaluated in Section 7.5.

7.2 Tracing the Non-Linear Ship's Engine Simulation by Solving a Linear Set of Differential Equations

The ship's engine is an eighth order non-linear simulation, the state equations of which are written in Appendix B. The non-linear terms of the [A] matrix (equation 4.1) are functions of the angular velocity ω_1 which can be expressed as:

$$\omega_1 = \frac{Y(7)}{J_1} \quad (7.1)$$

where $Y(7)$ and J_1 are the momentum and moment of inertia of the shaft connecting the turbine to the generator, respectively. By utilizing measurement point 1, FDLM results in a linear set of differential

differential equations which are written in Appendix C.

The non-linear simulation has been successfully traced by the linear equations. The simulated outputs, obtained by increasing the integration time step by a factor of 10, are satisfactory, as shown in Figure 7.4.

Since utilizing the outputs of measurement point 1 results in a linear FDLM model, measurement points 2, 3, and 4 have been applied together with point 1, as shown in Figure 7.5a, for measurement point 1 and 2.

7.3 Eliminating Derivative Calculations When Dependent Energy Storing Components are Included in the Model

Utilizing measurement points 2 and 3 are examples which require derivative calculations, as discussed in Section 4.3. Since the simulation includes stochastic processes, these time derivatives cannot be calculated. To eliminate time derivative calculations, the causalities of the submodels obtained by utilizing measurement points 1 plus 2 and 1 plus 3 are to be set as shown in Figure 7.5. This increases the model's order from 8 to 14, and the state equations of FDLM utilizing point 1 plus 2 are written in Appendix D.

7.4 Comparing ac Power Versus Its Corresponding Effort and Flow Variables

The system and model effort and flow variables of measurement points 2 and 3 are oscillatory in nature, as shown in Figure 7.6c (for the voltage of one of the phases at point 2). These oscillations cause difficulties to the operator to perform the system model comparison successfully.

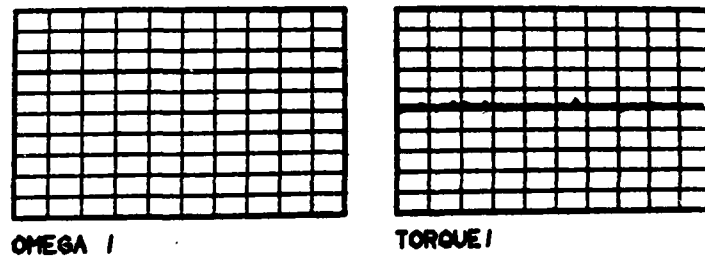
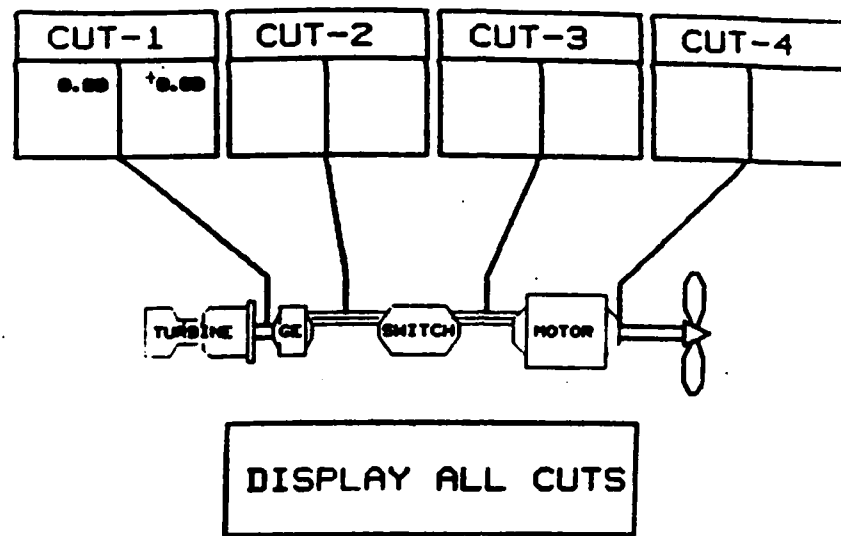


Figure 7.4 The system and model outputs of FDLM utilizing measurement point 1. The non-linear system is traced by a linear model.

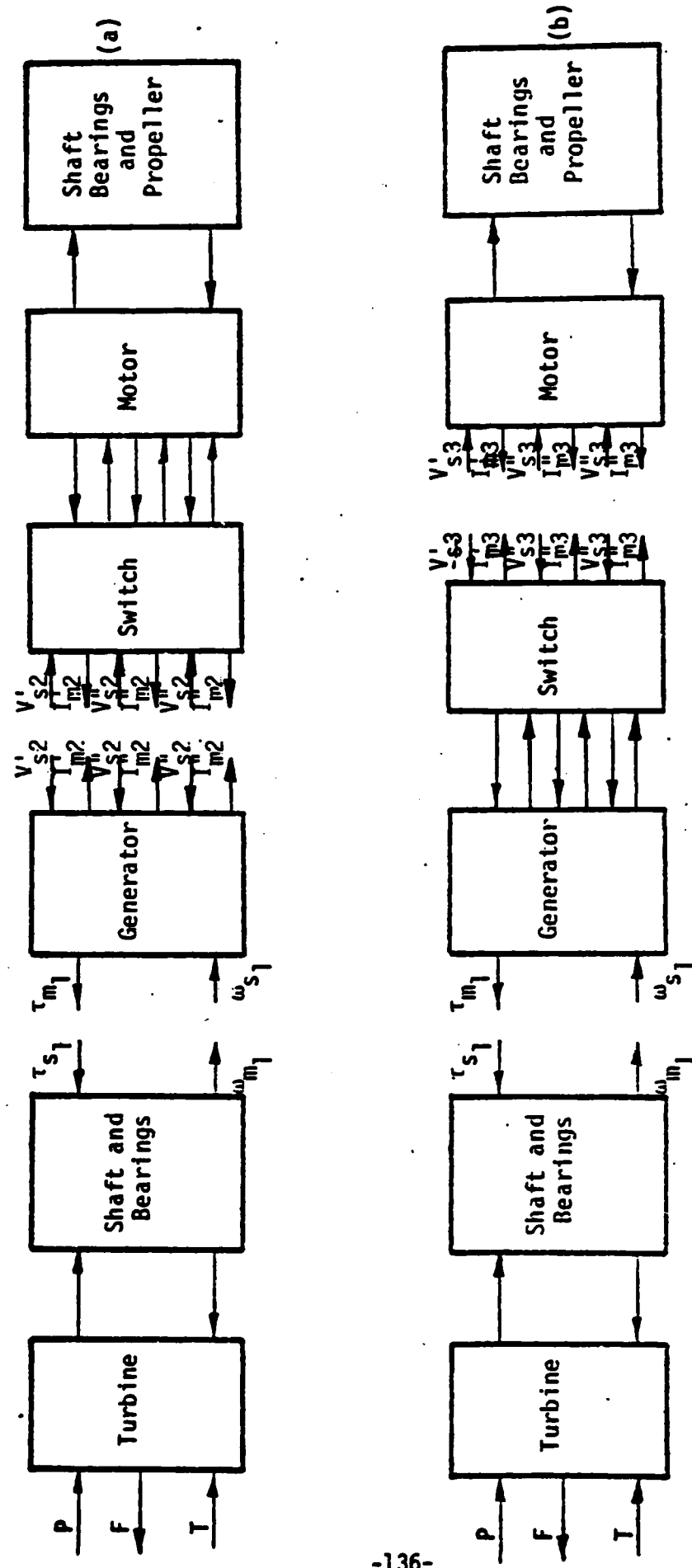


Figure 7.5: FDLM test applied utilizing measurement points 1 plus 2 (in 7.5a) and 1 plus 3 (in 7.5 b)

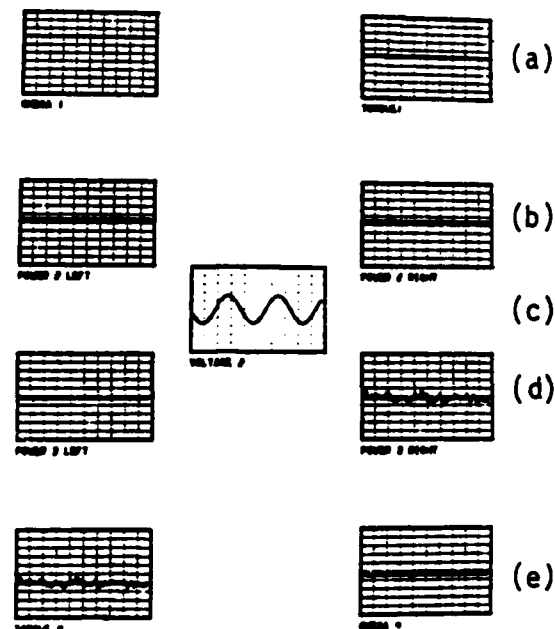


Figure 7.6 FDLM system and model outputs. The power of measurement point 2 in 7.6b, and the alternating voltage in 7.6c.

Therefore, it is proposed (section 2.3) to display to the operator the system-model power values, as shown in Figure 7.6b which are relatively constant.

7.5 Different Failure Location Procedures

The ship's engine simulation enables demonstrating the sequential and simultaneous failure location procedures, discussed in Section 2.3. A sequential and simultaneous location procedures of a single system failure are depicted in Figures 7.7 and 7.8, respectively. The three FDLM sequential tests shown in Figure 7.7a-c indicate that the switch has failed. This failure was located 227 seconds after it had been introduced. In contrast, the simultaneous FDLM application (Figure 7.8) results in locating the defective switch 5 seconds after it has failed.

The FDLM capability to locate a multiple system failure is demonstrated in Figures 7.9 and 7.10. The sequential FDLM tests (Figure 7.9a-d) indicate that the ac generator and motor have failed. The results of these tests are obtained 109 seconds after the system failures were introduced. These results do not clearly determine whether is or is not defective.

However, by utilizing the FDLM tests simultaneously, 4 seconds after introducing the failures it becomes clear that the ac generator and motor have failed, and the switch's status is normal.

These two examples demonstrate that the simultaneous FDLM application identifies the failure locations soon after they have occurred. Furthermore, in multiple failures, ambiguous results of the FDLM sequential tests are resolved by applying simultaneous FDLM mode.

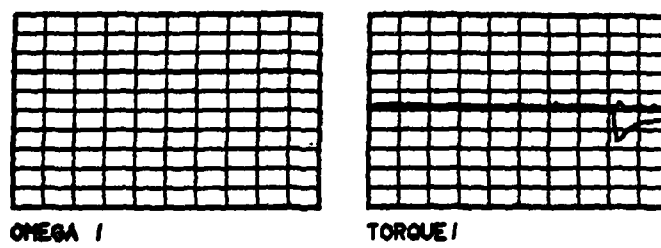
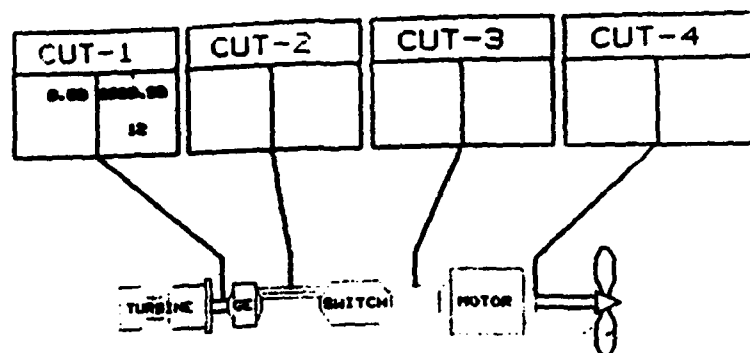
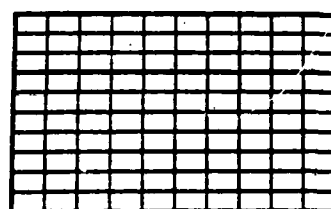
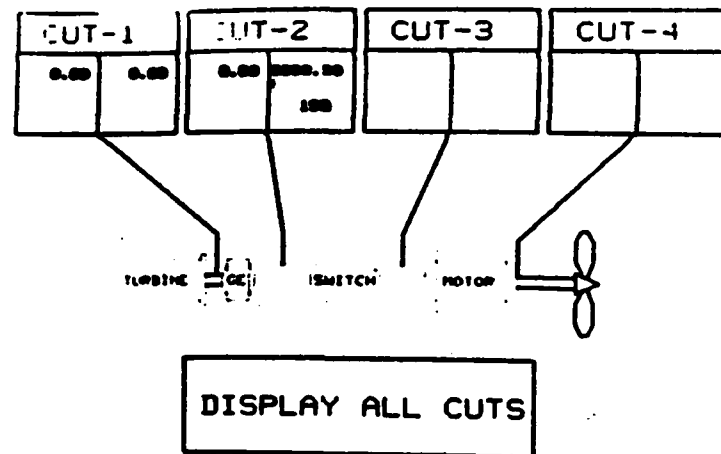
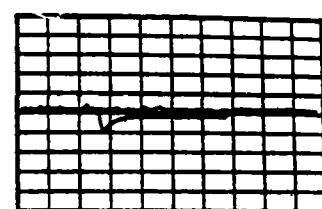


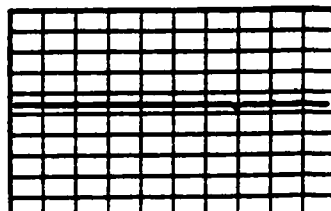
Figure 7.7a FDLM sequential test application utilizing measurement point 1. The failure is to the right of point 1.



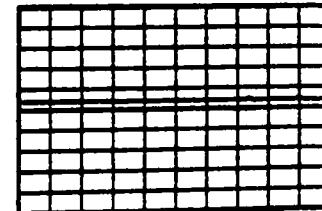
OMEGA I



TORQUE A



POWER 2 LEFT



POWER 2 RIGHT

Figure 7.7b FDLM sequential test application utilizing measurement point 1 plus 2. The failure is to the right of point 2.

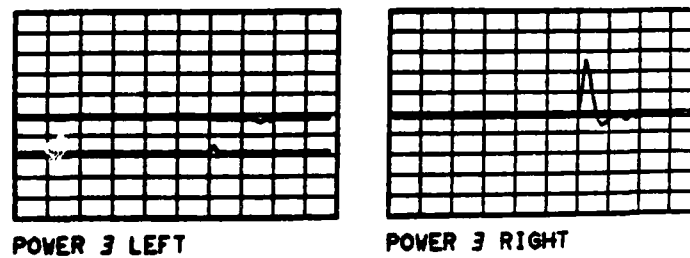
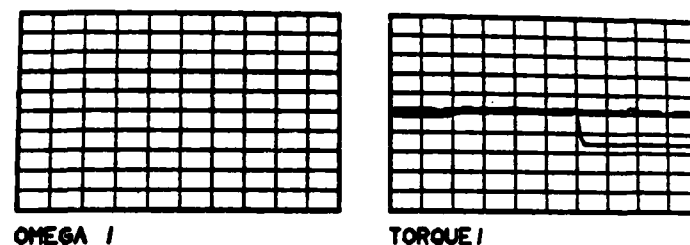
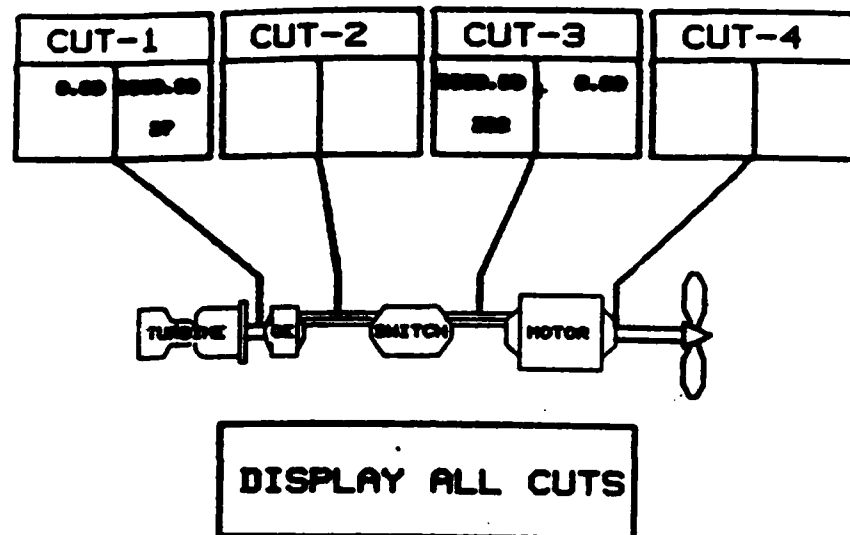


Figure 7.7c FDLM sequential test application utilizing measurement points 1 plus 3. The failure is to the left of point 3. Hence, the failure is between point 2 to 3.

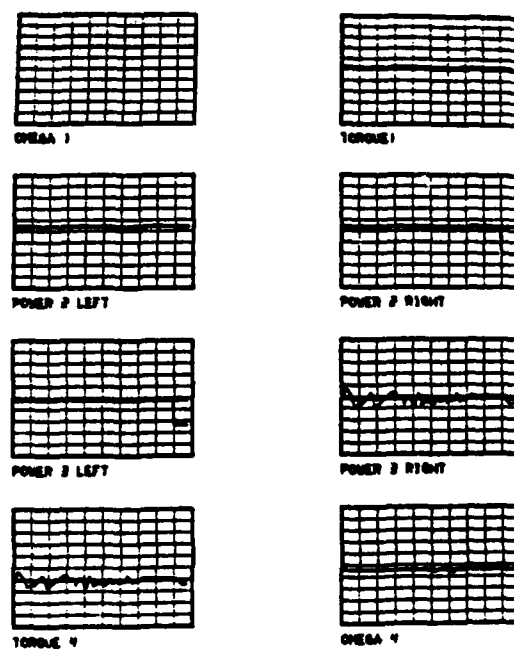
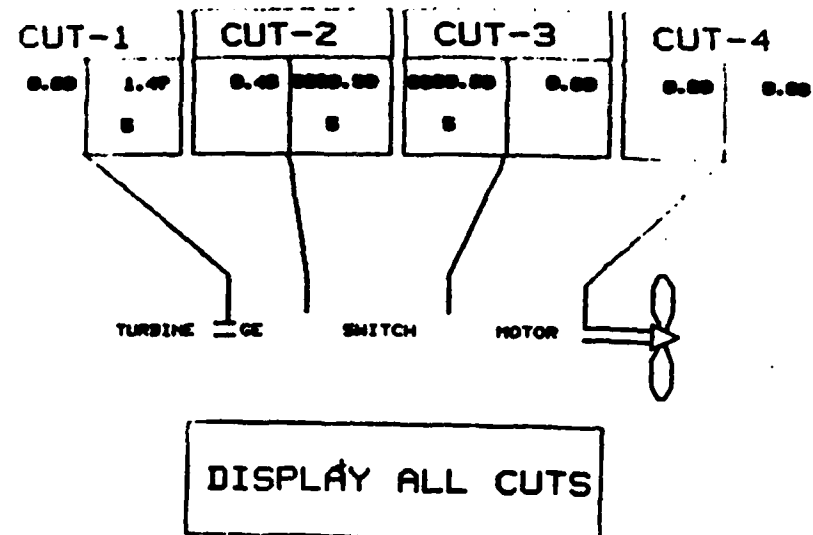


Figure 7.8 FDLM simultaneous test application the failure is between point 2 to 3.

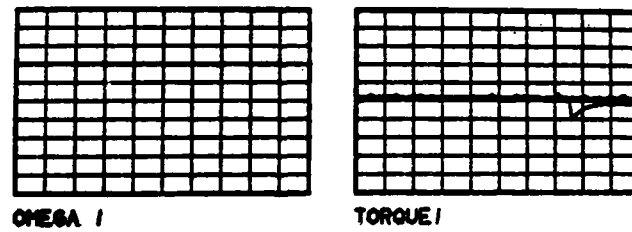
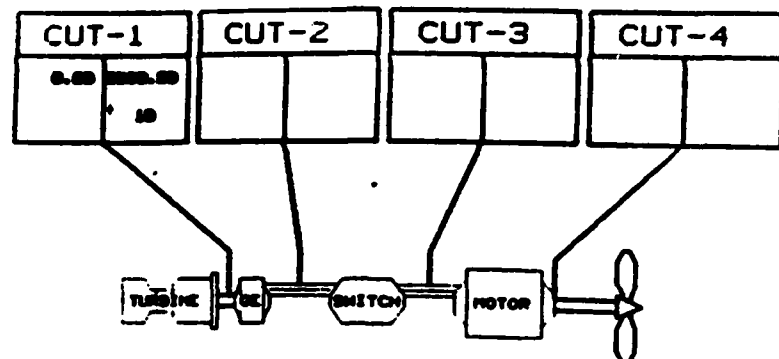
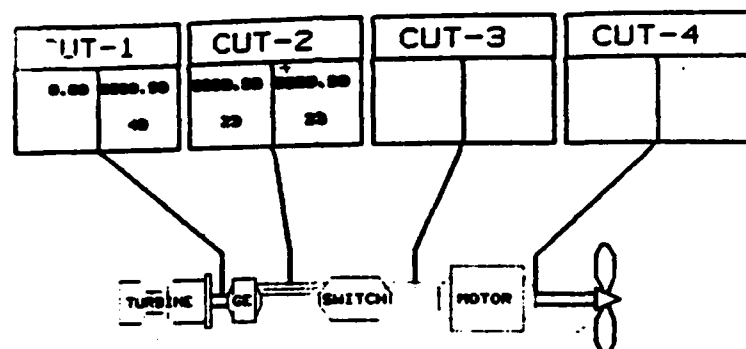
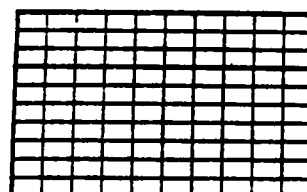


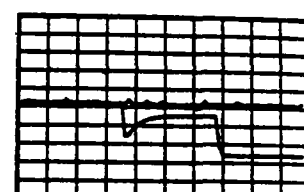
Figure 7.9a FDLM sequential test application utilizing measurement point 1. The failure is to the right of point 1.



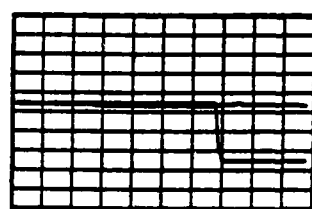
DISPLAY ALL CUTS



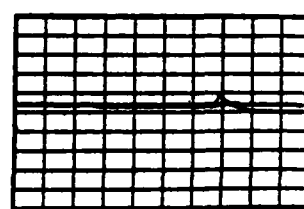
OMEGA 1



TORQUE 1



POWER 2 LEFT



POWER 2 RIGHT

Figure 7.9b FDLM sequential test application utilizing measurement points 1 plus 2. There is a multiple failure between points 1 and 2 and to the left of point 2.

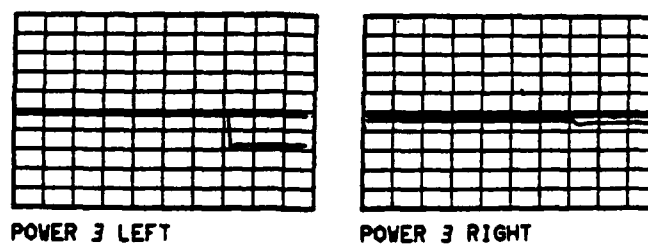
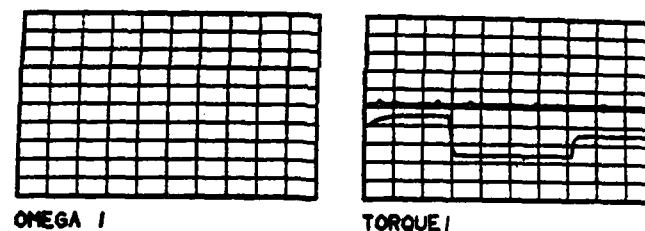
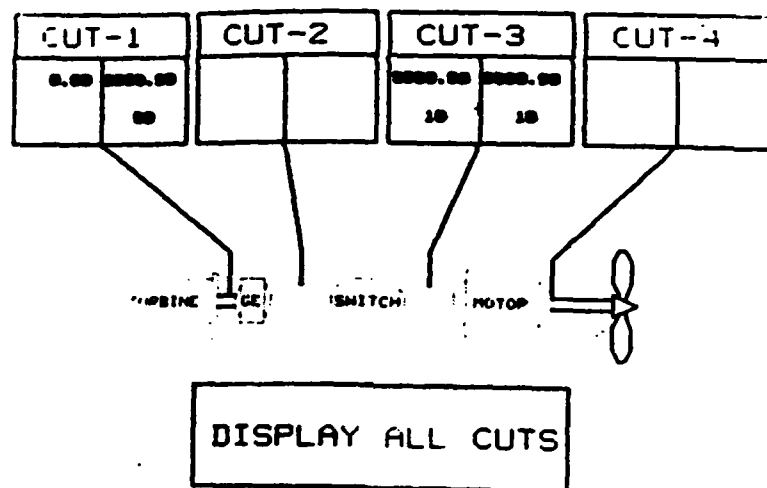


Figure 7.9c FDLM sequential test application utilizing measurement points 1 plus 3. There is a multiple failure between points 1 and 3 and on the right of point 3.

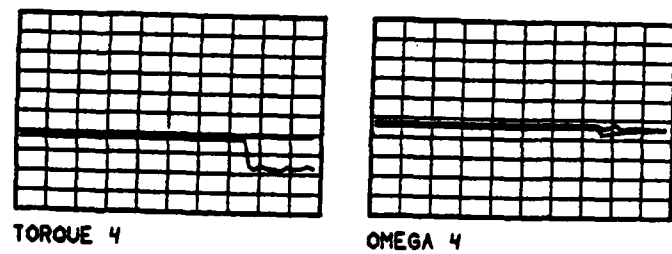
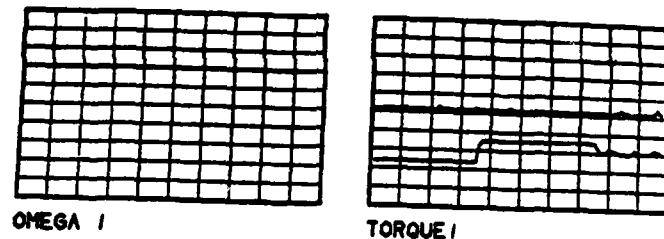
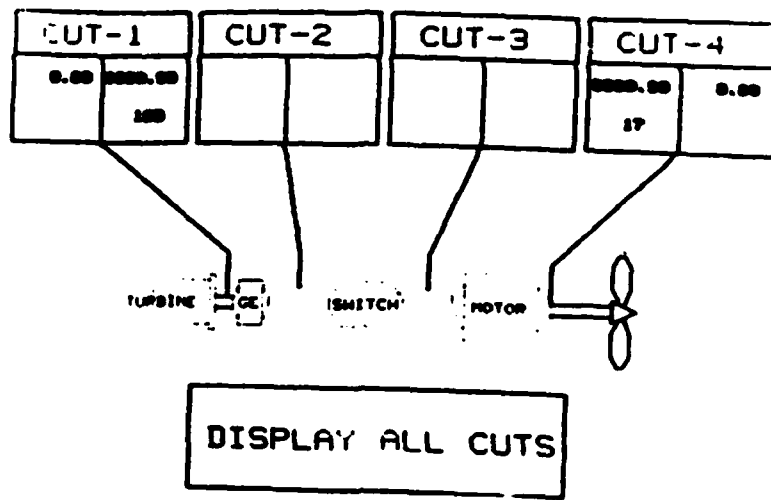
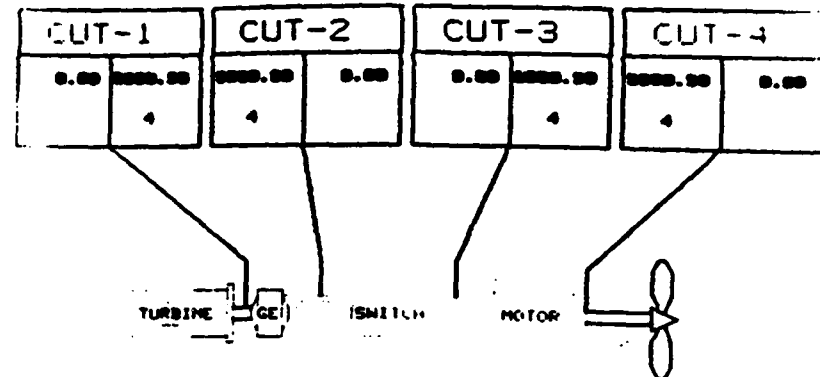


Figure 7.9d FDLM sequential test application utilizing measurement points 1 plus 4. The failure is between points 1 and 4.



DISPLAY ALL CUTS

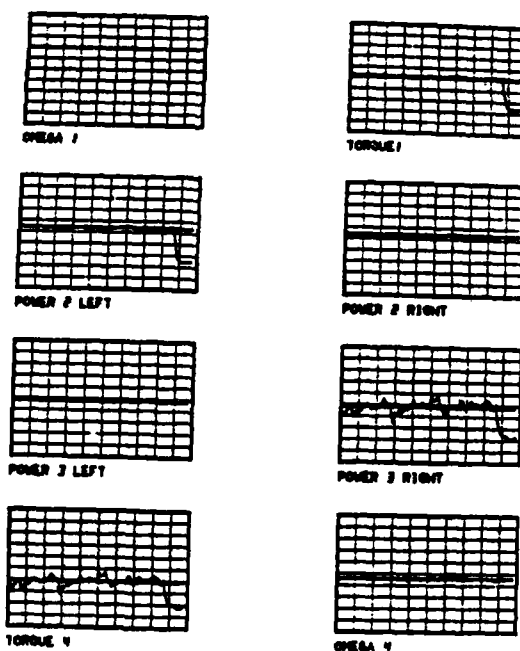


Figure 7.10 FDLM simultaneous test application. There is a multiple failure between points 1 and 2 and points 3 and 4.

CHAPTER 8

CONCLUSIONS AND FUTURE WORK

A new method which detects and locates system failures in real time is introduced in this thesis. This method is called Failure Detection and Location Method (FDLM). Significant deviations of the measured system power variables from their normal values constitutes the definition of a system failure. FDLM detects a failure by comparing the measured variables with the outputs of a computerized model of the system's normal operational mode. To locate the causes of the failure the model is disaggregated and according to the causalities of the resultant submodels, the measured system outputs are used as the submodel's inputs. The power covariables of these inputs are the submodel outputs which are compared with their corresponding system measured variables. Only the outputs of the submodels in which the failure causes are located deviate from their corresponding measured system variables. This enables FDLM to detect and locate system failures by utilizing a single computerized model of the system's normal operational mode, and its measured system outputs.

FDLM can identify $m+1$ system failure locations, where m is the number of available measurement points. Thus the number of measurement points determines how fine the locations of system failures can be identified. This is similar to the Failure Sensitive Filter technique, where the number of measurement points determines the number of failure modes which can be detected by a single filter.

FDLM can be applied to two distinct; sequential and simultaneous modes. In the sequential mode, FDLM utilizes the outputs of each measurement point sequentially. Here the number of compared system model outputs is minimized, but the location procedure is extensive. The simultaneous FDLM mode utilizes all the available system measurement points at once. This results in fast location but requires a comparison of many system and model outputs. In practical applications a combination of the simultaneous and sequential FDLM modes is recommended. An advantage of the FDLM sequential mode is its capability to distinguish between system and sensor failures. To detect system failures, one has first to validate the measurements, and use the validated signals to detect and locate system failures. FDLM assumes that the measured system outputs have been validated by other available techniques.

Where system failure is defined to be a process which causes the values of the system transferred power to deviate from the normal values. Such deviations can be detected by comparing the system with a single model of its normal operational mode. Constructing only one model is an advantage which requires the completion of the failure location task before the failed system outputs wander too far from their normal ranges. This can be achieved by early failure detection and efficient location procedure.

To obtain early failure detection FDLM is proposed to be applied to continuously monitored dynamic systems such as power plants, airplanes and ships. This system is to be continuously compared with a computerized model during their operation. Failure detection, based on deviations from

a model is in contract to fault/event tree analysis where failure is detected when measured system outputs reach their safety limit or abnormal range.

To obtain an efficient failure location procedure, it is proposed to cut the model such that the relative positions of its state variables during the location procedure will not be changed. This requires that the model be cut into submodels such that each submodel contains a minimum number of state variables (one if possible). It is shown in this work that the multiple cut approach also overcomes the problem of low sensitivity of system parameters.

Sensitivity is a measure of the size of a detectable failure. It depends on the noise levels of the measured system outputs, and the quality of the compared computerized model. In practical FDLM applications, a detailed model may detect small system model deviations but might require lengthy calculations and as a result, would not be implemented in real time. The questions of how detailed the model has to be, should be addressed in every FDLM application.

FDLM determines the status of a physical system by testing relatively few of its outputs. Therefore, FDLM is a promising candidate of the desired Nuclear Plant Surveillance and Diagnostic System (NPSDS) [15], which is under development now. NPSDS is designed to reduce the number of displayed variables in nuclear power control rooms.

FDLM, when utilizing certain system measured outputs transforms a non-linear model into a linear set of differential equations, forced by

non-linear inputs. This approach results in capabilities to detect failures of non-linear dynamic system by solving linear set of differential equations.

Calculating time derivatives of measured system outputs cannot be performed when the outputs are changing their values rapidly (not smooth functions). These derivative calculations can be eliminated by setting the causalities of the submodels promptly. This is achieved at the expense of increasing the number of the model state variables.

FDLM was successfully applied to multiconnected physical systems with bi- and uni-lateral energy bonds. It is shown how to expand FDLM to be applicable to systems with multi-lateral energy bonds. In the future, it is planned to apply FDLM to part of a fossil power plant, where the multi-lateral FDLM applications will be tested.

While FDLM was designed to detect system failure, it can also be used in a reverse way to update the model when the system is readjusted and model calibration is required.

A Bayesian statistical model was incorporated into FDLM and evaluated. This model calculates the probability that the system failed. This probability was found to be very useful. By displaying the probability to human operators as an odds ratio (failure/nonfailure), their miss and false-alarm rates, as well as their reaction times can be improved significantly.

The probability display can be used as a computerized alarm system which will call the operator's attention, once the odds ratio exceeds

a preset critical value. The operator's task will be to use FDLM and to confirm the location of the failure causes. The location can be identified up to two adjacent measurement points. To identify the system's defective components, inbetween measurement points, a simple fault/event tree analysis of the defective subsystem, and the operator's experience should be utilized.

In the future it is recommended to apply FDLM to a real thermo-fluidic system. In this application FDLM should be coupled with the available diagnostic methods which will be used to validate sensor signals, and detect failures between components between measurement points. The efficiency and reliability of this combined diagnostic system should be tested, and its sensitivity to a choice of measurement points, noise level, and model simplifications should be analyzed.

REFERENCES

- [1] Thomas B. Sheridan, "Understanding Human Error and Aiding Human Diagnostic Behaviour In Nuclear Power Plants", Human Detection and Diagnosis of System Failures, edited by Jens Rasmussen and William B. Rouse, Plenum Press N.Y., 1981.
- [2] Report of the President's Commission on the Accident at Three Mile Island, Washington, D.C., October 1979.
- [3] N. Moray, "Human Information Processing and Supervisory Control", MMSL report M.I.T., Cambridge, MA, May 1980.
- [4] D. Patterson, "Application of Computerized Alarm-Analysis System to a Nuclear Power Station", Proceedings IEE, Vol. 115, No. 12, 1968.
- [5] D. Welbourne, "Alarm Analysis and Display at Wylfa Nuclear Power Station", Proceedings IEE, Vol. 15, No. 11, 1968.
- [6] B. Frogner, and C.H. Meijer, "On-line Power Plant Alarm and Disturbance Analysis System", Final Report NP891, EPRI, Palo Alto, CA, February 1980.
- [7] W. Bastl, and L. Felkel, "Disturbance Analysis Systems, State of the Art", Human Detection and Diagnosis of System Failures, edited by Jens Rasmussen and William B. Rouse, Plenum Press, N.Y., 1981.
- [8] K.L. Gimmy, and E. Momm, "Automatic Diagnosis of Multiple Alarm for Reactor Control Rooms", Proceedings of ANS, Los Angeles, CA, June 1982.
- [9] J.C. Deckert, J.L. Fisher, D.B. Lanning, and A. Ray", A Signal Validation Methodology for Nuclear Power Plants", Proceedings of ACC, Washington, D.C., June 1982.
- [10] J. Gilmore, and R. McKern, "A Redundant Strapdown Inertial System Mechanization - SIRU", Presented at the AIAA Guidance, Control and Flight Mechanics Conference, Santa Barbara, CA, August 1970.
- [11] A.J. Pejsa, "Optimum Orientation and Accuracy of Redundant Sensor Arrays", Honeywell Aerospace Division, Minneapolis, MN, 1971.
- [12] R.B. Broen, "A Nonlinear Voter-Estimator for Redundant Systems", Proceedings IEEE Conference on Decision and Control, Phoenix, Arizona, 1974.

- [13] C.L. Louie, "Control Systems Reliability Using Redundant Instrumentation", Engineering Thesis, Ocean Engineering, M.I.T., Cambridge, MA, June 1982.
- [14] A. Ray, R. Geiger, M. Desai, and J.J. Deyst Jr., "Computerized Fault Diagnostics in a Nuclear Reactor via Analytic Redundancy", Proceedings ACC, Washington, D.C., June 1982.
- [15] P.J. Nicholson, and D.D. Lanning, "Requirements and Concepts for a Nuclear Plant Surveillance and Diagnostics System (NPSDS)", Presented at IAEA Specialists MTG on Distributed Systems for Nuclear Power Plants, Chalk River, Ontario, Canada, May 1980.
- [16] M. Lind, "The Use of Flow Models for Automated Plant Diagnosis", Human Detection and Diagnosis of System Failures, edited by Jens Rasmussen, and William B. Rouse, Plenum Press, N.Y. 1981.
- [17] M.R. Hassan, "Use of Disaggregated Model as an Aid to the Human Operator in Failure Diagnosis in Complex Automated Systems", MSc Thesis, Mechanical Engineering, M.I.T., Cambridge, MA, April 1981.
- [18] H.M. Paynter, "Analysis and Design of Engineering System", M.I.T. Press, Cambridge, MA, 1961.
- [19] H.M. Paynter, "Dynamics and Control of Thermofluid Processes and Systems", 2.155 Class Notes, Mechanical Engineering, M.I.T., Spring 1981.
- [20] M.L. James, G.M. Smith, and J.C. Wolford, "Applied Numerical Methods for Digital Computation", IEP-A Dun-Donnelley Publisher, N.Y., 1967.
- [21] B. Sheckel, Personal Communications, M.I.T., Cambridge, MA, December 1981.
- [22] Thomas B. Sheridan, and William R. Ferrel, "Man-Machine Systems Information, Control, and Decision Models of Human Performance", M.I.T. Press, Cambridge, MA, 1976.
- [23] A. W. Drake, "Fundamentals of Applied Probability Theory", McGraw-Hill, 1967.
- [24] E.G. Gai, and R.E. Curry, "A Model of the Observer in Failure Detection Tasks, IEE Transactions on System, Man, and Cybernetics, February 1976.
- [25] J. Tzelgov, "Providing the Operator with an Estimator of Failure Probability: A Theoretical Comparison of Two Statistical Models, MMSL report M.I.T., Cambridge, MA, April 1982.

- [26] W.G. Cochran, and G.M. Cox, "Experimental Designs", Wiley Publisher, N.Y., 1957.
- [27] G. Keppel, "Design and Analysis, A Researcher's Handbook", Prentice-Hall Publisher, 1973.
- [28] A.L. Markunas, "Modeling, Simulation, and Control of Gas Turbines", MSc Thesis, Mechanical Engineering, M.I.T., Cambridge, MA, June 1972.
- [29] M. Fujii, "Synthesis of a Multivariable Controller for Real/Reactive Power Dispatch", MSc Thesis, Mechanical Engineering, M.I.T., Cambridge, MA, February 1980.
- [30] H.M. Paynter, Personal Communications, M.I.T., Cambridge, MA, March 1982.

APPENDIX A

INSTRUCTIONS TO THE EXPERIMENTAL SUBJECTS

Purpose

This experiment explores what information should be displayed to an operator of a plant such that plant failures can easily be detected.

Background

You are participating in an experiment in which your task is to detect failures in a hydroelectric plant system. The system, shown in Figure A.1, utilizes hydraulic power to generate electricity. To detect failures in this system, measured system outputs and their corresponding model variables are to be displayed on a CRT screen as a function of time. In our case the measured variables are the torque and the angular velocity of the generator's shaft (as marked in Figure A.1).

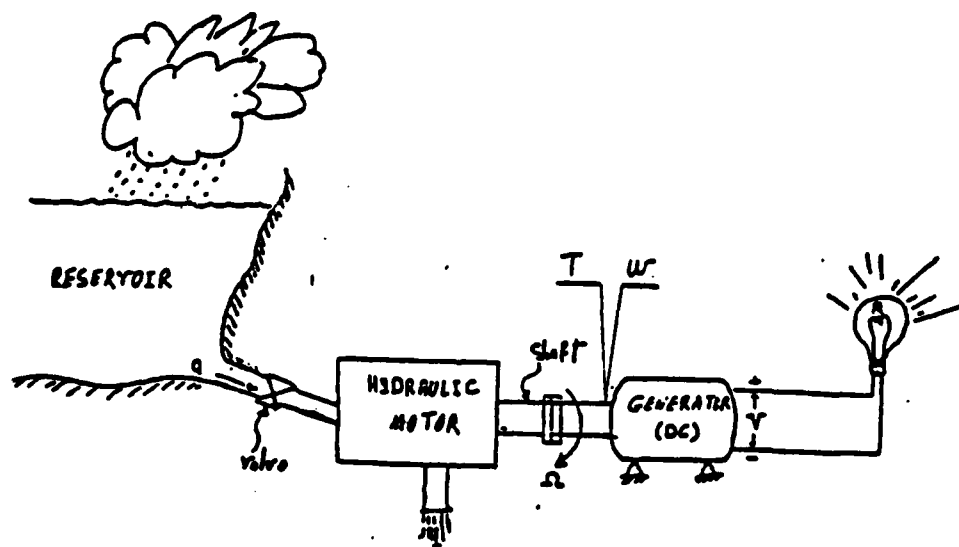


Figure A.1 A description of the hydraulic-mechanical-electrical system.

The measured system outputs are noisy in nature, whereas the model outputs are either noisy or smooth. That is, the model angular velocity is smooth whereas the torque is noisy. When the model output is noisy, a system failure results in a discrepancy between the system and the model outputs immediately. On the other hand, when the model output is smooth, the discrepancy appears only after a time delay. The time delay in our case is about 15 seconds. The experiment consists of two sessions, one devoted to smooth model output, and one to noisy output.

To explore the effect of noise on a failure detection task different kinds of output can be displayed:

1. Raw output variables.
2. Averaged model output.
3. Averaged system and model outputs.

Averaging the output is a simple way to smooth out the noise. In this experiment these three displays will appear equally in random order.

The effect of providing additional digital information is to be determined. Two kinds of digital displays will be tested.

1. The ratio of failure to no-failure probabilities [$p(\text{Failure})/p(\text{No-failure})$]. This ratio is smaller than 1 when $p(\text{Failure})$ is smaller than 0.5, and larger than 1 when $p(\text{Failure})$ is larger than 0.5.
2. The time during which the ratio of probabilities exceeds 1.

Each session will consist of four combinations of the digital displays:

1. No digital information provided.
2. Ratio of probabilities is displayed.
3. The time during which the ratio of probabilities exceeds 1 is displayed.
4. Ratio of probabilities and the time during which it exceeds 1 are displayed.

The type of digital information provided will be written on the screen.

In this experiment it is assumed that the hydroelectric plant is still being tested and, as such, is very unreliable. The probability that the system has failed is 0.5. Thus in 50% of the experimental trials the system is defective.

Using all the information displayed on the screen, you have to decide whether the system in any particular trial is, or is not defective.

Experimental Details

The experiment is to be performed in two sessions. Each session consists of 4 modes, differing in the digital information displayed. There are 60 experimental trials in each mode. To establish a certain level of familiarity with the system each one of the modes will start with 10 practice trials. In these trials you will be notified whether or not you made the right decision.

There are 2 control buttons:

1. Start
2. Alarm.

Each trial is initiated by pressing the Start button. The Alarm button should be pressed as soon as a system failure is detected. The total time for each trial is 35 seconds. Pressing the Alarm after the 35 seconds does not count. Attempt to avoid false alarms. That is, do not press the Alarm button unless you detect a failure. Speed and accuracy are of equal importance.

APPENDIX B: SHIP'S ENGINE SIMULATION

The bond graph description of the ship's engine is depicted in Figure B.1. This is an eighth order non-linear simulation, and the state equations can be written as:

$$\dot{y}(1) = (\frac{G10}{J_1} y(7) - \frac{2R_1 + R_2}{L_1} y(1) - \frac{G100}{J_2} y(8)) / (1 + \frac{L_2}{L_1})$$

$$\dot{y}(2) = (\frac{G11}{J_1} y(7) - \frac{2R_1 + R_2}{L_1} y(2) - \frac{G110}{J_2} y(8)) / (1 + \frac{L_2}{L_1})$$

$$\dot{y}(3) = (\frac{G20}{J_1} y(7) - \frac{2R_1 + R_2}{L_1} y(3) - \frac{G200}{J_2} y(8)) / (1 + \frac{L_2}{L_1})$$

$$\dot{y}(4) = (\frac{G21}{J_1} y(7) - \frac{2R_1 + R_2}{L_1} y(4) - \frac{G210}{J_2} y(8)) / (1 + \frac{L_2}{L_1})$$

$$\dot{y}(5) = (\frac{G30}{J_1} y(7) - \frac{2R_1 + R_2}{L_1} y(5) - \frac{G300}{J_2} y(8)) / (1 + \frac{L_2}{L_1}) \quad (B.1)$$

$$\dot{y}(6) = (\frac{G31}{J_1} y(7) - \frac{2R_1 + R_2}{L_1} y(6) - \frac{G310}{J_2} y(8)) / (1 + \frac{L_2}{L_1})$$

$$\dot{y}(7) = \tau_{in} - \frac{b_1}{J_1} y(7) - (y(1) \cdot G10 + y(2) \cdot G11 + y(3) \cdot G20 + y(4) \cdot G21 + y(t) \cdot G30 + y(6) \cdot G31) / L_1$$

$$\dot{y}(8) = y(1) \cdot G100 + y(2) \cdot G110 + y(3) \cdot G200 + y(4) \cdot G210 + y(5) \cdot G300 + y(6) \cdot G310 -$$

$$\frac{b_2}{J_2} y(8) - \frac{k}{J_2} y(8)$$

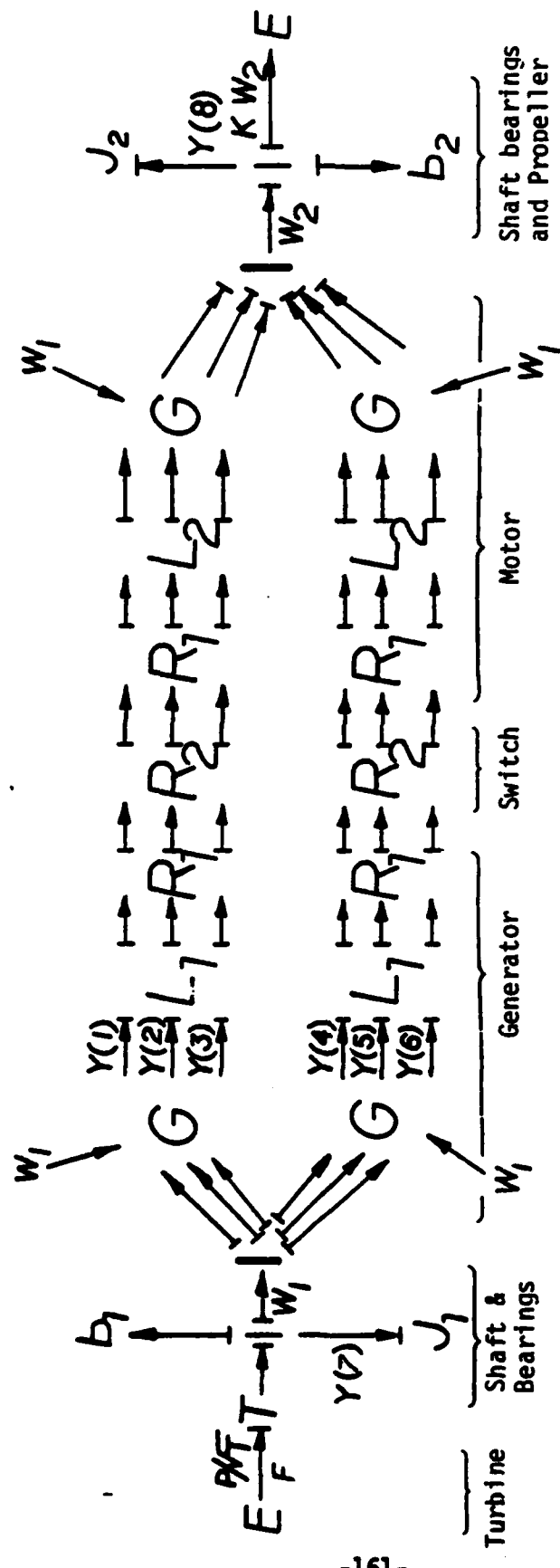


Figure B.1 Bond graph description of the ship's engine simulation.

where:

$$G10 = v_1 \cos\left(\frac{y(7)}{J_1} t\right)$$

$$G11 = v_1 \dot{m} \left(\frac{y(7)}{J_1} t\right)$$

$$G20 = v_1 \cos\left(\frac{y(7)}{J_1} t + \frac{2\pi}{3}\right)$$

$$G21 = v_1 \dot{m} \left(\frac{y(7)}{J_1} t + \frac{2\pi}{3}\right)$$

$$G30 = v_1 \cos\left(\frac{y(7)}{J_1} t + \frac{4\pi}{3}\right)$$

$$G31 = v_1 \sin\left(\frac{y(7)}{J_1} t + \frac{4\pi}{3}\right)$$

$$G100 = v_2 \cos\left(\frac{y(7)}{J_1} t\right)$$

$$G110 = v_2 \dot{m} \left(\frac{y(7)}{J_1} t\right)$$

$$G200 = v_2 \cos\left(\frac{y(7)}{J_1} t + \frac{2\pi}{3}\right)$$

$$G210 = v_2 \dot{m} \left(\frac{y(7)}{J_1} t + \frac{2\pi}{3}\right)$$

$$G300 = v_2 \cos\left(\frac{y(7)}{J_1} t + \frac{4\pi}{3}\right)$$

$$G310 = v_2 \sin\left(\frac{y(7)}{J_1} t + \frac{4\pi}{3}\right)$$

t is the current time and τ_{in} is the torque applied to the generator's shaft. τ_{in} is calculated using Markunas's model of gas turbines [31]. This model can be written as:

$$\tau_{in} = P C_p \frac{\left(\dot{F} \sqrt{\frac{T}{P}}\right) \left(1 - \frac{T_2}{T}\right)}{\frac{y(7)}{J_1 \sqrt{T}}}$$

$$\dot{F} = 1.006 \left(1 - \left(\frac{P_{at}}{P}\right)^{BT} 0.7\right)$$

$$BT = 3.1 + 1.62 / \left(\frac{y(7)}{J_1 \sqrt{T} w_{design} + 0.26} \right) \quad (B.3)$$

$$\frac{T_2}{T} = 1 - EFFT \left(1 - \left(\frac{P_{at}}{P}\right) \frac{\gamma-1}{\gamma}\right)$$

$$EFFT = DT \left(1 - \left(1 - \sqrt{\frac{1-ET}{1-P_{at}/P}}\right)^2\right)$$

$$ET = 1 - 0.8 \left(\frac{y(7)}{J_1 \sqrt{T} w_{design}} \right)$$

APPENDIX C: UTILIZING MEASUREMENT POINT 1 IN
APPLYING FDLM TO THE SHIP'S ENGINE

FDLM cut model using measurement point 1 is shown in Figure C.1. The state equations of this model can be written as:

$$\begin{aligned}
 \dot{y}(1) &= (w_{1s}G10 - \frac{2R_1 + R_2}{L_1} y(1) - \frac{G100}{J_2} y(8)) / (1 + \frac{L_2}{L_1}) \\
 \dot{y}(2) &= (w_{1s}G11 - \frac{2R_1 + R_2}{L_1} y(2) - \frac{G110}{J_2} y(8)) / (1 + \frac{L_2}{L_1}) \\
 \dot{y}(3) &= (w_{1s}G20 - \frac{2R_1 + R_2}{L_1} y(3) - \frac{G200}{J_2} y(8)) / (1 + \frac{L_2}{L_1}) \\
 \dot{y}(4) &= (w_{1s}G21 - \frac{2R_1 + R_2}{L_1} y(4) - \frac{G210}{J_2} y(8)) / (1 + \frac{L_2}{L_1}) \\
 \dot{y}(5) &= (w_{1s}G30 - \frac{2R_1 + R_2}{L_1} y(5) - \frac{G300}{J_2} y(8)) / (1 + \frac{L_2}{L_1}) \\
 \dot{y}(6) &= (w_{1s}G31 - \frac{2R_1 + R_2}{L_1} y(6) - \frac{G310}{J_2} y(8)) / (1 + \frac{L_2}{L_1}) \\
 \dot{y}(7) &= \tau_{in} - \frac{b_1}{J_1} y(7) - \tau_{1s} \\
 \dot{y}(8) &= G100 \cdot y(1) + G10 \cdot y(2) + G200 \cdot y(3) + G210 \cdot y(4) + G300 \cdot y(5) + \\
 &\quad G310 \cdot y(6) - \frac{b_2}{J_2} y(8) - \frac{k}{J_2} y(8)
 \end{aligned} \tag{C.1}$$

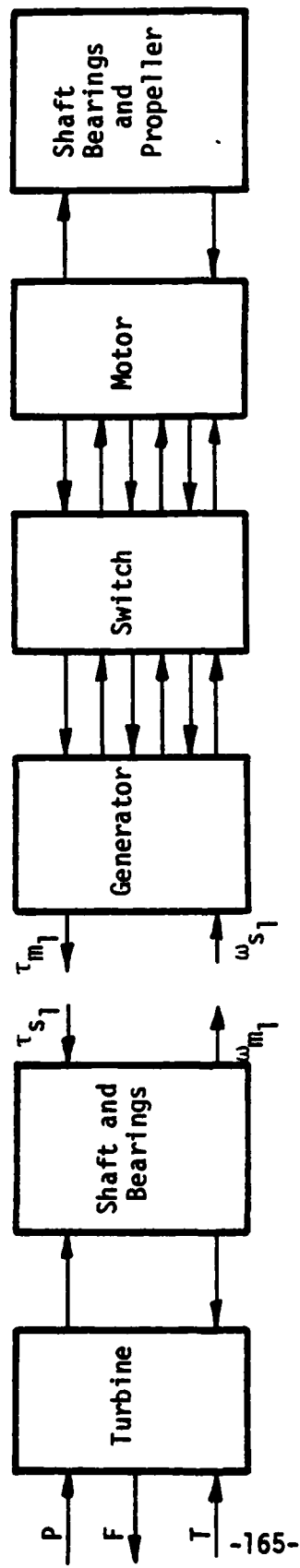


Figure C.1 FDLM test applied utilizing measurement point 1 results in transforming the non-linear model to a linear one.

where:

$$G10 = V_1 \cos(w_1 t_s)$$

$$G11 = V_1 \sin(w_1 t_s)$$

$$G20 = V_1 \cos(w_1 t_s + \frac{2\pi}{3})$$

$$G21 = V_1 \sin(w_1 t_s + \frac{2\pi}{3})$$

$$G30 = V_1 \cos(w_1 t_s + \frac{4\pi}{3})$$

$$G31 = V_1 \sin(w_1 t_s + \frac{4\pi}{3})$$

(C.2)

$$G100 = V_2 \cos(w_1 t_s)$$

$$G110 = V_2 \sin(w_1 t_s)$$

$$G200 = V_2 \cos(w_1 t_s + \frac{2\pi}{3})$$

$$G210 = V_2 \sin(w_1 t_s + \frac{2\pi}{3})$$

$$G300 = V_2 \cos(w_1 t_s + \frac{4\pi}{3})$$

$$G310 = V_2 \sin(w_1 t_s + \frac{4\pi}{3})$$

and τ_{in} is calculated by using equations (B.3).

APPENDIX D
UTILIZING MEASUREMENT POINTS 1 AND 2
IN APPLYING FDLM TO THE SHIP'S ENGINE

The FDLM cut model using measurement points 1 and 2 is shown in Figure 7.6a. The state equations of this cut model can be written as:

$$\begin{aligned}
 \dot{y}(1) &= w_{1s} G10 - v_{21s} - \frac{R_1}{L_1} y(1) \\
 \dot{y}(2) &= w_{1s} G11 - v_{22s} - \frac{R_1}{L_1} y(2) \\
 \dot{y}(3) &= w_{1s} G20 - v_{23s} - \frac{R_1}{L_1} y(3) \\
 \dot{y}(4) &= w_{1s} G21 - v_{24s} - \frac{R_1}{L_1} y(4) \\
 \dot{y}(5) &= w_{1s} G30 - v_{25s} - \frac{R_1}{L_1} y(5) \\
 \dot{y}(6) &= w_{1s} G31 - v_{26s} - \frac{R_1}{L_1} y(6) \\
 \dot{y}(7) &= \tau_{in} - \frac{b_1}{J_1} y(7) - \tau_{1s} \\
 \dot{y}(8) &= (G100 \cdot v(9) + G110 \cdot y(10) + G200 \cdot y(11) + G210 \cdot y(12) \\
 &\quad + G300 \cdot y(13) + G310 \cdot y(14)/L2 - \frac{b_2}{J_2} y(8) - \frac{k}{J_2} y(8) \\
 \dot{y}(9) &= v_{21s} - \frac{R_1 + R_2}{L_2} y(9) - G100/J_2 y(8) \\
 \dot{y}(10) &= v_{22s} - \frac{R_1 + R_2}{L_2} y(10) - G100/J_2 y(8)
 \end{aligned} \tag{D.1}$$

$$\dot{y}(11) = v_{23s} - \frac{R_1+R_2}{L_2} y(11) - \frac{G200}{J_2} y(8)$$

$$\dot{y}(12) = v_{24s} - \frac{R_1+R_2}{L_2} y(12) - \frac{G210}{J_2} y(8)$$

$$\dot{y}(13) = v_{25s} - \frac{R_1+R_2}{L_2} y(13) - \frac{G300}{J_2} y(8)$$

$$\dot{y}(14) = v_{26s} - \frac{R_1+R_2}{L_2} y(14) - \frac{G310}{J_2} y(8)$$

where τ_{in} is calculated by using equations B.3, and G10-G310 are calculated by solving equations (C.2).

DISTRIBUTION LIST

Capt. Paul R. Chatelier
Office of the Deputy Under
Secretary of Defense
OUSDRE (E&LS)
Pentagon, Room 3D129
Washington, DC 20301

Engineering Psychology Group
Office of Naval Research
Code 442EP
Arlington, VA 22217

Dr. Eugene Silva
Ocean Sciences, Code 421
Office of Naval Research
800 North Quincy Street
Arlington, VA 22217

Communication & Computer Technology
Programs
Code 270
Office of Naval Research
800 North Quincy Street
Arlington, VA 22217

Manpower, Personnel, and Training
Programs
Code 270
Office of Naval Research
800 North Quincy Street
Arlington, VA 22217

Information Sciences Division
Code 433
Office of Naval Research
800 North Quincy Street
Arlington, VA 22217

Personnel & Training Research Group
Code 442PT
Office of Naval Research
800 N. Quincy Street
Arlington, VA 22217

Special Assistant for Marine
Corps Matters
Code 100 M
Office of Naval Research
800 North Quincy Street
Arlington, VA 22217

Dr. Edgar M. Johnson
Technical Director
U.S. Army Research Institute
5001 Eisenhower Avenue
Alexander, VA 22333

Technical Director
U.S. Army Human Engineering Labs
Aberdeen Proving Ground, MD 21005

U.S. Air Force Office of
Scientific Research
Life Sciences Directorate, NL
Bolling Air Force Base
Washington, DC 20332

Chief, Systems Engineering Branch
Human Engineering Division
USAF AMRL/HES
Wright-Patterson AFB, OH 45433

Director, Human Factors Wing
Defence & Civil Institute
of Environmental Medicine
Post Office Box 2000
Downsview, Ontario M3M 389
CANADA

Defense Technical Information Center
Cameron Station, Bldg. 5
Alexandria, VA 22314

Dr. Craig Fields
Director, System Sciences Office
Defense Advanced Research
Projects Agency
1400 Wilson Boulevard
Arlington, VA 22209

Dr. M. Montemerlo
Human Factors & Simulation
Technology, RTE-6
NASA HQS
Washington, DC 20546

Dr. Jesse Orlansky
Institute for Defense Analyses
1801 N. Beauregard Street
Alexandria, VA 22311

Dr. A. K. Bejczy
Jet Propulsion Laboratory
California Institute of Technology
Pasadena, CA 91125

Dr. Robert D. Ballard
Department of Ocean Engineering
Woods Hole Oceanographic Institution
Woods Hole, MA 02543

Dr. Douglas M. Towne
University of Southern California
Behavioral Technology Laboratory
1845 S. Elena Avenue
Redondo Beach, CA 90277

Dr. Julian M. Christensen
General Physics Corporation
1010 Woodman Drive
Suite 240
Dayton, Ohio 45432

Dr. Harry Snyder
Department of Industrial Engineering
Virginia Polytechnic Institute and
State University
Blacksburg, VA 24061

Dr. Robert T. Hennessy
NAS - National Research Council
2101 Constitution Ave., N.W.
Washington, DC 20418

Dr. Amos Freedy
Perceptronics
6271 Variel Avenue
Woodland Hills, CA 91364

Dr. Robert Williges
Human Factors Laboratory
Virginia Polytechnic Institute
and State University
130 Whittemore Hall
Blacksburg, VA 24061

Dr. Christopher Wickens
University of Illinois
Department of Psychology
Urbana, IL 61801

Dr. Edward R. Jones
Chief, Human Factors Engineering
McDonnell-Douglas Astronautics Co.
St. Louis Division
Box 516
St. Louis, MO 63166

Dr. Babur M. Pulat
Department of Industrial Engineering
North Carolina A&T State University
Greensboro, NC 27411

Dr. Richard W. Pew
Information Sciences Division
Bolt Beranek & Newman, Inc.
50 Moulton St.
Cambridge, MA 02138

Dr. J. Lester
ONR Detachment
495 Summer Street
Boston, MA 02210

CDR James Offutt, Officer-in-charge
ONR Detachment
1030 East Green Street
Pasadena, CA 91106

Director
Naval Research Laboratory
Technical Information Division
Code 2627
Washington, D.C. 20375

Dr. J.E. Franklin
Navy Center for Applied Research in A.I.
Code 7510
Naval Research Laboratory
Washington, D.C. 20375

Dr. J.R. Davis
Information Technology Division
Code 7500
Naval Research Laboratory
Washington, D.C. 20375

Dr. Robert G. Smith
Office of the Chief of Naval
Operations, OP 987H
Personnel Logistics Plans
Washington, D.C. 20350

Dr. Andreas B. Rechnitzer
Office of the Chief of Naval
Operations, OP 952F
Naval Oceanography Division
Washington, D.C. 20350

Human Factors Department
Code N215
Naval Training Equipment Center
Orlando, FL 32813

Dr. Gary Pooch
Operations Research Department
Naval Postgraduate School
Monterey, CA 93940

Mr. H. Talkington
Ocean Engineering Department
Naval Ocean Systems Center
San Diego, CA 92152

Mr. Paul Heckman
Naval Ocean Systems Center
San Diego, CA 92152

Mr. Warren Lewis
Human Engineering Branch
Code 8231
Naval Ocean Systems Center
San Diego, CA 92152

Dr. A.L. Slafkosky
Scientific Advisor
Commandant of the Marine Corps
Code RD-1
Washington, DC 20380

Human Factors Technology Administrator
Office of Naval Technology
Code MAT 0722
800 N. Quincy Street
Arlington, VA 22217

Mr. Phillip Andrews
Naval Sea Systems Command
NAVSEA 0341
Washington, DC 20362

Mr. Milon Essoglu
Naval Facilities Engineering Command
R&D Plans and Programs
Code 03T
Hoffman Building II
Alexandria, VA 22332

CDR Robert Biersner
Naval Medical R&D Command
Code 44
Naval Medical Center
Bethesda, MD 20014

Dr. George Moeller
Human Factors Engineering branch
Submarine Medical Research Lab
Naval Submarine Base
Groton, CT 06340

Dr. Robert Blanchard
Navy Personnel Research and
Development Center
Command and Support Systems
San Diego, CA 92152